NTNU

Norwegian University of
Science and Technology

DEPARTMENT OF GEOSCIENCE AND PETROLEUM

TPG 4920- PETROLEUM ENGINEERING, MASTER`S THESIS

CO$_2$ STORAGE IN DEPLETED GAS FIELD RESERVOIR MODEL AND SENSITIVITY ANALYSIS USING NUMERICAL SIMULATION TECHNIQUES

By

Nabeel Ahmed Khan

Supervisors: Ashkan Jahanbani Ghaforokhi & Alv-Arne Grimstad

Date of Submission: 08/07/22

CO₂ STORAGE IN DEPLETED GAS FIELD RESERVOIR MODEL AND SENSITIVITY ANALYSIS USING NUMERICAL SIMULATION TECHNIQUES

By

N.A KHAN

in partial fulfillment of the requirements for the degree of

Master of Science
in Petroleum Reservoir Engineering and Petrophysics

at the Norwegian University of Science and Technology

Student number: 546777

Supervisors: Assoc. Prof Ashkan Jahanbani Ghahfarokhi- NTNU
Alv-Arne Grimstad –Sintef

NTNU
Norwegian University of
Science and Technology

Abstract

Worries are growing with the upsurge of GHG emissions and accumulation into our atmosphere where the chief producer of GHG is the combustion of fossil fuel for producing useful energy. Energy scientists, researchers and technologists have been working relentlessly to provide solutions to limit this frightening issue and have suggested numerous measures, including wind, solar and hydroelectric power to name a few, as alternative energy solutions. But this is not enough to decrease the impact of the already present GHGs that are becoming foremost influence to the global warming issue. A comparatively fresh and an innovative solution is the use of CCUS for mitigating these GHGs. Out of the three branches of this proposed solution, the one concerning petroleum engineers the most, is storage. The first storage project in an aquifer commenced in Norway in the Sleipner field in 1996 and since then this project has successfully managed to store amounts in Mega tonnes of CO_2 into the geological formations. Many countries like USA, UK, Netherlands, China, and South Korea have shown a great curiosity in this field and have realized its significance in attaining the global net zero target of 2070.

Out of the three prominent options available for storage, depleted oil and gas reservoirs are one of them. In this thesis, which is a preparation of the work for alliance with ACT RETUN project, CO_2 injection in a depleted gas reservoir is studied and sensitivity analysis of the impact of storage on reservoir, based on different reservoir heterogeneities, initial fluid properties, end point saturations of the relative permeability data, reservoir properties and characteristics, injection rates and aquifer support is performed. Key concepts related to the storage process and special considerations regarding it are presented initially which gives a greater insight of important reservoir engineering concepts revolving around, capacity injectivity, containment and monitoring of CO_2 storage. The reservoir modelling and simulation was done using Eclipse 300 (a compositional simulator) and the Norne field model was used from open source (grid properties). The results of simulation revealed that reservoir heterogeneity impacted the storage efficiency slightly. The injection rates must be controlled to avoid fractures and leakages, having high initial reservoir temperature is not advisable for injection, having a lower initial water saturations is favorable for increased capacity, high critical gas saturation is needed for enhanced residual gas trapping and aquifer can be very useful for storage activities provided it is a strong one (having large aquifer volume).

Overall, this thesis opens up windows to explore on working with larger data sets and actual depleted gas models where even more comprehensive studies (like thermal runs, fault scenarios, monitoring wells etc.) can be performed using the knowledge gained and skills developed within this thesis.

Preface

In the name of Allah, the most Merciful and the most Significant.

The MSc. thesis is an indication that a remarkable two year journey at NTNU has come to an end. During these hard times when Covid-19 had taken over the globe and things were difficult, being able to successfully complete the degree and write this thesis is a fantastic achievement which gives extreme satisfaction to me.

I would like to express my gratitude to my supervisor Assoc. Prof Ashkan Jahanbani Ghaforukhi and Alv-Arne Grimstad. They have been a constant support throughout this entire process of completing this thesis. It started from topic selection, to conducting relevant research and gathering data, learning simulation techniques, performing reservoir simulations. During these past 20 weeks both my supervisors constantly and critically evaluated my work in the weekly online meetings. Their guidance, knowledge and help is of immense value to this thesis and I look forward to build on it further in my professional career to come.

I would specially like to thank my parents who have constantly supported me during this period away from home and have kept me motivated. A big shout out to them!

Table of Contents

List of Figures

List of Tables

Nomenclature

P_C: Capillary Pressure

γ_{b-co_2}: Interfacial Tension between brine and Carbon dioxide

<: greater than

>: less than

∇: gradient operator

A: reaction surface area

c: capillary, critical

C: specific heat capacity

CO: Carbon Monoxide

CO_2: Carbon Dioxide Gas

D: diffusivity

E_a: activation energy

eq: equilibrium

f: function

fms: formations

g: gravitational acceleration assuming in the negative coordinate direction

g: magnitude of gravitational acceleration

Gt: Giga tons

h: grid spacing in the computational domain

h: Reservoir Thickness

H: specific enthalpy

H_2: Hydrogen gas

H_2O: Water

I: kinetic rate

k: permeability tensor

K: rate constant of chemical reaction

K: relative permeability

K; Permeability

m: meters

mD: milli Darcy

N/G: Net to Gross

o.e: oil equivalent

P: Pressure

p: pressure

P_{res}: Reservoir Pressure

P_{wf}: Wellbore Flowing Pressure

q: filtration velocity (Darcy flux)

Q: ion activity product

r: Pore Radius

R: universal gas constant

s: saturation

S: source/sink term

Sgr: Residual Gas Saturation

S_H: source/sink term of energy

Sm^3: Standard cubic meter

S_w: Water saturation

S_{wc}: Connate Water Saturation

T: temperature

t: time

U: specific internal energy

v: velocity vector

w.r.t: with respect to

x, y, z: Cartesian coordinates

X: mole fraction

α, β: fluid phase

ΔH: Change in enthalpy

ΔP: Change in Pressure

ΔT: Change in Temperature

θ: Contact angle for determining the wettability

λ: conductivity

μ: dynamic viscosity

v: stoichiometric reaction coefficient

ρ: density

Σ: summation

τ: tortuosity

ϕ: porosity

Abbreviations

CCS: Carbon Capture and Storage
CCUS: Carbon capture, Utilization and Storage
CO2CRC: Cooperative Research Centre for Greenhouse Gas Technologies
EM: Electromagnetic
EOR: Enhanced Oil Recovery
FDP: Field Development Plan
GWC: Gas Water Contact
IEA: International Energy Agency
IPCC: International Panel on Climate Change
O&G: Oil and Gas
Ppm: Parts per million
PVT: Pressure Volume Temperature
R&D: Research and Development

1 Introduction

With the growth in world`s population, the demand for energy consumption has witnessed a severe upsurge. This demand is catered for, chiefly, by the combustion of fossil fuels. For electricity generation and in the industrial sector, primarily in the manufacture of steel, cement, chemicals and fertilizers fossil fuels are a key play a key role. Based on preliminary analysis, the global average atmospheric carbon dioxide in 2020 was 412.5 ppm, setting a new record high amount despite the economic slowdown due to the COVID-19 pandemic. (LINDSEY, 2021) As stated by the International Panel on Climate Change, the use of fossil fuels for the industrial and other sectors will continue to rise in the near and far future. Unfortunately, the combustion of fossil fuels is one of the foremost causes of atmospheric GHG emissions and causative towards global warming. This poses a staggering threat to the environment making survival of the living beings very difficult. Technical solutions are consequently necessary to lessen the emitted CO_2 volume from the atmosphere and curtail the impact of it. CCUS is one significant, relatively new and an innovative process that aids in achieving this goal to a certain extent (Svalestuen, Park, DePaola, & Powell, 2017). It encompasses separating CO_2 from the effluents of industrial plants or power stations, and then lastingly storing it deep underground in various geological formations. In recent years, plentiful successful large scale CCUS projects have been initiated around the globe which undoubtedly set a standard for others to work on and provide a prospect to further improve performance, cut cost and make future CCUS projects become more practicable and certain in accomplishing their goals (Khan N. A., 2021).

1.1 Thesis Motivation

This thesis is a continuation of the specialization project completed here at NTNU and is an inspiration from the ongoing ACT RETURN project which is launched by a group of oil and gas operators, which emphasizes on safe and efficient CO_2 injection into depleted oil and gas reservoirs. The eventual target of the ACT RETURN project is to determine the prospects of large-scale CO_2 storage in oil and gas fields that have matured, become uneconomic and have depleted. CCS via depleted O&G sources is particularly interesting for the countries neighboring the North Sea. Norway, the UK, Netherlands, Germany and Canada along with Italy (represented by ENI) are the companies that are partners for this project. The ACT RETURN project targets to develop practicable solutions for seeing off the technical challenges related with the injection of CO_2 into the O&G formations and guarantee a safe and cost efficient use of these storage sites. The challenges stated in the executive summary include (i) Coupled reservoir flow modelling, (ii) Near wellbore processes, (iii) Wellbore integrity and (iv) Enabling cold CO_2 injection (Khan N. A., 2021).

The scope of this thesis is to determine the exact total number of moles of CO_2, distribution of CO_2 after storage, the dominant trapping mechanism and final reservoir pressure after the gas is injected into a real Norne reservoir model that was publicly available for academic and research purpose. The outcome of varying reservoir heterogeneity, relative permeability for end point saturations, reservoirs properties, rate of injection, and the effect of aquifers on the final simulation results for parameters stated above is established. Reservoir modelling strategies are in line with the previous studies on reservoir simulation for CO_2 storage in depleted gas fields like the study (Raza, et al., 2017) that debates the effect of residual gas saturation on CO_2 storage and the study by (Akai, Okabe, Hiyama, & Saito, 2021) which revolves around

the impacts of aquifer encroachment and reservoir heterogeneities on CO_2 storage in depleted gas reservoirs. Prior projects related to this field of study are discussed throughout the sections of the thesis and how every step was linked to a previously conducted work is vividly enlightened and referenced (Khan N. A., 2021).

1.2   Research Objectives

According to the SINTEF website, the RETURN project aims at enabling safe and cost-efficient long-term CO_2 storage in depleted O&G reservoirs by understanding and handling cooling and CO_2 phase change effects during injection with the following secondary objectives:

- o   Having coupled well-reservoir flow modelling with having effects of strong cooling and phase changes of the CO_2 during injection. Confirm the coupled flow model using experimental and field testing and apply the validated model to actual field cases.
- o   Study the behavior of temperature and pressure during CO_2 injection in depleted gas reservoirs in the near well regions Understand how low temperatures, strong temperature variations and strong pressure variations expected during CO_2 injection into depleted reservoirs will affect the near-well region (reservoir and caprock), as well as their effects on storage capacity (depletion/re-pressurization effects) and injectivity.
- o   Researching about the details of risks related to well integrity during CO_2 injection into depleted reservoirs consequential from cold temperatures, and strongly varying downhole pressures and temperatures

In this thesis, the primary focus was to estimate a volumetric capacity of the reservoir for injecting CO_2 and study the migration of CO_2 from the well towards the boundaries of the reservoir using numerical simulation techniques. The pressure buildup near the well and the reservoir is to be determined with a focus on initial depletion and then re-pressurization. Containment of injected CO_2 in the reservoir is also to be studied by evaluating the leakage pathways across the regions created in the reservoir.   Determine the trapping mechanisms including dissolution, structural and residual in the gas reservoir. A comparison of results between two approaches of numerical simulation is to be defined. A sensitivity analysis based on variable reservoir heterogeneity, different initial fluid saturations and deeper GWC, variable injection rate, varying reservoir fluid properties and compositions, and aquifer support is to be conducted for all of the above. Thermal effects and salt precipitation are not studied in this research mainly because of the limitation of the software used.

1.3   Thesis Outline

The master's thesis was carried out for CO_2 injection simulation in a depleted gas reservoir by using the Norne field geological properties. Before moving on to discussing the, softwares involved, methodology used and the results and discussion of the project, a literature research section focusing on what CO_2 storage is and what its major technicalities are is researched and presented. In Section 2 fundamental of CO_2 sequestration are discussed that accurately enlightens the concept of CCUS, storage in depleted oil and gas fields, pros and cons of injecting CO_2 into depleted reservoir, and finally previous CCS projects are

mentioned. Section 3 focuses on the special considerations involved in the process of CO_2 injection particularly the geo-mechanical, chemical, thermal and some general considerations. The actual Norne reservoir model and its properties are introduced in Section 4. A detail study regarding numerical simulation and the relevant concepts it is based upon is highlighted in the Section 5. Details of the methodology used and the main software of concern is explained in Section 6. Furthermore, a comprehensive discussion of all the results obtained is given in Section 7. Finally, a conclusion is provided along with the areas of further research, improvements and suggestion in Section 8.

2 Fundamentals of CO$_2$ sequestration

2.1 The Need for CCUS

A lot of the anthropogenic CO$_2$ levels have increased severely, from pre-industrial levels of 280 ppm a 100 years ago to over 400 ppm since 2013 (Svalestuen, Park, DePaola, & Powell, 2017). The rising economic and population growth results in the upsurge of CO$_2$ emissions levels, and if left unattended, are projected to surpass 530 ppm by the 22nd century (Svalestuen, Park, DePaola, & Powell, 2017). These levels have to be kept minimum to a set limit, as they can enhance the greenhouse effect. This effect ultimately leads to the rise in global temperatures which in turn destroys the global ecosystems, causes natural disasters like storms, floods and droughts, consequently destruction of natural habitat. According to the IPCC 2007 report (Parry, et al., 2007), goals for steadying CO$_2$ levels at ≤450 ppm were fixed in 2007 to avoid serious blows to the environment and health. To achieve these targets, however, IPCC 2014 report (Edenhofer, et al., 2014) suggests, considerable enhancements in energy efficiency, increased deployment of renewable and nuclear energy, and the development of new technologies for lessening CO$_2$ emissions as a result of the use of fossil fuels which amounted almost 9855 million metric tons or nearly 36 Gt in 2014 (Boden, Marland, & Andres., 2017) and other anthropogenic sources is needed (Khan N. A., 2021).

"Reaching net zero will be virtually impossible without CCUS", (IEA, 2020). CCUS is projected to contribute to dropping 600 billion tonnes of CO$_2$ over the following 50 years which is almost 17 years` worth of annual emissions from the power and industrial plants. In the IEA`s Sustainable Development Scenario, according to which the energy sector has to reach net zero by 2070 on global CO$_2$ emissions, CCUS will play a key role here and accounts for nearly 15% of the collective reductions. If this goal has to be achieved twenty years earlier, then CCUS deployment should rise to 50%. In addition to the environmental benefits, CCUS can provide social benefits such as job protection and creation, and energy safety and access, in addition to the main objective of CO$_2$ emissions` reduction. These factors and statistics mentioned above clearly reflect the importance of CCUS and demonstrate the reasoning of an urgent need of its research, expansion and deployment (Khan N. A., 2021).

2.2 What is CCUS?

Carbon capture, utilization and storage is one of the progressive and valuable technologies newly deployed around the globe to curb the anthropogenic CO$_2$ levels present in the atmosphere. Fossil fuels combustion for power and heat production, transport sector along with manufacturing of steel, cement, chemical, fertilizers and hydrogen is prevalent and releases CO$_2$ in gigatonnes scales per year. Sectors such as power and transport, have substitute resources like wind, solar and hydropower to supply for their needs to a certain extent. However, industrial processes like the ones stated above, have restricted accessibility of alternatives to fossil fuels. Therefore CCS is deployed. Figure 2-1 and Figure 2-2 help in envisioning and clarifying the work flow of CCUS respectively. This section will provide a detailed description of procedures/theory of storage. Carbon capture and utilization is, however, beyond the scope of the literature research conducted (Khan N. A., 2021).
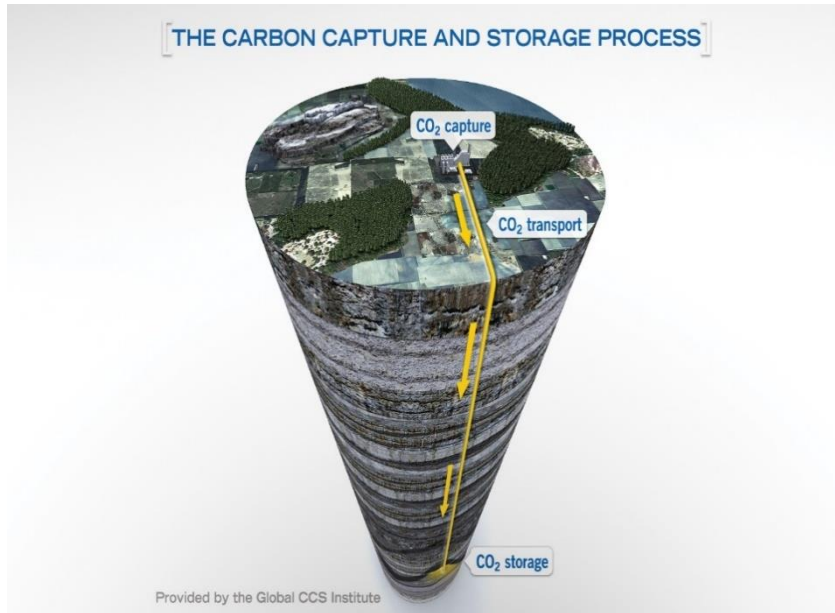
Figure 2-1 Carbon capture and storage (GLOBAL CCS, 2021) (Khan N. A., 2021)
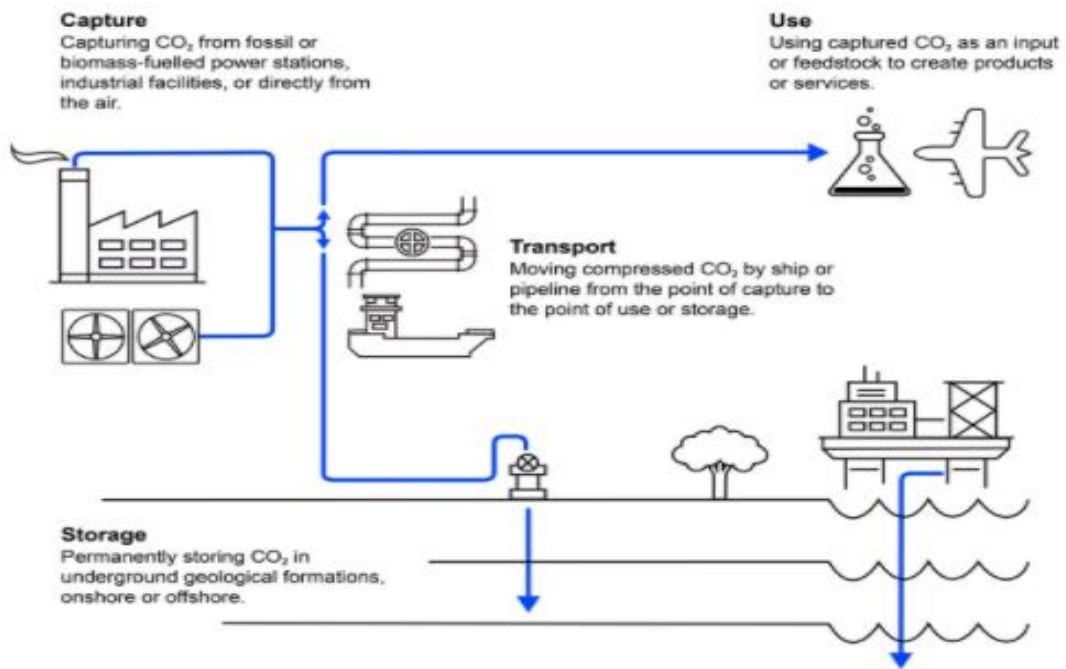
Figure 2-2 CCUS flow diagram (IEA, 2021) (Khan N. A., 2021)

2.3 A Complete CO_2 Storage Overview

CO_2 storage is the ultimate phase of the CCS process, where the captured CO_2 is injected into subsurface formations. The usual type of formations include (I) Deep saline aquifers (II) Depleted O&G reservoirs (III) Coal bed methane. Figure 2-3 below illustrates the varieties of sequestration sites. This diagram displays the positioning of the probable storage sites for injection along with fields where CO_2 injection is used for enhanced recovery for oil and/or methane. Over the years, there have been incessant enhancements in the knowledge and ruling required for successfully storing the CO_2 gas in the subsurface and there are at present numerous megaton-sized pilot projects that provide an insight of proceeding with the sequestration processes while evading former mistakes and bettering on them (Svalestuen, Park, DePaola, & Powell, 2017). The behavior of CO_2 is dissimilar at various P and T conditions, hence, it is imperative to forecast and define its physical properties in the subsurface environment and the kinds of physical and/or chemical reactions can occur between CO_2 and the subsurface constituents like hydrocarbons, H2O and minerals. The target is to ramp up the injection amount to gigatonnes/year mark by improving R&D in the following areas: (1) Injectivity and capacity; (2) Monitoring, verification and performance metrics; (3) Forecasting and managing induced seismicity and (4) Well Integrity (Svalestuen, Park, DePaola, & Powell, 2017). A key factor that determines storage capacity of a site is the pore volume of the geological formation and the long term storage safety. This guarantees that the injected volume of the CO_2 stays in the formations for long periods of times, more than centuries, and does not harm the adjacent environments like potable aquifers. These related problems and parameters determining successful storage will be discussed in details in the upcoming sections.

These sections have been an adaptation of my previous research and work (Khan N. A., 2021) conducted for the same topic.
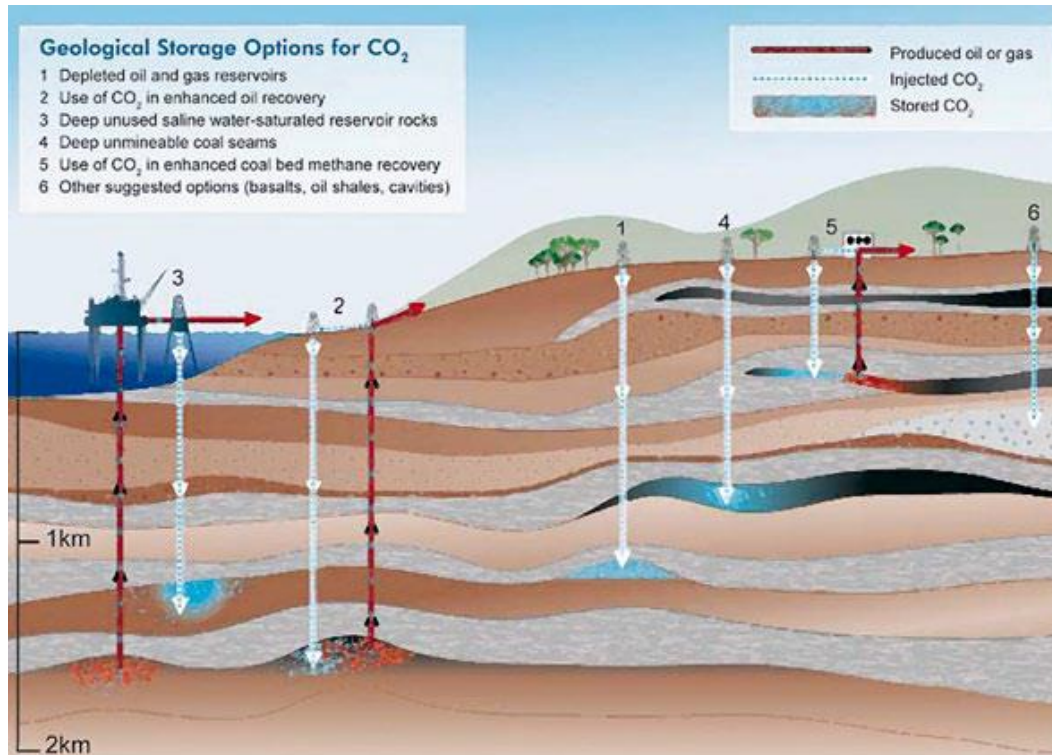
Figure 2-3 Potential CO$_2$ Storage sites (IPCC, 2007) (Khan N. A., 2021)

2.3.1   Types of Potential Storage Sites

There are three main types of geological formations (i) Saline aquifers (ii) Depleted O&G reservoirs and (iii) Coal bed methane reservoirs, that are appropriate as storage sites for anthropogenic CO$_2$. It is evident from the existing data that saline aquifers are potentially a better choice in terms of capacity, however, it comes with a cost of ambiguity and lack of data availability making it more liable to risks and challenges in comparison with the O&G depleted reservoirs. Since the thesis concerns the depleted gas reservoir, details are provided for this only.

2.3.1.1   *Depleted oil and gas reservoirs.*

The rate at which the hydrocarbon reserves are being produced and utilized is increasing in spite of the green initiative and the limitations on petroleum trade. This is due to the swelling global population and eventually the increase in demand for energy consumption. This depletion of hydrocarbons reservoirs, their status as uneconomical for further production makes them vital geological spots where CO$_2$ can be injected back and stored. Before injection it has to be ensured that the CO$_2$ is in a supercritical state that makes its density similar to that of a liquid while viscosity becomes more gaseous at P > 73.8 bar and T >31°C as shown in the phase diagram in the Figure 2-4 below. This is done so that the denser state CO$_2$ dissolves in water easily and mixes with resident hydrocarbon gas, stays immobilized, and a larger volume of CO$_2$ can be injected in this way. The injected CO$_2$ is stored in the reservoir as a free or trapped gas. The mechanisms of trapping are explained in detail in the Section 2.3.3 of this report.
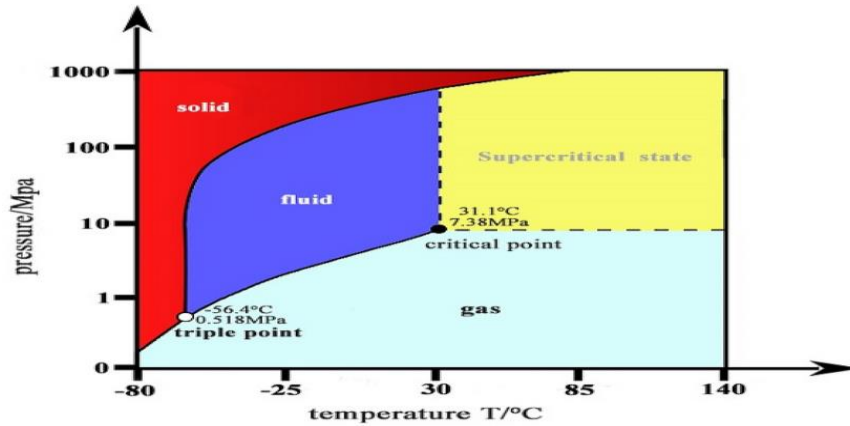
Figure 2-4 Phase Diagram of CO2 gas (Yang, Lian, & Li, 2020) (Khan N. A., 2021)

 The likely storage capacity is around 900 Gt CO_2 (IPCC, 2007) which as compared to the saline aquifer is a lesser value, however, the number has larger confidence due to the obtainability of formation data from earlier hydrocarbon production projects making the data about reservoir parameters like permeability, porosity, stratigraphy and structural geology more concrete. The trapping mechanisms in these reservoirs are similar to the ones in saline aquifer formations with slight differences because of the presence of an additional phase of hydrocarbon and these are elucidated in Section 2.3.3. O&G reservoirs have some obvious advantages and disadvantages as potential sites for CO_2 sequestration and are covered as separate sections later.

2.3.2   Features Leading to Effective Storage

The previously mentioned storage sites can be regarded as good candidates only if they fulfill the criteria of long term storage with full safety. According to the previously conducted researches, the following parameters ensuring good storage are proposed.

- o   One of the most significant reservoir rock properties that must be present is a seal which is an extremely low permeability rock (<1mD) present in the formation that prevents the injected CO_2 to migrate upwards and reach the ground surface or nearby water aquifers. (Agartan, Gaddipati, Yip, Savage, & Ozgen, 2018)
- o   Depth of the reservoir must be high enough to make sure that the P and T is sufficient to keep the CO_2 in the supercritical state that supports in trapping, and provides the opportunity of storing greater volumes of the CO_2. However, care must also be taken not to inject into too deep formations (>2500m), (Agartan, Gaddipati, Yip, Savage, & Ozgen, 2018) as at deeper levels higher compaction of reservoir rocks diminishes the pore space and eventually lessens the capacity.
- o   Having a large storage capacity is needed to store the CO_2 injected. This is guaranteed by having large effective porosity in the reservoir usually >20%. Another aspect determining the capacity is the P and T of the reservoir. It is important that the pressure and geothermal gradient is high enough to keep the CO_2 in supercritical state. (Razaa, et al., 2016)
- o   There should not be any pathways present for CO_2 to leak out of the formation. These pathways include feeble top seal, faults or fracture zones, in the case of saline aquifers and depleted O&G

formations, and abandoned wellbores with lower reliability for the case of O&G depleted reservoirs only.

o Since the injected fluid must flow into the geological formation, it is essential that the permeability is reasonably large (>300mD). This ensures that the injected CO_2 is well spread into the formation and does not result in additional pressure buildup. This buildup in turn can lead to injectivity issues and activate fracturing and/or seismic events like minor earthquakes (Gasda, Bachu, & Celia, 2004).

o Reservoir thickness must be large >50m as it is directly related to injectivity (Razaa, et al., 2016). This is to safeguard that the pressure buildup in the near well regions is not very high and is dissipated towards the boundaries laterally farther from the near well area.

o The pore throat distribution of the rock matrix must be thin as it is more advantageous than a wider pore because the high aspect ratio (i.e., pore-body radius to pore throat radius) affects the fluid interface and results in the flow of the wetting phase to go into the pore throats offering a high non-wetting phase (CO_2) saturation. This narrow pore throat size results in higher capillary pressure eventually leading to improved trapping section (Grobe, Pashin, & Dodge, 2009) (Pentland, Iglauer, Gharbi, Okada, & Suekane, 2012). This will be explained further in the next section.

2.3.3 Trapping Mechanisms

Trapping is the most important aspect of geological storage without which injection of CO_2 into the subsurface would be merely a waste. Trapping mechanisms are categorized into two main groups: (I) Physical and (II) Chemical. As the name suggests physical trapping mechanism is the one in which CO_2 is physically trapped without any change in the chemical properties of CO_2. The process usually take place immediately after injection and can continue for centuries. Chemical trapping happens as a result of chemical reactions between CO_2 and the reservoir fluids, rock and minerals where CO_2 doesn't remain a separate phase and its chemical properties are reformed. This is a long term process (>50 years) and usually the time of occurrence is greater than the physical trapping mechanisms (Khan N. A., 2021). These are further characterized as follows:

2.3.3.1   Physical Trapping

a) Structural trapping Structural Trapping is generally the first form of trapping that happens as soon as the CO_2 is injected into the geological formation and is similar to how hydrocarbons had been stored underground for thousands of years. CO_2 present as a supercritical or mobile phase inside the geologic formations are trapped by the help of structures like cap rocks and stratigraphic traps. After injection, in the subsurface, the CO_2 is dense but not more than the reservoir fluid (brine or hydrocarbons) present. This density difference creates a buoyancy force that aids in the upward movement of CO_2 through the porous and permeable rock until a stratigraphic trap (fault) or a caprock is reached as shown by the Figure 2-5. In O&G depleted reservoir fields this movement can also come to a stop once a sealed abandoned well is reached (Ajayi, Gomes, & Achinta, 2019) (Khan N. A., 2021).
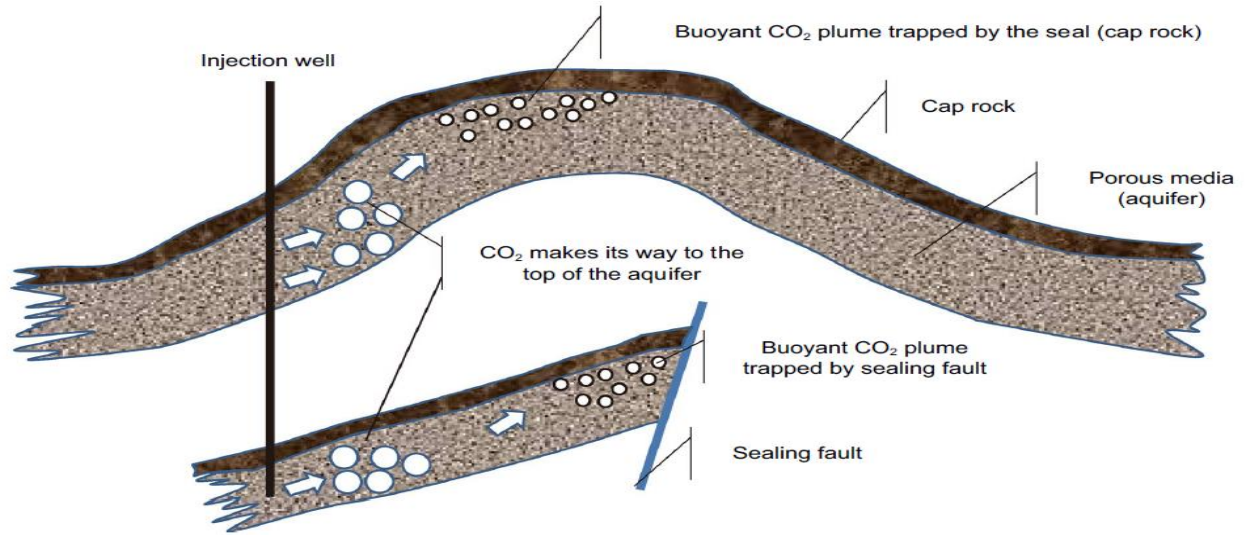
Figure 2-5 Structural trapping of injected CO2 (Ajayi, Gomes, & Achinta, 2019) (Khan N. A., 2021)

b) Capillary/ Residual Trapping After injection the CO_2 moves through the reservoir pore spaces in two directions; upwards and lateral, and relocates the reservoir fluids present. This causes the reservoir fluids to fill up the pore spaces available. This movement is not totally the case for all CO_2 droplets and some of them are left behind as residual droplets. This is shown in Figure 2-5 and it can be seen that CO_2 gets trapped in the pore throats of the porous media. Surface tension between the reservoir fluid and CO_2 causes the latter to be immobilized. The geometry of pore spaces, communications between rock-fluid and fluid–fluid play important roles in storage in geological formations (Razaa, et al., 2016). The Laplace model given by the Eq.1 below show these interactions which affect the flow process and in the long-term, control the capillary-sealing (Raza, et al., 2017). This equation shows the capillary pressure is inversely related to the pore radius.

$$P_C = P_{CO_2} - P_{brine} = \frac{2\gamma_{b-co_2}\cos\theta}{R} \qquad (1)$$
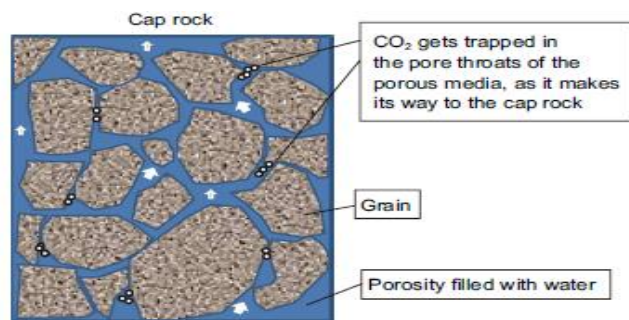
Figure 2-6 Residual trapping due to formation pore structure (Ajayi, Gomes, & Achinta, 2019) (Khan N. A., 2021)

Residual trapping is more effective than the other mechanisms involved in trapping CO_2 in the short term. Capillary forces are stronger than the buoyant forces hence CO_2 is trapped as small bubbles rather than being trapped structurally underneath a caprock. This type of trapping can be most easily be compared with that of a sponge being filled with water where the liquid is contained in many individual containers within it (Berge, et al., 2011) (Khan N. A., 2021).

2.3.3.2   Chemical Trapping

a) Solubility Trapping Solubility trapping is fundamentally due to a chemical reaction between formation brine and the injected CO_2. Just as sugar dissolves in tea, CO_2 dissolves into water establishing a dense CO_2- saturated brine mixture. This heavy mixture is dense enough to avoid the buoyant forces due to density differential and descents to the lower part of the reservoir and gets trapped. This dissolution results in the formation of weaker carbonic acid that disassociates into H^+ ion and HCO_3^- and thus forming insoluble ionic compounds by reaction with the cations present in the formation. CO_2 solubility in formation water decreases as temperature and salinity increase. (Ajayi, Gomes, & Achinta, 2019).

b) Mineral Trapping Mineral trapping happens when CO_2 that is in an aqueous state reacts with solid rock minerals and transforms into heavier compounds like calcite, muscovite or quartz. The variation in compounds is governed by the mineralogy of the formation. It is a comparatively slower process and occurs after or during solubility trapping and can be thought of as the most permanent form of storage since the compounds formed are irreversible. This trapping mechanism is dependent on the pressure of the gas (CO_2 injection), T and P of the formation, and ultimately the reservoir`s permeability and porosity. (Ajayi, Gomes, & Achinta, 2019).
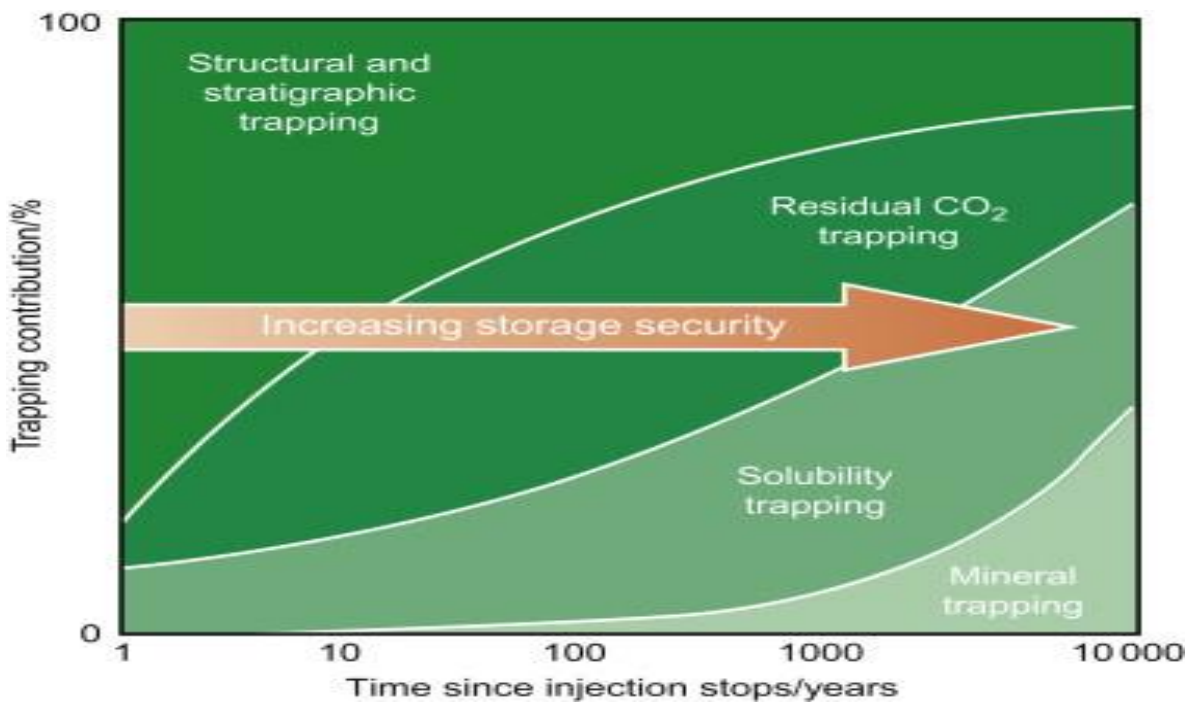
Figure 2-7 Trapping mechanism and time dependency (Rosenbauer & Thomas, 2010) (Khan N. A., 2021)

Figure 2-7 shows the relationship between trapping mechanism and time. It is apparent from the figure that at the start of injection the largest contribution to trapping is from structural and stratigraphic traps. With time the residual trapping shows dominance followed by solubility trapping. At extremely later times, the mineral trapping is the most obvious mechanism for immobilizing the injected CO_2 back. There is an increase in storage security with time for all the mechanisms (Khan N. A., 2021).

2.4　Pros and Cons of O&G Fields as Potential Storage Sites

With more and more interest in CCUS and better technological developments, oil and gas depleted fields are becoming a very prevalent storage options. It is therefore important to understand their pros and cons and make a careful analysis before they are used (Khan N. A., 2021).

Pros

One of the evident benefits of making use of O&G depleted fields as sequestration sites include: the fact that at lower pore pressures at the time of injection initiation can allow the refilling of reservoir until it reaches its original reservoir pressure. Additionally, a greater and tested knowledge like history matched geological and petrophysical data is available making the estimation of total capacity more solid in comparison to the saline aquifers. Furthermore, O&G reservoirs have an already built-in wells` infrastructure obtainable. Some of the already present production or injection wells can be used as CO_2 injection wells, with slight modifications and upgrade if necessary. Previous production history provides a guarantee that the reservoir that has been a home to a great amount of hydrocarbons for thousands of years can have proven containment like a seal on top of the reservoir. (Loizzo, Lecampion, Berard, & Jammes, 2010)

Cons

As a matter of fact, although O&G reservoirs offer certain benefits but it is wise to reflect upon some of the disadvantages of using them as storage sites for anthropogenic CO_2. Accessibility of abandoned sites is mainly dependent on when operating companies choose to consider their time off. Mostly field abandonments are reliant a lot on profitability which in turn depends on the prices of petroleum. Unfortunately, these are unstable, making the abandonment deferred or sudden. Usually, these depleted reservoir have a greater number of wells drilled. Some of the wells may have been drilled long time ago with old technology and out-of-date materials, which can become the leakage pathways for the injected CO_2 to discharge towards the surface and hence the containment is affected negatively. Additionally, it is also important to note that the overall capacity of O&G depleted reservoirs is lower than the saline aquifer. When CO_2 is injected to the reservoir, re-pressurization occurs. This although can provide room for refilling of the reservoir, but may cause an adverse effect on the seal integrity and weaken the rock structure (Loizzo, Lecampion, Berard, & Jammes, 2010).

Overall, O&G have their own pros and cons that are needed to be carefully assessed before a storage project begins. If the possible disadvantages are carefully monitored and efforts are taken to avoid them, O&G can safely be considered as an excellent choice for sequestration of CO_2 (Khan N. A., 2021).

2.5　Earlier Works and Lessons Learned

Of the two main geological formations including saline aquifers and depleted O&G reservoirs, relatively slight consideration has been given to mature gas reservoirs. In total almost four to five projects have been

started, completed or are under planning. Out of these projects, the ones which have been successfully initiated and stored large volumes of CO_2 are discussed in the following sections.

2.5.1 In Salah, Algeria

The In Salah CO_2 storage project is the world's ground-breaking onshore project which has supplied massive experience applicable to the ongoing CCS projects worldwide. In Salah gas fields produced CO_2 as a waste (1-10%) together with their hydrocarbons` production. Produced CO_2 was compressed and injected back into the Krechba field, a carboniferous sandstone unit, at a depth of 1900 meters using long reach horizontal wells. The start of injection was in 2004, and over 3.8Mt of CO_2 has been stored in the field until its closure. Monitoring was performed using diverse geophysical and geochemical methods including time-lapse seismic, micro-seismic, wellhead sampling using CO_2 tracers, well logging, core analysis, surface gas monitoring and satellite InSAR data (Khan N. A., 2021).

Before the start of injection, risk calculation for injection scenario was carried out and monitoring activities strategy was set out. Key risks comprised of the injectivity problems, early CO_2 breakthrough into the hydrocarbon production wells, dangers of migration to outside Krechba region, vertical leakages and wellbore leakages. A significant attribute of the monitoring program was the ability to use the observed data and respond swiftly to reduce risks. A vital lesson learned from this project is to include monitoring in FDP and in routine field operations. Additionally, the storage monitoring program must be designed to address site-specific leakage risks, and should be pointed out during site selection as well as during in operation phase. (Ringrose, et al., 2013)

In 2011, injection operations were deferred for the time being due to concerns over seal integrity, although no leakage was reported, the project was still shut off in the same year.

2.5.2 Otway, Australia

Otway Project is Australia`s first CCS project and is started by CO2CRC in the year 2007 after a couple of years taken in planning stage. After the end of first stage of the project, 65000 tonnes of CO_2 rich (80% CO_2 and 20% methane) had been injected through a well drilled at a depth of 2003 -2014 meters into a depleted natural gas reservoir. An extensive range of pre and post injection data is consequently available to learn about the vital project findings and the guidelines across atmospheric, near surface and subsurface regions. The second stage of this project is grounded on injection into a heterogeneous formation with no seal present to comprehend residual trapping mechanism in detail. (Jenkins, et al., 2011)

The stage 1 of the project included successfully injecting CO_2 in the down dip side of a fault bounded Waarre-C reservoir formation. Monitoring results gave consistency with the modelling predictions, therefore, adding guarantee to both approach and validity of the sub-surface realizations. Key monitoring strategies involved to monitor the ecological impact of CO_2 plumes included the atmospheric measurements, groundwater measurements, soil gas measurements and micro-seismic. (Jenkins, et al., 2011)

The joint leakage rates from all the assessments including well-design, CO_2 leakage through seals and finally through faults were fewer than the limit set by IPCC of 0.1 % making the storage a victory. The project is still operational and is in the second stage of storage (Khan N. A., 2021).

2.5.3 K12-B, Netherlands

The K12 –B is a mature gas field located in the Dutch sector of the North Sea. It is a deep reservoir with the top depth of 3800 meters below the sea level. The field has a large CO_2 component (13 %) present in it, which is why this had to be separated from the produced hydrocarbon and injected back into the gas field since 2004. In total in excess of 100 k-ton of CO_2 had been injected until this project was called off in 2017. The entire project has been conducted without any serious events of leakages or fractures. This was guaranteed by initially a successful storage job and later use of proper monitoring techniques. It is so far the only gas reservoir in the Netherlands into which captured CO_2 was reinjected. (Vandeweijer & Hofstee, 2018)

Monitoring and reservoir simulation program was constantly carried out throughout the injection period. This was accompanied by geo-mechanical studies, risk assessment and geo-chemical assessments. The field has an overlying extremely impermeable Zechstein salt layer that made leakage through it tremendously unlikely. The only conceivable leakage pathway was the wells drilled through the top seal. Therefore, strong weight was kept on monitoring and maintenance mainly of the K12 B-6 well that was used for reinjection of CO_2 back to the field. Some of the tools used to monitor its integrity include multi finger calipers and the EM based tool to view well thickness. Chemical tracers that could attach on to the injected CO_2 were used as well to monitor the extent of its movement. Last but not the least, history matching and reservoir simulations were conducted to compare past productions and injection predictions with the actual current rates. This was helpful to predict and evade any injectivity problems. (Vandeweijer & Hofstee, 2018)

Overall, this project was an accomplishment and the first of its kind in this region. It delivers some useful knowledge and training to apply during the future projects involving CO_2 storage in depleted gas reservoirs (Khan N. A., 2021).

2.6 Properties of CO₂ –methane, brine and their mixtures.

A multiphase and a multi component system is formed once the CO_2 is injected in depleted gas reservoirs. It contains several phases including aqueous and non-aqueous phases as well as a solid phase. Water determines the aqueous phase where other components like salts and injected CO_2 gets dissolved. Methane and carbon dioxide interaction is considered as the non -queous phase where pure CO_2 or pure CH_4 can be present. These phases exists together in the reservoir and can sum up to a total of four phases in the system. A phase diagram is a famous approach to represent the relationship of the components in a system at equilibrium as a function of P&T. Figure 2-8 below shows a phase envelope of a Changsen reservoir given in the study by (Chen, et al., 2015) which reflects that the phase envelopes, consisting of a dew-point and bubble point line originating from the critical point, encompass the two phase liquid-vapor region. The critical pressure and temperature of pure CO_2 are 73.9 bar and 31.1°C respectively shown by the Figure 2-4. Variation of temperature and pressure conditions in depleted gas reservoirs, multiple phases can coexist. Alterations of these conditions triggered by the CO_2 injection can result in phase transitions in the reservoir. The understanding of pressure and temperature behavior in the reservoir is hence very important for geological CO2 sequestration. At a supercritical state density and viscosity of CO2 is higher than that of methane making it more mobile and able to displace the in-situ methane. But once the conditions reach the critical point of the mixtures, these properties change drastically and hence the flow is also altered.
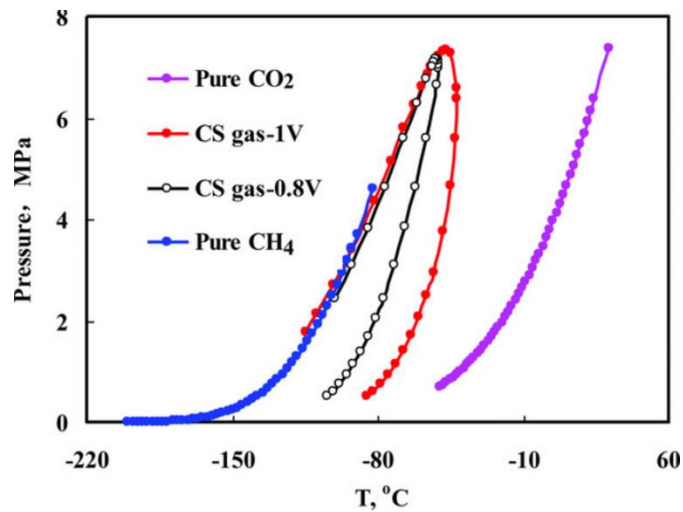
Figure 2-8 Phase diagram of Changshen reservoir for pure methane, pure carbon dioxide and their mixture (Chen, et al., 2015)

As far as solubility of CO_2 and CH_4 is concerned, it increases with greater pressure and decreasing salinity of the water phase. Dissolution of CH_4 in brine is approximately one tenth of magnitude lesser than CO_2. Increasing temperature causes an increase he amount of water components that dissolves or evaporates, into the non-aqueous phase increases with increasing. However, in the presence of a secondary non-aqueous component in a full CO_2-CH_4-brine mixture system, the solubility of the other component in the brine phase gets slightly enhanced. Study of dissolution/mutual solubility is again important to consider as it causes change in temperature, which could ultimately impact injectivity and long term immobilization of CO_2. Further details related to this topic is presented in Section 3.2.1 of the thesis.

3 Special considerations for CO$_2$ injection

This section discusses the main problems of storage in geological formations with particular focus on the depleted gas fields. Although such fields are very popular geological formations chosen for CO$_2$ storage, key challenges that they bring along are needed to be addressed before they can be made useful to their full potential. The main issues related to it are subdivided into mechanical, thermal and geochemical impacts and are discussed in detail in the following sections.

3.1 Geo-mechanical impacts of CO$_2$ injection

As mentioned in Section 2 of this thesis, one of the most important aspect of a successful storage in depleted oil and gas reservoirs is the hydraulic integrity of both the geological formation that encircles it and the wellbores that are drilled through it. In this section, a review of critical geo-mechanical factors that pose risks to the integrity of the bounding seal system is discussed in detail. Most of the literature found in this section are adapted from the works of (Hawkes, McLellan, & Bachu, 2005) and (Orlic, 2016).

Geo-mechanical effects related to CO$_2$ injection are caused due to the buildup of pore pressure and cooling of the injection reservoirs when a cold CO$_2$ is injected into a reservoir rock at a higher temperature. The increase in pressure and cooling effect causes an initiation of elastic and thermal stresses that can change the pre-injection state of stress within the near well bore region and beyond. Mostly reservoirs and imminent surrounding rock formations: overlying seals, lateral seals and base rock during injection witness the largest induced stresses and deformations. CO$_2$ injection can result in significant geo-mechanical responses such as reactivation of pre-existing fractures and faults in the reservoir and in the overlying formations. Some of the connected fractures even act as the leakage pathways for unwanted fluid migration out of the storage reservoir. In addition to this, injection of CO$_2$ can induce uplift of the ground surface and cause felt seismicity due to sudden slip on pre-existing faults. This rupture usually begins at the reservoir level, but the dynamic rupture may go beyond the reservoir and affect the integrity of overlying seals or trigger larger earthquakes along the critically stressed faults. Some of the geo-mechanics related risks are summarized in the Figure 3-1 and detailed explanations are given in each sub sections below.
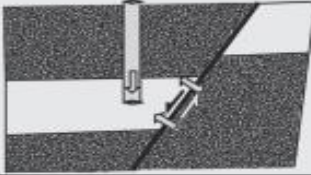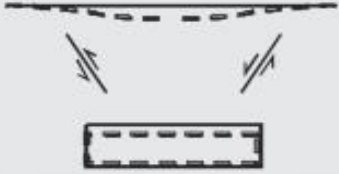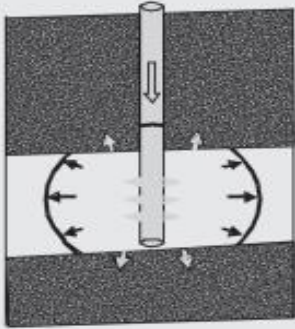
Risk Factor		Mechanism	Methods of Assessment and Mitigation
Reactivation of faults within or bounding the reservoir: (1) Pressure change in the fault plane		Local pressure increase near a fault during injection reduces effective normal stress → reducing the shear strength of the fault.	Geomechanical analyses to determine maximum safe pressure. Inject into reservoir "sweet spots" to avoid locally high pressures. Preferential selection of injection wells that are distant from faults.
Reactivation of faults within or bounding the reservoir: (2) Pressure changes that are pervasive throughout the reservoir		Pressure changes that are pervasive throughout the reservoir cause a change in the in-situ stress magnitudes. The risk of fault reactivation is generally greatest when reservoir pressure is depleted.	Geomechanical analyses to determine if stresses at minimum reservoir pressure (i.e., prior to CO_2 flooding) were capable of causing slip. Review records for any indications of seismicity during primary or secondary recovery operations.
Reactivation of faults in the overburden or caprock		Pressure depletion → reservoir compaction → reservoir subsidence. Shear stresses develop in overburden in the regions overlying the lateral limits of the reservoir.	Geomechanical analyses to assess if subsidence-induced shear stresses at minimum reservoir pressure were capable of reactivating faults. Review historical data for any indications of seismicity during primary or secondary production.
Induced shear failure		Expansion or contraction of reservoir during injection or production, respectively, results in shear stresses at the reservoir-caprock boundary. For domed or anticlinal reservoirs, large horizontal compressive stresses can develop at the apex of the structure.	Geomechanical analyses to identify maximum safe Δp. Was this exceeded during production? Will it be exceeded during injection? Use caution for reservoirs that experienced high-temperature, high pressure injection.
Out-of-zone hydraulic fractures: (1) Prior to CO_2 injection		Fracture treatments or high pressure squeezes are the most obvious causes; waterflood-induced fracturing is also a possible cause. Fractures induced within reservoir grow out of zone if stress contrast is low. Caprock or overburden fracturing during cementing or workovers are also possible.	Operational history (e.g., post-frac height measurements using thermal or radioactive logging; reservoir response during production/injection) should indicate if containment has been lost. Review cementing and workover reports for records of significant losses or high ECDs.
Out-of-zone hydraulic fractures: (2) During CO_2 injection		Injection above fracturing pressure induces fractures within reservoir. If stress contrast is low, fractures grow into caprock, overburden and/or underburden.	Avoid fracturing. Identify safe upper pressure limit (e.g., σ_j) and maintain a reasonable safety margin below it. Inject into reservoir "sweet spots" to avoid locally high pressures, and select high-permeability storage reservoirs that don't require fracturing for high injection rates.
Leakage outside of casing due to poor cement emplacement in yielded and enlarged boreholes		Near-well stresses that are high wrt rock strength can result in extensive rock yielding, detachment, and enlargement. Cement emplacement may be poor in severely enlarged or rugose hole sections. Zones of high near-well permeability may exist if induced shear fractures and microcracks are not penetrated by cement.	New wells – drill with a mud type and mud density sufficient to mitigate severe yielding and enlargement. Existing wells – identify and preferentially monitor high-risk wells; e.g., use well age, documented cementing problems (e.g., uncemented zones due to losses), cement bond logs, caliper logs etc. as risk indicators.

Figure 3-1 Summary of Geo-mechanical problems related to CO2 injection (Hawkes, McLellan, & Bachu, 2005).

3.1.1   Fault Reactivation

Inducing slip on an inactive fault provides a possible leakage pathway. When the maximum shear stress acting in the fault plane exceeds the shear strength of the fault, it causes slip. Considering a simple 2D case of a fault oriented parallel to the intermediate principal in-situ stress (σ_2). The magnitudes of the shear stress (τ) and normal stress (σ_n) acting on the plane are given by the following equations

$$\tau = \frac{(\sigma_1 - \sigma_3)}{2} \sin2\delta$$

and

$$\sigma_n = \frac{(\sigma_1 + \sigma_3)}{2} + \frac{(\sigma_1 - \sigma_3)}{2} \cos2\delta$$

Where: σ_1 = maximum principal in situ stress (Pa) σ_3 = minimum principal in situ stress (Pa)
δ = angle between the fault plane and the σ_3 direction (rad) = dip angle of the fault (w.r.t. horizontal) for a normal fault stress regime = angle between the fault and vertical for a thrust fault stress regime = angle between the strike of a vertical fault and σ_{Hmin} for a strike-slip fault stress regime

According to Mohr-Coulomb shear failure criterion to characterize the fault strength, the slip criterion can be written as:

$$\tau_{slip} = C_{fault} + (\sigma_n - p)\tan\phi_{fault}$$

Where: τ_{slip} = critical shear stress for slip to occur (Pa) C_{fault} = fault cohesion (often assumed to be 0 for conservative fault slip risk analyses) (Pa) ϕ_{fault} = fault friction angle (often in the 30 to 40 degree range for faults, although it can be significantly less for clay rich faults (rad), p = pore pressure in the fault plane (Pa) A parameter which indicates the risk of slip on a fault, similar to the fault slip tendency, is the ratio of resolved shear stress on the fault plane to the critical shear stress for slip. This parameter is referred to as the modified slip tendency (Tsm):

$$T_{sm} = \frac{\tau}{\tau_{slip}}$$

Defined below, fault reactivation is predicted when $T_{sm} \geq 1$ and substituting these equations together and solving for T_{sm} gives:

$$T_{sm} = \frac{(\sigma_1 - \sigma_3)\sin2\delta}{[(\sigma_1 + \sigma_3) + (\sigma_1 - \sigma_3)\cos2\delta - 2p]\tan\phi_{fault}}$$

As shown by this equation that the fault slip risk is a function of the in-situ stress magnitudes, the pore pressure in the fault plane, the orientation of the fault plane and the fault friction angle.
Existing faults can be reactivated by a number mechanisms either during production or injection which are discussed below.

Faults Within or Bounding the Reservoir—Pressure Change in the Fault Plane

If injection occurs into a reservoir that is intersected or bounded by an inactive fault, the injection induced pore pressure increase reaches the fault plane causing an increase in the risk of reactivation of fault. According to the equation above, an increase in the pore pressure will lead to an increase in the slip tendency of the fault (keeping all else constant i.e. there is no fluid pressure leak off into the surrounding rock matrix. One strategy to avoid such a scenario would be to conduct a geo-mechanical analyses to identify the maximum permissible injection pressure and this limit would surely predict the suitability of the reservoir as a good storage site. Secondly, it should be made sure that the injection wells are placed at a reasonable distance from faults that are at risk of reactivation. In this way the near wellbore pressure buildup would not reach the fault planes.

Faults Within or Bounding the Reservoir—Pervasive Pressure Changes

Previously it was discussed about a fault reactivation case in localized region. For pore pressure changes that are more pervasive throughout the reservoir, induced alterations in the in-situ principal stresses will occur. The intensity of these changes are dependent on the pressure change and depends on some other petrophysical factors like thickness, lateral extent and shape of the reservoir and properties of the faults under influence.

For a reservoir with no preexisting active faults, the vertical stress magnitude is not affected but the horizontal stress is predicted to be changed with the change in formation pressure given as the following equation:

$$\gamma_h = \frac{\Delta\sigma_{Hmin}}{\Delta P_{fm}} = \alpha\frac{1 - 2\vartheta}{1 - \vartheta}$$

$$\gamma_v = \frac{\Delta\sigma_v}{\Delta P_{fm}} = 0$$

Where,

γ_h, γ_v = horizontal and vertical stress path coefficients, α = Biot's coefficient = $1 - \frac{K_{bulk}}{1 - K_{grain}}$, K_{bulk} = bulk modulus of porous rock (Pa), K_{grain} = bulk modulus of constituent mineral grains (Pa), ΔP_{fm} = pore pressure change and ϑ = Poisson's ratio

Moreover, the effective stress change can be expressed as a function of the stress path coefficients

$$\frac{\Delta\sigma\,{}^{`}_v}{\Delta P_{fm}} = \alpha$$

$$\frac{\Delta\sigma\,{}^{`}_h}{\Delta P_{fm}} = \alpha(1 - \gamma_h)$$

Where,

$\Delta\sigma\,{}^{`}_v$ is the vertical effective stress and $\Delta\sigma\,{}^{`}_h$ is the horizontal effective stress.

To assess the risk of this fault reactivation mechanism, it is mandatory to determine the current stress regime, the orientation and strength properties of any faults that intersect or bound the reservoir, the reservoirs` response of depletion, the minimum pressure experienced during depletion, and the maximum pressure anticipated during CO2 injection.

Faults in the Overburden

With the change in pore pressure, during injection or production, expansion or contraction can occur leading to displacements of the rock mass overlying the reservoir. If the downward displacement is considerably large flexure of the overburden overlying the flanks of the reservoir can result in large shear stresses. Furthermore, presence of high angle faults in the overburden pose a risk that the induced shear stresses will reactivate them. A simple solution for an idealized reservoir compaction scenario, magnitude of compaction in a linear elastic reservoir can be predicted using the following equation.

$$\Delta H = HC_m \Delta P_{fm}$$

and

$$C_m = \frac{(1 + \vartheta)C_b}{3(1 - \vartheta)}$$

Where,
Is C_m= uniaxial compaction coefficient (Pa^{-1}) and C_b= bulk compressibility
Therefore, these relationships suggest that fault reactivation risks can be attributed to reservoir compaction and increases with the following:

- Higher reservoir thickness
- Greater pressure change
- Higher uniaxial compaction coefficient.

As this mechanism relies on uniaxial compaction coefficient, risks of fault reactivation are higher in soft sedimentary rocks like unconsolidated sandstones and chalks.

As a conclusion, this mechanism in itself, only poses a threat to the integrity of the overburden strata, this type of fault reactivation does not a pose a real threat CO_2 containment within the zone of injection. However, fault slip in the overburden could result in casing deformation and well failure if it crosses theses faults. Additionally, the increase in permeability related to these faults, will decrease their ability to act as a secondary seal for the CO_2 to be stored and leak through them. Leakage could also be through wellbores and large reservoir displacements in the near reservoir area as explained in the upcoming sections.

3.1.2 Induced Shear Failure

Significant shear stresses can develop at the reservoir –caprock interface due to negligible fluid flow into or out of overlying caprock resulting in no direct driving force for lateral deformation of the caprock. The most important parameters affecting the magnitude of this risk mechanism can be identified by considering the analytical solution for induced shear stress in an isotropic, elastic half-space overlying reservoir. The following equation analytically shows the relationship of induced stress in the lateral direction.

$$\tau_{xy}(x_0, y_0, z_0) = \frac{C_b E_o}{12\pi(1-\vartheta)} \int \Delta p(x, y, z) G(x, y, z) dV$$

Where:

C_b = bulk compressibility of the reservoir, Pa, E_o = Young`s modulus of the overburden (with caprock), Pa, ϑ = Poisson's ratio, Δp = pressure change at a point x,y,z within the reservoir, Pa, x_0, y_0, z_0 = cartesian coordinates for the point of interest, m, $G(x, y, z)$ = distance function that imparts a reservoir shape effect on the magnitude of the shear stress, m^{-3}. From the above equation the parameters that could induce the risks of shear failure can be pointed out which can be given as the following:

- o Increased caprock stiffness
- o Increased pressure changes
- o Increased reservoir compressibility (for instance: unconsolidated ss, chalk fms)
- o Lower strength of caprocks
- o Shallower depths; this is because the normal stress acting across the reservoir-caprock interface and the weak bedding planes in the caprock, will be relatively small.
- o Domed or anticlinal reservoirs (since at the apex of the structure high compressive stresses can be developed)

In addition to pore pressure effects stated earlier, temperature changes within the reservoir can also induce shear stresses as follows

$$\tau_{xy}(x_0, y_0, z_0) = \frac{\alpha_T E_o}{12\pi(1-\vartheta)} \int \Delta T(x, y, z) G(x, y, z) dV$$

Where:

α_T = Volumetric thermal expansion coefficient of the reservoir $^\circ$ K^{-1} and $\Delta T(x, y, z)$ = temperature change at a point x,y,z within the reservoir, $^\circ$ K.

Generally, temperature induced shear failures are less as compared to pore pressure induced ones as the reservoir temperatures are mostly constant throughout the injection and the production period.

3.1.3   Borehole Instability

Borehole stability is determined by the response of the subsurface rock surrounding a well when it is being drilled, completed and later produced. A borehole is stable if the strength of these rocks is more than the induced stresses, otherwise, rock yielding may happen and the yielded rock could be detached from the borehole wall leading to a borehole that is very large and/or is encompassed by a region of rock that is extremely fractured. It is something of concern for reservoir being used as CO_2 storage sites as cement job may be poor and ultimately cement would not penetrate the drilling induced shear fractures and micro-cracks in weak rocks. This can ultimately result in leakage pathways for CO_2.

3.1.4   Casing deformation and failure

Like all the above mentioned geo-mechanics related risk factors is the deformation and failure of casing. It can be a result of one or more of the risk mechanisms described in previous section. As an example, induction of shear failure in casing strings that transect the rock failure plane can occur with fault reactivation and caprock-rock interface induced shear failure. In the same way, extreme reservoir

compaction can apply high axial loads on casing strings within the reservoir which can lead to buckling failure of it, mostly when the cement job is not properly done and can also result in tensile failure as well at the reservoir-caprock interface. Risks related to fault slip, or rock failure due to the mechanisms mentioned earlier and casing shear, buckling and tensile failure risks can be considered to be directly proportional.

CCUS is a recent technological development in curbing the global threat posed by the accumulation of CO_2 in the atmosphere. This section gives a detailed account of what CCUS is, it`s history, technical aspects of storage (including types of storage sites) and the associated problems, trapping mechanisms, advantages and disadvantages of storage in gas depleted reservoirs, lessons learned from previously completed/ongoing projects.

3.2 Geochemical impacts of CO_2 storage

As discusses in previously, the selection of suitable reservoirs and their caprocks as potential storage sites has to be done after performing detailed studies to understand the geological conditions and structure of the whole basin (porosity, permeability, geometry, capacity, mineralogy etc.). Many geochemical reactions can occur in the subsurface in the presence of CO_2 that can lead to a change in the reservoir integrity and trapping potential. The changes include: (i) acidification of pore waters, dissolution of primary minerals, changes in porosity and permeability. (Nikolaos, et al., 2018) Sometimes these changes can be beneficial and sometimes the opposite, therefore, a detailed investigation of lithology and mineralogy is needed before injection of CO_2 is done. Figure 3-2 is a diagrammatic representation of the chemical impacts of CO_2 injection in the formation. They are discussed in details in the sections below.
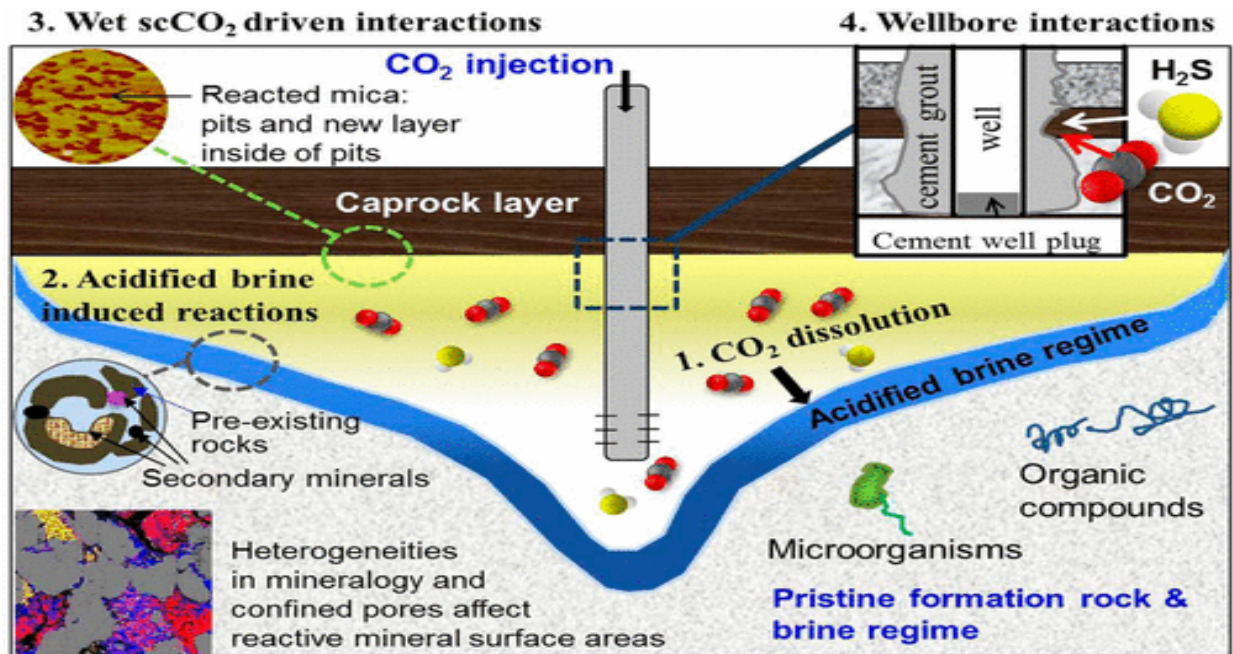
Figure 3-2 Summary of Geochemical Effects of CO2 injection (Jun, Giammar, & Werth, 2013)

3.2.1 Mineral reactions with acid

Once the CO_2 dissolves in water, it breaks the water components and forms carbonate ions by initiating a series of chemical reactions. This is chain of reaction starts by aqueous CO_2 reacting with formation water forming carbonic acid, which dissociates into H+ ions and HCO3- ions. HCO3- ions further break down into CO3- (carbonate) ions. This lowers the pH of the water and further leads to reaction of formation minerals with the carbonic acids and the CO3- ions. These minerals include CaCO3, $MgCO_3$ and $FeCO_3$. These chemical reaction result in changes to the reservoir porosity and permeability. This is of greatest concern for the caprock, as it is an integral part of the containment of the CO_2 gas in the subsurface. Hence, it is vital that these geochemical reactions are well predicted and defined in advanced. Mineral composition of the formation, temperature, pressures, salinity of reservoir fluids, and the pH of the aqueous phase are some of the factors affecting these chemical reactions. These reactions can be divided into two timescales long and short term. The short term effects include the dissolution of CO_2 in water and the formation of carbonic acid and the long term effects include the formation of precipitates after reaction with the carbonic acid. For this thesis, the geochemical effects were not studied due to the limitation of the software used and because of the fact that Norne field model is used that is a sandstone reservoir which is composed of quartz that is relatively unreactive to weak carbonic acid.

3.2.2 Precipitation of salt in the well nearby area (Drying out zone)

Formation damage occurs as a result of drying-induced salt precipitation in the target reservoirs during CO_2 injection operations (Talman, Shokri, Chalaturnyk, & Nickel, 2020). According to the studies by (Lorenz & Muller, 2003) the initial salinity and residual water saturation are critical parameters in depicting the potential for salt induced damage. The mass and the spatial distribution of salts precipitated are controlled by the following factors; the efficiency of brine displacement by the injected CO2, the solubility of water in the CO_2 stream, the water kinetics, capillary forces, salt diffusion down the concentration gradient induced by evaporation and large scale flows associated with gravity override induced by buoyancy of CO2. These factors are responsible for salt precipitation in the previously water wet regions and not directly to the salts formed in the near wellbore regions (Talman, Shokri, Chalaturnyk, & Nickel, 2020). The presence of injected CO_2 and the vaporization of the formation water present in the near well area causes the precipitation of salts and results in a reduced permeability. Since injection of CO_2 is constantly supplied vaporization is an ongoing process and if there is no external source to replace the formation brine along with no movement of water towards the drying out zone, the aqueous phase saturation constantly decreases. This results in an increase in an increase in the concentration of the dissolved salts and leads to precipitation upon further reduction in the brine saturation. The drying out zone can further travel into the formation with more salts being precipitated in area adjacent to the near well area.

The salt precipitation is an issue of concern for CO_2 injection projects as it leads to a reduction in local porosity and negatively impacts the permeability of the storage reservoirs, which in turn cause problems of injectivity. The magnitude of the flow reduction through the pore network is determined by the location of salt precipitates. If they form at the pore throat, the permeability is greatly reduced. The injected CO_2 acts

as the non-wetting phase in depleted gas reservoirs which are considered as water-wet, brine being the wetting phase (ShojaiKaveh, Rudolph, Rossen, Van Hemert, & Wolf, 2013). Due to this, the salt precipitates not only accumulates at the pore throat but also occurs along the whole surface of the grain shown by the laboratory experiments in the studies conducted by (Muller, Qi, Mackie, Pruess, & Martin, 2009). A number of operational problems can occur as a result of salt precipitation which include: (i) Well perforations appear to be partially plugged (ii) scale which is dislodged will fall further, clogging the lower portion of the injection wells and (iii) the falling debris cause any water at the bottom to become saline and highly corrosive.

As mentioned above, capillary forces particularly capillary backflow play an import role in salt precipitation. Capillarity affects the spreading of the liquid saturation profile across the drying fronts. By definition, capillary backflow is a return flow of brine into the dry out zone formed after brine evaporation from a region beyond this zone moving in an opposite direction of the CO_2 stream. (H.Ott, Roels, & Kloe, 2015) This brine backflow is caused by the capillary pressure evolving due to the significant disparity in brine saturation between the dry-out zone, where the saturation is zero, and the higher brine saturation outside the dry-out zone. The backflow is initiated once the pressure front formed due to injection of CO_2 is at a relatively lower value as compared to the capillary pressure gradient. This backflow results in more water being evaporated in the dry out region causing increased salt precipitation and consequently more reduction in permeability and a higher pressure buildup. (Norouzi, Babaei, Han, Kim, & Niasar, 2021)

3.2.3   Formation of Hydrates

At low medium-to-high pressures and low temperatures, guest molecules like CH_4 or CO_2 react with water to form ice-like crystalline substances called gas hydrates. Natural gas hydrate reservoirs found in permafrost-affected and offshore deep-sea sediments are likely targets for CO_2 storage. With the injection of CO2 in methane reservoirs, spontaneous CH4/CO2 exchange occurs caused be the differences in the chemical potentials between each of the hydrates. This exchange is determined by favorable thermodynamics and primarily characterized by the following two stages: a quick reaction on the surface with partial dissociation and then a complete diffusion of guests' molecules penetrating through the formed mixed hydrate layer and deeper into the hydrate crystal (Falenty, Qin, Salamatin, Yang, & Kuhs, 2016). Due to the constant rate transformation process CH_4 hydrate crystals that get exposed to CO_2 reduce in size and even vanish over time. (Pan, Ismail, Luzi-Helbing, Koh, & Schicks, 2020). Nonetheless, during CO_2 injection many different hydrates can be formed where compositions ranging from pure CH_4 to pure CO_2 hydrates. The nearby already present methane hydrates can be dissociated due to the heat released when CO_2 reacts with formation water while forming CO_2 hydrates. As a whole, there are numerous phase transitions occurring while each type of hydrates are being formed. Accurate modelling of CO_2 injection into methane hydrate reservoirs and greater understanding of CH_4/CO_2 exchange process, based on the substantial knowledge of these phenomenon is necessary (Pandey, Strand, Solms, Ersland, & Almenningen, 2021).

Free water interacts with the injected carbon dioxide gas, forming carbon dioxide hydrate and releasing heat resulting in a significant temperature rise. This causes an incomplete conversion of gas into hydrates. At low injection pressures (<=3.5MPa) this effect is insignificant while at higher pressures liquid CO_2 is

present and this phenomenon is observed greatly. Consideration is restricted to the low injection pressures ($\leq$ 3.5 MPa) since at the higher pressures carbon dioxide exists in the liquid state. According to (Tsypkin, 2016) as compared with injection of the gas phase, no significant reservoir heating takes place in the case of injection of liquid carbon dioxide. At the high injection pressures formation of CO_2 hydrate on the front along with the formation of CH_4. At the moderate injection rates only CO_2 hydrate is formed, while at the low rates boiling of liquid CO_2 with formation of the gas phase also occurs. Critical diagrams which illustrate the parameter ranges corresponding to three possible regimes of injection of the liquid phase are given in the Figure 3-3 below. (Tsypkin, 2016)

Hydrates although can be beneficial in terms of CO_2 storage capacity, as large amount of CO_2 can be stored in the form of solids, however, they can cause serious injectivity issues. They directly impact the permeability of the reservoir and therefore can lead to higher pressure buildup in the near wellbore region and beyond. The favorable conditions (High P and low T) of hydrate formation can be provided by Joule Thomson cooling effect. Hence, it is necessary to model the thermal effects along with the chemical effects in order to ensure that the reservoir remains above the hydrate formation region. The JT Thomson cooling and the temperature effects are discussed in detail in the next section of the thesis.
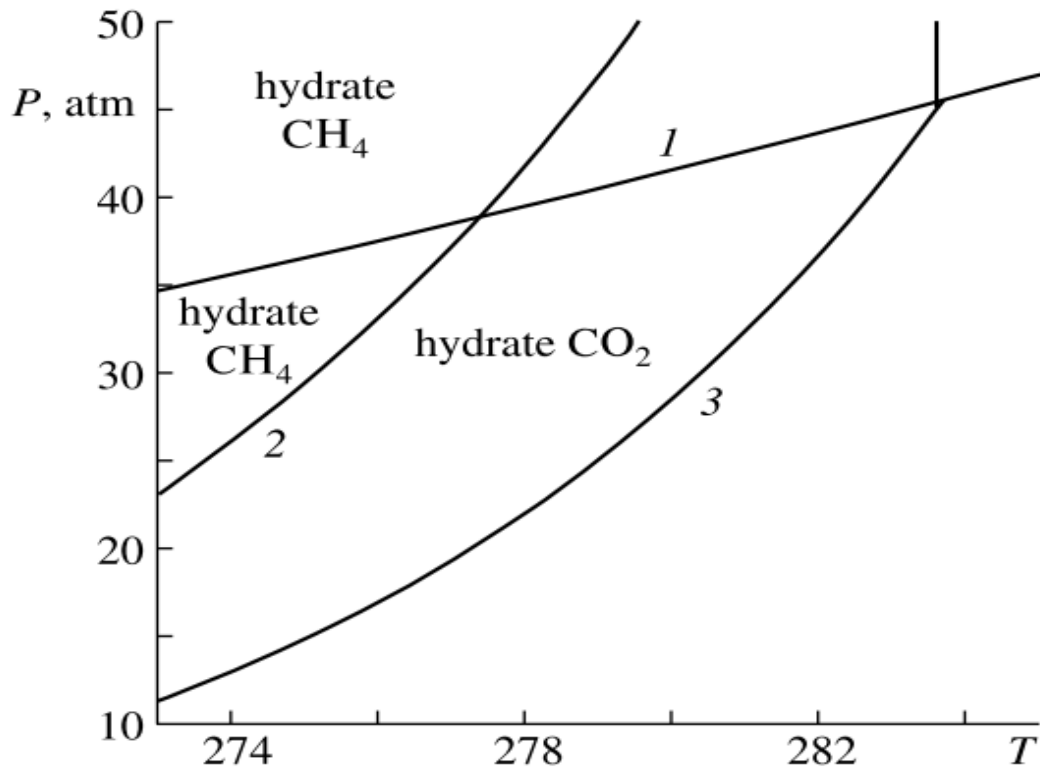
Figure 3-3. Regions of formation of methane hydrate and carbon dioxide in the P&T diagram. Curve 1 is the curve of thermodynamic equilibrium of the liquid and gaseous phases of carbon dioxide and curves 2 and 3 are the curves of dissociation of CH4 and CO2 hydrates respectively. (Tsypkin, 2016)

3.3 Geothermal effects of CO₂ injection

Injection of CO_2 in deep geological formations results in temperature changes caused by processes like JT cooling, endothermic water vaporization, exothermic CO_2 dissolution (mentioned in Section 3.2), resulting in CO_2 reaching the storage formation at a colder temperature than the corresponding geothermal gradient. With the entry of CO_2 into the storage formation, the temperature drops slightly in the near wellbore region as a result of the JT cooling (Vilarrasa & Rutqvist, Thermal effects on geologic carbon storage, 2016) This cooling results in negative impacts on the injectivity of CO_2 injection process as it causes the formation of hydrates that could clog the well and also lead to thermal stresses that impairs the wellbore stability (Jamaloei, 2015). The concept of JT cooling and its effects are explained in detail below.

3.3.1 Joule-Thompson effect

The importance of JT effect in downstream and upstream petroleum industry applications has been studied and discussed in multiple works previously and evaluating this effect in depleting hydrocarbon reservoirs is extremely important (Jamaloei, 2015). Joule-Thomson effect occurs in a dense phase and in gaseous pipelines/ injections wells during the emptying of such mediums. Cold temperatures are generated when pressure of the fluid present inside these mediums decreases or decompression occurs when they are deposited into their respective destinations (James, 2006). This effect usually occurs in real gases such as N_2 or CO_2 and occurs at constant enthalpy. (Oldenburg, 2006). According to the Joule-Thomson expansion experiment, the absence of heat exchange the total work done is equal to the internal energy of the system given by the following equation.

$$w = \Delta U = P_1 V_1 - P_2 V_2$$

For ideal gases, $P_1V_1=P_2V_2$, making JT expansion occur at constant internal energy (Oldenburg, 2006). For real gases such as CO_2, the change in enthalpy is given by $\Delta H = \Delta U + \Delta(PV)$ and substituting these two equations together gives the result of $\Delta H = 0$ making the JT expansion occurring at constant enthalpy. This means that the change in pressure and the corresponding change in temperature would depend on the JT coefficient as ΔT and ΔP are directly related. The plot of ΔT vs ΔP would be a straight line with a linear relationship, with its slope being the JT coefficient. The precise determination of this coefficient and the JT inversion curve is significant to predict the behavior of the injected CO_2 in the geological formation. By definition, the JT inversion curve is the locus of the points at which JT coefficient becomes zero and separates the region of +ve JT from -ve JT. The sign of the JT coefficient determines how the temperature of a real gas changes by isenthalpic expansion. The positive values indicate the cooling of stream under consideration when it passes through an isenthalpic pressure change (Farzaneh-Gord, Rahbari, & Zangeneh, 2020). JT cooling is an intrinsic thermodynamic effect, which depends on the mixture composition and the operational conditions. According to the **Error! Reference source not found.** given below, that Joule-Thomson coefficients are greater at low pressure than at pressures >7 MPa, i.e. about 0.5 K/MPa at 40 °C and 20 MPa and about twenty times higher at the same temperature and a pressure of 5 MPa. This explains why the JT effect will be greatest in cases of CO_2 storage in depleted gas reservoirs with low pressure (André, Azaroual, & Menjoz, 2009).
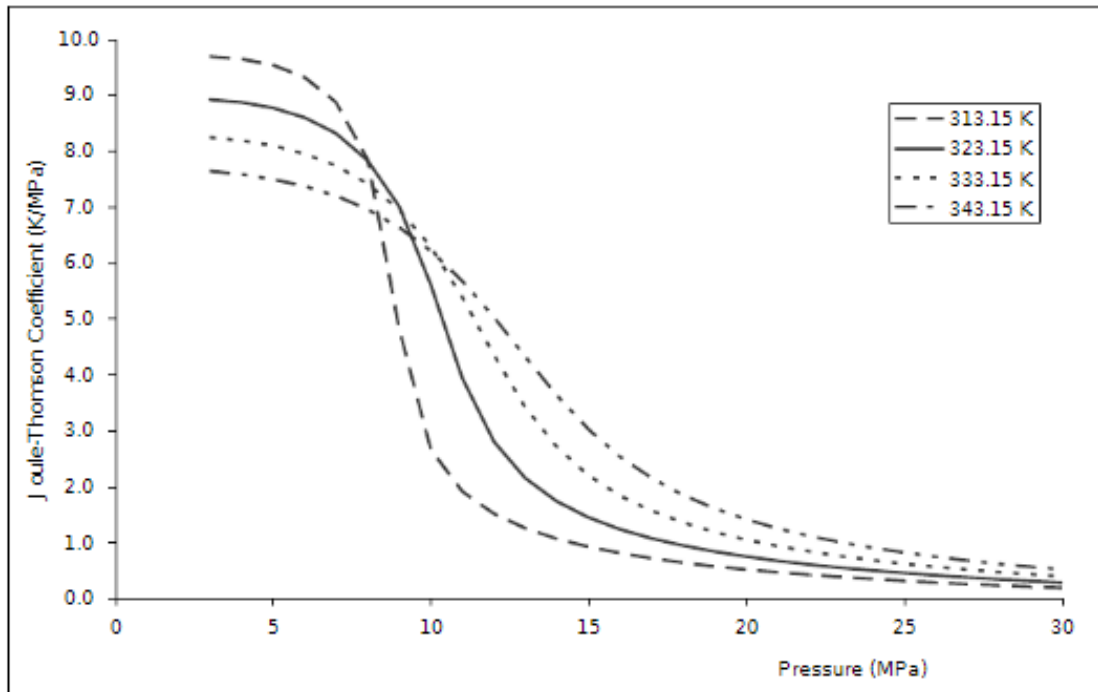
Figure 3-4 JT coefficient for CO2 as a function of P and T (data from NIST webbook) (André, Azaroual, & Menjoz, 2009)

When CO_2 is injected into a geological formation, irrespective of why it is being injected, there will always be a pressure drop from the injection well to the reservoir. This ΔP is dependent on the rate of injection, and how well the reservoir responds to this injection. The pressure drop results in a cooling effect and can cause the formation of induced thermal stresses and ultimately faults. (Oldenburg, 2006) This effect is prominent in scenarios involving high injection rates, with high pressures (100 bars) and is relatively lower in regions with permeability < 200 mD. In regions with lower permeability, pressure drop will be greater ultimately causing a greater JT effect and increases chances of thermal stresses and fractures. Large Joule-Thomson cooling during expansion can cause an alteration in injectivity and formation permeability due to the formation of hydrates, freezing of residual water, and fracturing due to thermal stresses. (Jamaloei, 2015). The total cooling of injected CO_2 is a combination of the magnitude of the pressure differential between the bottom hole and the average reservoir pressure and the Joule Thompson coefficient. Another important concern related to thermal effects in the subsurface due to CO_2 injection is the wellbore instability. It can greatly increase the cost of drilling and completing the wells and even create problems for preexisting wells. The near wellbore rocks are mainly affected by the geochemical, geo-mechanical and the geothermal effects which are discussed in detail previously. Thermal stresses are initiated with the change in well temperatures therefore it is highly advisable to monitor the wellbore conditions during well drilling, completions and injection/production through them. In this study, mostly all simulations are run in an isothermal state and dynamic reservoir modelling is done without the coupling with wellbores.

Overall, these thermal effects need to be properly addressed in the ongoing and planned CO_2 storage projects. Precautions must be taken according to the type of geological formations, PVT properties of the injected and the reservoir fluid, and also the saturations of reservoir fluids.

3.4 General Considerations

This section discusses some of the more general considerations of storage in geologic formation with particular focus on the gas fields. Although depleted gas fields are very popular geological formations chosen for CO_2 storage purpose, key challenges that they bring along are needed to be addressed before they can be made useful to their full potential. In addition to the geo-mechanical, geochemical and the geothermal issues discussed earlier there are certain other generic issues that should be addressed as well.

- o Before injecting CO_2 into a gas reservoir, it is important to understand the pressure response of depletion, whether it is with or without aquifer support. For the latter, the pressure decline will be linear and pressure at abandonment will be extremely low along with a high RF (>90%). In the presence of a strong aquifer, the depletion will be very little and will have lower RF. Both these types of reservoir are suitable for injection. With no aquifer present, there is a big sink into which CO_2 can be injected and with a strong aquifer case, it is evident that as water replenishes easily during hydrocarbon production so it can drive away easily during injection. On the contrary, a weak aquifer support is not ideal for storage. (Hughes, 2009)
- o Density of CO_2 is lower than that of hydrocarbons produced, which makes the pore space to store more CO_2 than the amount that is produced from it, particularly at shallower depths. It is important to find the optimal depth of injection where max volume of CO_2 can be injected in a given pore space. At greater depths (for example >2500m), the P &T of CO_2 can be very large making density closer to that of hydrocarbons and hence reduced storage volume. (Hughes, 2009) In this thesis, as shown in later sections, the reservoir is at a depth above 2700 m making the injected CO_2 well and truly in the supercritical region.
- o For the case of depleted O&G reservoirs, presence of abandoned wells can cause leakage issues. The abandoned wells are old and weak and have been plugged in via older infrastructure making high probability of leakages trough them. Developments in well diagnostics, predominantly in present infrastructure, are compulsory to comprehend leakage risk and mitigation measures (Svalestuen, Park, DePaola, & Powell, 2017).
- o A high residual gas saturation in a reservoir is a problem. This leads to a decrease in storage capacity and injectivity as the hydrocarbon gas mixes with the supercritical CO_2 that reduces its density and viscosity (negatively affecting trapping) and relative permeability of gas is affected due to high residual gas saturation (Raza, et al., 2017) (Lekic, Jukic, Arnaut, & Macenic, 2019).

4   Norne Reservoir

The Norne pilot project is the first benchmark case that has been made publicly available for academic and commercial purposes including the area of integrated operations (i.e. Smart fields, fields of the future, Digital oilfields and the e-fields) that is based on real field data. The available field data is a key benchmark for petroleum industries which has been used to assess and compare mathematical methods for history matching and closed loop reservoir management. This benchmark pilot project was formed with mutual discussions between IO Center, NTNU and Norne field operations (Equinor (formerly Statoil), ENI and Petoro) (Rwechungura, Suwartadi, Dadashpour, Kleppe, & Foss, 2010). The field has been divided into different segments as shown later and for this thesis the E-segment has been used to consider for the purpose of sequestration of CO_2. Working on a real field data instead of a synthetic one gives an opportunity to engage with the most realistic problems and challenges that can be faced while studying different aspects of CO_2 storage. How this field`s fluid properties and some of the grid properties were updated for the purpose of CO_2 storage in a depleted gas reservoir are explained in the Section 6.

4.1   Location, stratigraphy and petrophysical properties

The Norne Field is situated in the blocks 6608/10 and 6508/10 on a horst block between the Vøring and Møre basins as shown in Figure 4-1a , approximately 9 km x 3 km in size, in the southern part of the Nordland II in the Norwegian Sea that is 80 km north of the Heidrun field. (Rwechungura, Suwartadi, Dadashpour, Kleppe, & Foss, 2010). December 1991 was the year of its discovery and the field developmental drilling started in August 1996 and oil production in November 1997. The field contains both oil and gas and they are found in sandstone from the Middle and Early Jurassic age which are subdivided into four different formations from the top to the bottom that include major tectonic faults and diagenetic carbonates, which also tend to avoid pressure communication between reservoir segments and hamper fluid flow. These are: the Garn and Ile formations of the Fangst Group; and the Tofte and Tilje formations of the Båt Group. Figure 4-1b shows this geological arrangement. Burial depth of these sandstones which are affected by diagenetic process is 2500-2700 m, causing a reduction in reservoir quality due to effect of mechanical compaction, however, most of the sandstones are good reservoir rocks. The porosity is in the range of 25-30 percent while permeability varies from 20 to 2500 mD (Rwechungura, Suwartadi, Dadashpour, Kleppe, & Foss, 2010). It consists of two separate oil components, the Norne main structure (C, D and E segment) and the Northeast segment (G segment) of which 98 % of oil in place is situated at the Norne main structure. The distribution of the segments is shown in the Figure 4-2 below. The total hydrocarbon column (based on well 6608/10-2) is 135 m which contains 110 m oil and 25 m gas. Approximately 80% of oil is located at Ile and Tofte formation and gas in the Garn formation. (Rwechungura, Suwartadi, Dadashpour, Kleppe, & Foss, 2010). The Ile and Garn formations are separated by the shaly non-reservoir Not-1 Formation. The Not-1 Formation is a relatively thin layer but acts as an effective seal, hindering the communication between the reservoirs above and below it. The top of the heterolithic Aare Formation is the base of the reservoir and the shaly Not-3 Formation acts as a cap rock (Maleki, Davolio, & Schiozer, 2017). Further details on Norne field stratigraphy are presented in the works of (Swiecicki, Gibbs, Farrow, & Coward, 1998) and (Dalland, Worsely, & Ofstad, 1988) and (Correia & Schiozer, 2016).
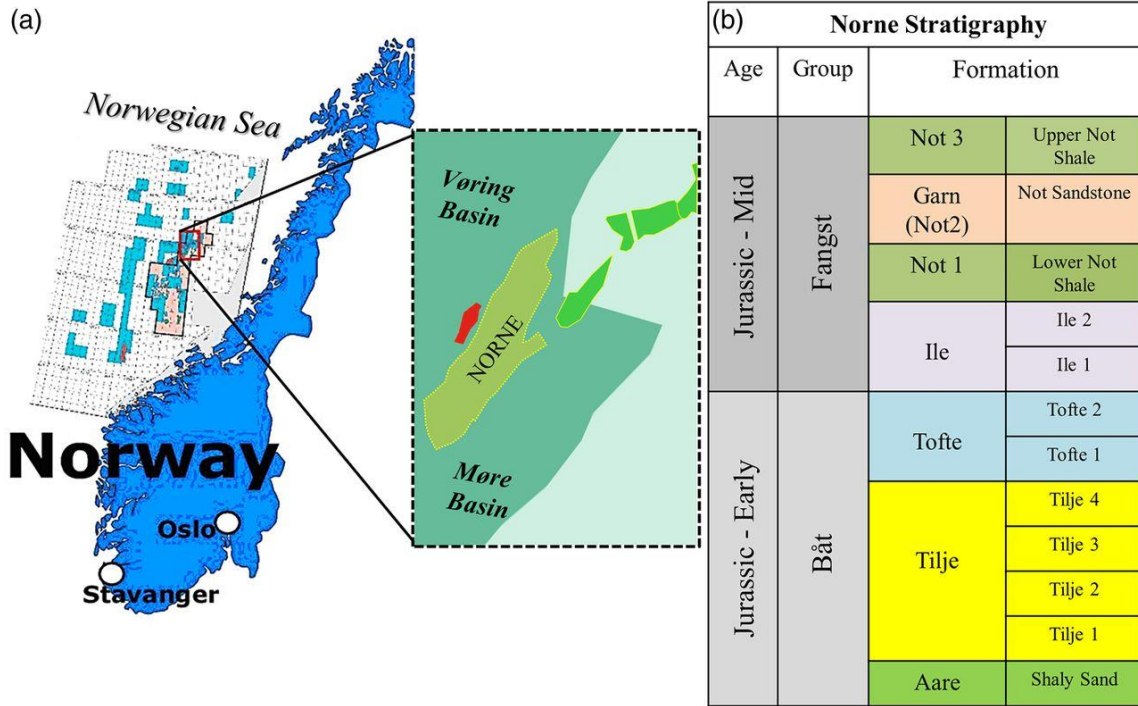
Figure 4-1 (a) Location of the Norne Field in the Norwegian Sea (modified from Huang et al. 2013). (b) Stratigraphy of the Norne field (Maleki, Davolio, & Schiozer, 2017).
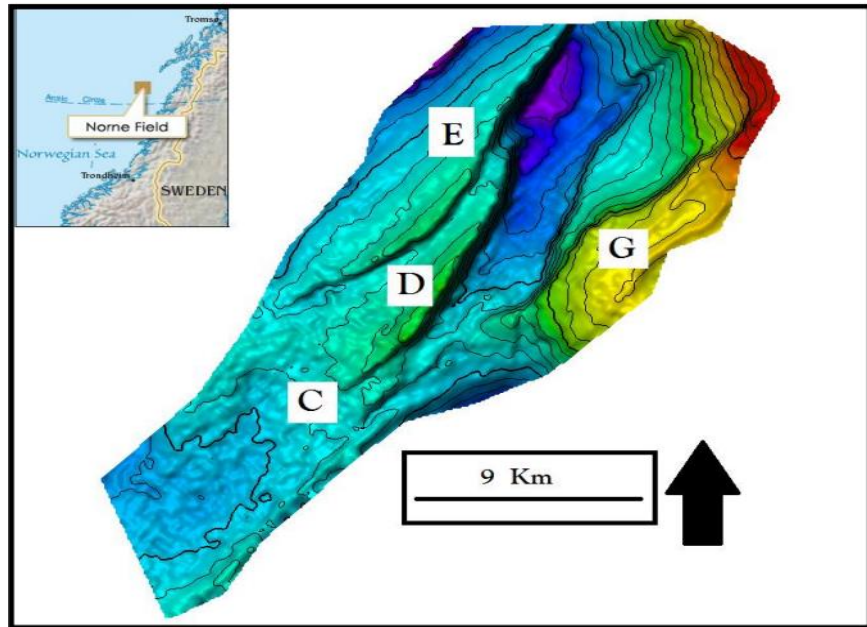
Figure 4-2 Segments of the Norne field (Khan A. , 2014)

At present, the geological model consists of 17 reservoir zones and the current reservoir zonation is slightly changed from earlier subdivisions. A pictorial representation of the zonation from 2001 can be seen in Figure 4-3. The distribution of the average permeability and porosity and permeability can also be seen. Faults, especially major faults, play a significant role in the anisotropic flow of fluids and thus being vital

30

to be modelled correctly in the simulations. Each sub-area of the fault planes are assigned transmissibility multipliers. In the reservoir simulation model, the faults are described by dividing the fault planes into sections which follow the reservoir zonation, and are a function of fault rock permeability, fault zone width, the matrix permeability and the dimensions of grid blocks (Rwechungura, Suwartadi, Dadashpour, Kleppe, & Foss, 2010).

Reservoir Subdivision	Permeability (mD)	Porosity average (%)	Grain size (mm)	Average Thickness (m)
	-		CLYST (<0.002)	
GARN	29		VF-F SST (0.088-0.177)	9
GARN	23		VF-F SST (0.062-0.177)	11
GARN	18		VF SST (0.062-0.125)	11
NOT	-		CLYST (<0.062)	8
ILE	23		VF-F SST (0.088-0.177)	19
ILE	25		F SST (0.125-0.177)	12
ILE	27		F SST (0.125-0.177)	3
TOFTE 4	23		VF-F SST (0.088-0.177)	9
TOFTE 3	28		F SST (0.125-0.177)	29
TOFTE 2	22		VF SST (0.088-0.125)	6
TOFTE 1	24		F-M SST (0.125-0.500)	13
TILJE 4	19		VF-F SST (0.062-0.250)	12
TILJE 3	24		F SST (0.125-0.250)	17
TILJE 2	16		VF-F SST (0.062-0.250)	35
TILJE 1	25		VF-M SST (0.062-0.500)	26
			Total:	224

Legend:
- Channelized sandstones
- Shallow marine, shoreface deposits
- Lower shoreface to offshore transtion
- Cemented horizons
- Tidally influenced deposits
- Bay deposits
- Mouth bars
- Unconformity/sequence boundary

Figure 4-3 Zonation of Norne Field (STATOIL, 2006)

The initial drainage strategy, well locations and the cross-sectional fault structure is depicted in the Figure 4-4. The distribution of the fluid contacts is shown in the Table 4-1 below.

(N.B: The fluid model has been updated for this thesis and it is explained in detail in the Section 6.3 and changed from these contacts!)
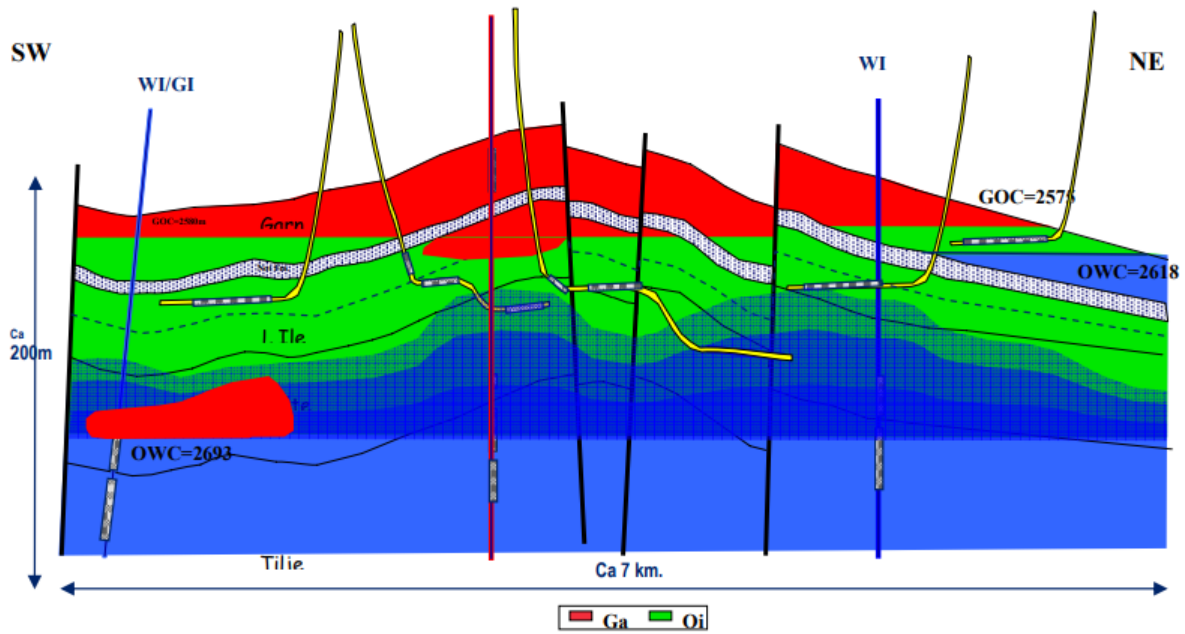
Figure 4-4 NE-SW running structural cross section of the Norne Field with initial depths of fluid contacts, and drainage strategy until the year 2006 (STATOIL, 2006).

Table 4-1 Original fluid contacts of the Norne field in meters (STATOIL, 2006).

Formation	C-segment		D-segment		E-segment		G-segment	
	OWC	GOC	OWC	GOC	OWC	GOC	OWC	GOC
Garn	2692	2582	2692	2582	2618	2582	2585	No gas cap
Ile	2693	2585	2693	2585	2693	2585	Water filled	Water filled
Tofte	2693	2585	2693	2585	2693	2585	Water filled	Water filled
Tilje	2693	2585	2693	2585	2693	2585	Water filled	Water filled

4.2 Historical production

As mentioned previously, Norne is a field in the Norwegian Sea, 80 kilometers north of the Heidrun field with a water depth of 380 meters. The field has been developed with a production, storage and offloading vessel (FPSO), connected to seven subsea templates. Production started in 1997. An amended PDO for several deposits in the area around the Norne and Urd fields was approved in 2008. The Alve, Urd, Skuld and Marulk fields are tied-back to the Norne FPSO as shown in Figure 4-5. According to the NPD, the current resource estimates are presented in the Table 4-2. In addition to this, the yearly production from this field is given in Figure 4-6. The field has been an oil producer from the start of the production reaching its maximum oil production in the year 2001 of about 11.25E06 Sm^3. After the early years of production, gas has once again been produced in a larger amount ($\pm$ 0.8E06 Sm^3 o.e) in recent years of 2019 and 2020. The field therefore has considerable potential based on its volumetric capacity to be considered for CO_2 storage in the years to come.
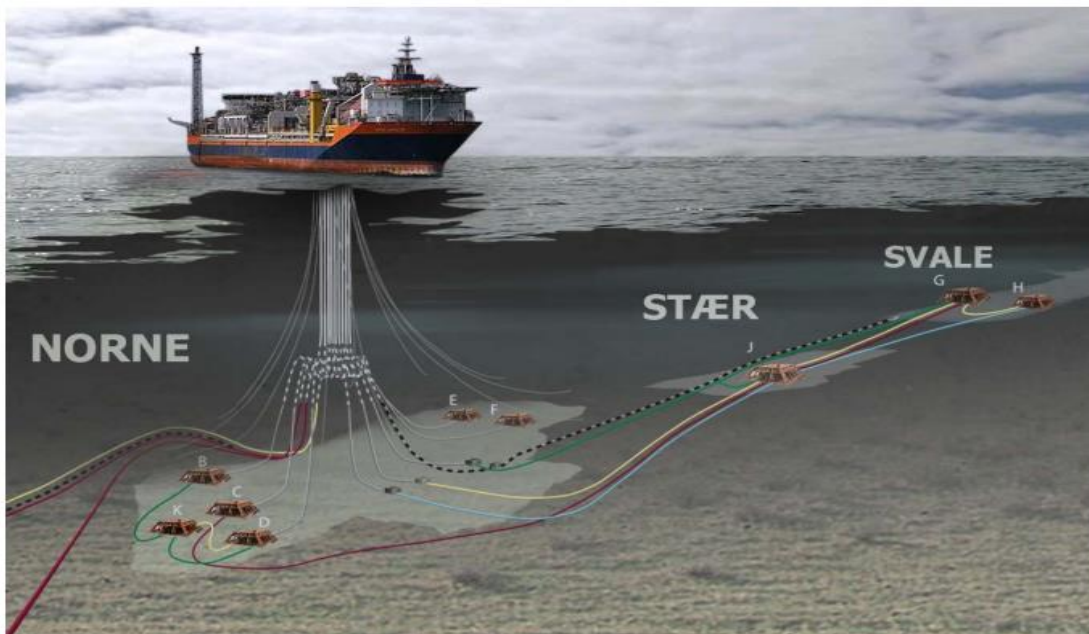
Figure 4-5 Norne FPSO (STATOIL, 2006)

Table 4-2 Total reserves of Norne (NPD, Norne Field, 2022)

NPD`s CURRENT RESOURCE ESTIMATES					
All numbers in million Sm3 o.e					
	Oil	Gas	NGL	Condensate	Sum
Recoverable reserves originally	95.2	12.9	3.1	0	111.1
Remaining reserves	3	3.2	0.8	0	7
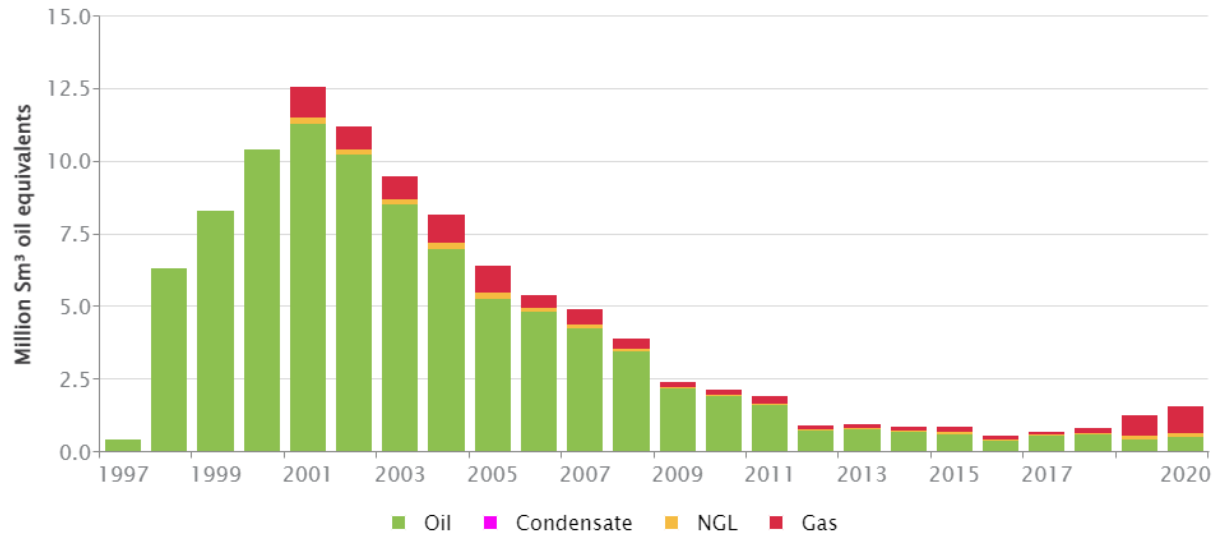
Figure 4-6 Historical hydrocarbon production from Norne field, (NPD, 2022)

5   Numerical Reservoir Modelling

Experimentation and careful monitoring of the sequestration sites is used to understand the geological storage of CO_2. Analytical and numerical approaches are useful for predicting CO_2 migration or dispersion. Although analytical and/or semi analytical solutions of CO_2 sequestration in reservoirs can be helpful, but because they are based on simplifications, they are considered to be limited in their applicability. Simulations that use physical modelling techniques and numerical solution of the governing equations can be proven as the only reliable way to address the processes related to carbon storage and its long term containment in the subsurface environment. Simulating CO_2 flow behavior in these geological formations is not an easy task as it depends on a number of physical factors including probable phase change, composition, reservoir heterogeneity and computational demand these factors bring along. According to a previous benchmark study, (Class, et al., 2009), comparing different mathematical and numerical models applied to particular problems for various aspects of CO_2 storage, numerical performances varied considerably for each scenario depending on differing processes like advective multi-phase flow, compositional effects due to dissolution of CO_2 into the ambient brine and non-isothermal effects due to temperature gradients. As a conclusion, this study explained the need of research in the crucial field of improving the numerical performances by optimizing discretization methods, solvers and parallelization methods (Jiang X. , 2011).

Modelling and simulations can predict where the CO_2 is likely to flow, its volume and spatial distribution and is beneficial for optimizing CO_2 injection operations. The CO_2 sequestration is dependent upon on flow and transport phenomenon in porous media occurring at different time and space. As an example, transport phenomenon like species` diffusion and viscous fingering occurs at a relatively small scale of time and space, while CO_2 storage can be extended to hundreds of kilometers and years. Hence, computational fluid dynamics (CFD) is not a viable option for modelling and simulating the CO_2 storage processes due to their increased lengths in time and space and especially because they require grid dimensions to be made adequately fine to begin to resolve the coupling between flow and phase behavior (Jiang X. , 2011). The following sections cover the theoretical modelling of flow and transport in carbon storage and the respective governing equations. Additionally, numerical methods used in simulations of CO_2 storage is also highlighted.

5.1   Theoretical modelling and governing equations for CO_2 storage

As explained in the Section 2.3.3, there are different trapping mechanisms to store CO_2 underground based on the properties of CO_2 at different P and T and at standard conditions CO_2 is a gas with a density higher than air. For CO_2 storage explained in section 2.7, T and P are above the critical conditions making the CO_2 supercritical fluid. This causes CO_2 to attain a liquid like density and gas like viscosity. In most cases however, injected CO_2 is buoyant and lies on top of water. Other than this, its solubility in water decreases with increasing temperature and water salinity, and converse is true with an increase in pressure. As explained previously, after CO_2 is injected, it is hydro-dynamically trapped (physical structural trapping) and with time due to secondary trapping mechanisms like residual trapping, mineralization and dissolution trapping (long term) more CO_2 is secured and leakage risks are avoided (Jiang X. , 2011). Since geologic

storage of CO_2 is a complex physicochemical process involving flow and transport phenomenon in porous media, primary and secondary trapping mechanisms must be addressed via a theoretical description that includes all the physical and chemical reactions. Furthermore, relevant reservoir rock properties and CO_2 properties must be included in the theoretical approach. Theoretical modelling and numerical simulation of CO_2 storage is challenging due to the unusually long time scale and the large spatial scale it involves. Some of the descriptions of these theories and numerical approaches are given in the following sub-sections.

5.1.1 Modelling of physical process and the governing equations

Flow in porous media is defined by the most famous Darcy`s law, that is a constitutive equation describing the physics of this flow. It was derived by Henry Darcy and initial results were based on experimental evaluation of flow of water through sand beds. The equation in a vector form can be defined as:

$$q = \frac{k}{\mu}(\nabla p - \rho g)$$

Where,

q is a vector quantity in a 3D coordinate system representing discharge per unit area, with the unit of velocity. The permeability tensor **k** signifies the ability of the medium to transmit fluids through the pore spaces, ∇p represents the pressure change, ρ is the fluid density and g is the gravitational field acceleration. The pore (interstitial) velocity through the porosity $\emptyset$ of the medium is given by:

$$v = \frac{q}{\emptyset}$$

Additionally, the effects of permeability in the three dimensions can be accounted for in the symmetric tensor o permeability given as:

$$\begin{Bmatrix} k_{xx} & k_{xy} & k_{xz} \\ k_{yx} & k_{yy} & k_{yz} \\ k_{zx} & k_{zy} & k_{zz} \end{Bmatrix} \text{ and } k_{ij} = k_{ji}$$

The validity of this law is for steady state, slow viscous flow. For the carbon storage process, Darcy`s law is applicable as a simple multiphase add-on of the Darcy`s law. In carbon storage different phases like brine, carbon and solid are present, which leads to replacing the absolute permeability with phase permeability. Additionally, relative permeability i.e. flow of a fluid in the presence of other fluids, accounts for a reduced flow of each phase that is caused by mutual interaction of the different flowing phases. The multiphase extended version of the Darcy`s law where z-direction is +ve upwards can be given as:

$$v_\propto = \frac{q_\propto}{\emptyset} = \frac{kk_\propto}{\mu_\propto \emptyset}(\nabla p_\propto + \rho_\propto g \nabla z)$$

In addition to the Darcy`s equation, it is significant to define the equation of mass conservation for each component of the fluid present for the description of geological carbon storage as is done for oil, water and gas flows through reservoirs. This is given as:

$$\frac{\partial}{\partial t}\left[\emptyset \sum_{\alpha}(\rho_\alpha S_\alpha X_i)\right] + \sum_{\alpha}\nabla \cdot (\rho_\alpha q_\alpha X_i) - \sum_{\alpha}\nabla \cdot (\emptyset S_\alpha \tau_\alpha D_\alpha \rho_\alpha q_\alpha \nabla X_i) = S_i$$

For the purpose CO_2 sequestration, the flow has to be modelled as a multiphase and a multicomponent (like CO_2, water, hydrocarbons etc.) system. These components can differ depending on the type of storage systems. The above equation of conservation of mass represents how four mass transfer mechanisms including: the time derivative of mass at a fixed point (or the local derivative or storage term), convective and diffusive transports, and source/sink term of mass respectively are balanced. τ, i.e. tortuosity represents the ratio of the diffusivity in free space to that in the porous medium and S_i is the source/sink term which is present due to the geo-chemical reactions (Jiang X. , 2011).

Additionally, there is an energy balance as well that is based on the time derivative of change of energy in the fluid phases in the formation matrix, convection/advection, conduction and also the possible source or sink terms of energy. Formally, the energy conservation equation is:

$$\frac{\partial}{\partial t}\left[\emptyset \sum_{\alpha}(\rho_\alpha S_\alpha U_\alpha) + (1-\emptyset)\rho_s C_s T\right] + \sum_{\alpha}\nabla \cdot (\rho_\alpha q_\alpha H_\alpha) - \sum_{\alpha}\nabla \cdot (\lambda \nabla T) -- = S_H$$

Here, U_α is the specific internal energy, H_α is the specific enthalpy, T is the temperature is the specific heat capacity. Subscript s represents the solid phase. The energy transport due to species diffusion has been omitted in this energy conservation equation. Moreover, this equation is further simplified by ignoring the dissipative effects such as work done by the viscous forces and the heat transport by the molecular diffusion of the species. As the flow velocities are small, the assumption of local thermal equilibrium is valid. The source/sink term here can be linked to the possible geochemical reactions as was the case in mass conservation equation.

All the above equations, for the multiphase flows in porous media for CO_2 storage, work simultaneously as the governing equations for the numerical simulations. These include the geo-mechanical effects such as the permeability and porosity of the rock matrix, fluid properties, like density and viscosity, in multiphase and even geochemical reactions that govern the flow and transport behavior. The equations supplied must be in harmony of constitutive relationship and supplementary constraints for fluid saturations, compositions of components and pressures. Fluid saturations for the empty space in a reservoir rock is given by:

$$\sum_{\alpha} S_\alpha = 1$$

And for two phases the difference in their pressures is given by:

$$P_\alpha = P_\beta - P_{c,\alpha,\beta}$$

Here, $P_{c,\alpha,\beta}$ is the capillary pressure as a function of saturation. As a matter of fact, in addition to these fundamental equations, there can be additional auxiliary equations that depend on the complexity of the system mainly determined by the number of phases involved and the components of interest (Jiang X. , 2011).

5.1.2   Limitations, uncertainties and issues for investigation of modelling

As explained previously, CO_2 flow and transport behavior in a geological storage medium is not simple and involves physiochemical processes and therefore requiring the mathematical models to take fully into considerations these processes. As an example, the hydraulics of the fluid flow of CO_2 dispersion is greatly impacted by physical properties, like permeability and porosity, of the porous media. Capillary pressure curves and the relative permeability as a function of saturations that indicate the interactions between the fluids of interest and the reservoir need to be defined by constitutive relationships. The figure below summarizes the sub-processes need to be considered for modelling of CO_2 storage. Out of various model inputs, the most underdeveloped area is of kinetic modelling mainly due to the excessively long durations of some reactions, for e.g. mineral carbonation. Input parameters also play major role in each of type of simulations, as an example; for a short term injection project, geochemical reactions will be less important as compared to the one that is long term. Thus, each process leads to the complexity in mathematical problems that involve coupled non-linear PDEs which are difficult to be solved analytically. In addition to these numerical issues, certain boundaries and uncertainties concerning these mathematical formulations can also arise (Jiang X. , 2011).

Momentum balance based on multiphase extension of Darcy`s law can be one of the main limitation of the numerical formulations. As a matter of fact, continuum approximation, a superposition of several continua, according to which each of it filling the whole medium forms the porous medium. This is used in general studies of multiphase flows at greater speeds in non-porous media for different applications (Crowe, 2006) (Jiang X. , 2011). For flows in porous media, one of the key factors of continuum approximation explained above is simply an extension of the Darcy`s equation. The Navier-Stokes momentum equations and the conservation of momentum equations are replaced by Darcy law at the macroscopic level. In addition to this, although, an extension of Darcy`s law has been used on multiphase systems, it is has its own limitations. During active injection of CO_2, it is not completely correct to assume a steady state flow. The flow, in such cases, may be unsteady with comparatively high speeds thereby challenging Darcy`s law`s validity. With all the limitations of the Darcy`s law, it is still widely acceptable in petroleum engineering and hydrogeology and its multiphase extension can be considered as more of a working approach than a fundamental physical law. Generally, numerical formulations depend greatly on the validity of continuum approximation, applicability of Darcy`s equation along with its extension to multiphase flow and also the correct models for the relative permeability (Jiang X. , 2011).

Furthermore, as discussed earlier, broad times and lengths scales are critical aspects of consideration while dealing with CO_2 storage and one way to deal with such large scales differences is a multi-scale approach. CO_2 dispersion using multi-scale modelling provides accurate prediction with minimal computational costs therefore making it a feasible option. Modelling of complex multiphase, multi-species heterogeneous systems while taking into consideration the locally occurring processes is the requirement of multi-scale modelling. Coarser grids containing various fine-scale elements are used to deal with macroscales. Upscaling of grids is done to apply the governing equations on such coarser grids (Niessner & Helmig, 2006). This would make the variables merge into the coarse-grid mean values and local fluctuating part, similar to the way filtrations of large-eddy simulations of CFD occur. These up-scales equations are solved on the coarse mesh, on the other hand, the fine-scales processes are only regarded in a relatively small domain of interest. Although such approaches have been proposed, yet, this area is open for more research and development (Jiang X. , 2011).
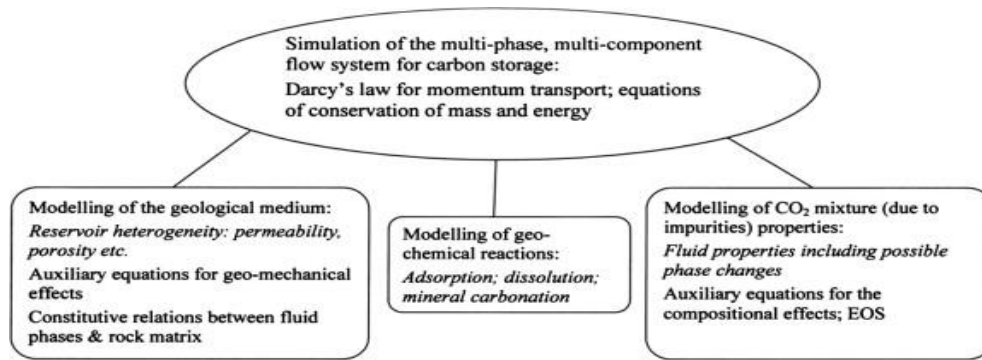
Figure 5-1 Summary of simulation types

5.2   Methods and Challenges of Numerical Simulations

For carbon sequestration in a geological media, the governing equations involved, are some of the coupled, non-linear, PDEs that include the 1st and 2nd order, temporal and spatial derivatives. Analytical solutions are not always applicable in many cases, thereby making numerical solutions based on discretization of the computational domain and the related equations a requirement. The discretization in time and space and numerical treatment of non-linearity are significant considerations for computations. In particular, accuracy, stability and computational speed are the primary concerns in discretization and numerical solution which are both significant for both temporal and spatial discretization, and integration. Most of the simulators developed for this purpose have a range of application ability of modelling that base on various methods of discretization and ultimately producing different levels of numerical accuracies (Jiang X. , 2011). Many software, either commercial or academic are available for the purpose of carbon storage and reservoir management, in the following section and overview is provided, and a detailed discussion of Schlumberger`s Eclipse is given in the later section separately as it has been used for this thesis.

5.2.1   Overview of simulators used

The governing equations explained in the previous sections, are translated into a finite form, making them applicable for computational handling and analysis use the simulation codes that depend on the type of numerical methods are used. These methods include, finite difference, finite element and finite volume method. All of these have been used ubiquitously in different simulators used for this purpose. The number of fluid phases, the number of components, and also the discretization methods used determine the complexity of the simulators. As part of the thesis, numerical simulation was needed to see how a reservoir model would behave according to the changes made in its input data. Currently, there are many available simulation tools in the market like CMG, ResInsight, TOUGH, Schlumberger`s Eclipse software etc., for this work, the latter were used.

Some of the most commonly used software, their main applications and the methods employed for discretization/integration are given in a tabulated form in the **Appendix C**. Each of the software has its own strength and weakness and is used mainly according to the purpose it serves.

The performance of the simulators is greatly influenced by the numerical methods used. One benefit of using the finite difference method, that reduces the solutions to differential equations by replacing derivative expressions with almost equal difference quotients, is that it can attain high order of accuracy without using over complex formulations. Taylor series expansions are also used to establish these finite difference solutions. On the contrary, finite volume method is dependent on the integral form of the governing equation in which the divergence terms are converted to integrals of the surface which are then evaluated as fluxes at the surface of each control volume. For complex geometries unstructured meshes, these can be conveniently formulated. The FEM is appropriate for solving PDEs over complex domains, which acts as an advantage for CO_2 storage simulations that involve a change of phase during fluid migration. In this method, the PDE are translated into an approximating system of ODEs, which are numerically integrated using techniques like Euler`s methods and Runge-Kutta method. Detailed explanation, numerical algorithms and standard numerical techniques are available in studies such as (Teukolsky, Vetterling, & Flannery, 2007) (Jiang X. , 2011).

5.2.2 Numerical issues for investigation and challenges

Numerical simulations of CO_2 are dependent on the suitability of the numerical and physical methods used. The order of truncation and the discretization schemes of the schemes determine the numerical accuracy. Generally, lower-order discretization schemes use fewer grid or mesh points in space and less data points in time, therefore requiring less computing resource and ultimately less time of computation in comparison to higher order schemes. In advanced numerical simulations like those of direct and large-eddy simulations of turbulent flows in the context of CFD, it is widely agreed that high-order numerical schemes should be used. Although studies on numerical simulations of CO_2 dispersion under geological storage conditions do exist, as of now, common understanding of the behavior of numerical algorithms for these simulations covering a broad range of scales is not available. Direct and large-eddy simulations (Jiang & Lai, Numerical techniques for direct and large-eddy simulations, 2009) (Jiang & Luo, 2001) and computational aeroacoustics involving modern high-order numerical schemes, is not available in the current studies of CO_2 flow and distribution (Jiang X. , 2011).

The error in the functional approximation reduces faster with the grid spacing in the higher-order scheme as compared to the lower-order scheme as the error is proportional to h^n for a nth order accurate numerical scheme. h has to be a minute quantity to ensure sufficient resolution occurs when considering local transport calculations. During practical simulations, complexity of the method and the grid resolution determine the computing time. Also, for simulation, when accuracy is crucially required and a small truncation error is targeted, inducting the application of high-order schemes gives access to a coarser mesh compared to lower-order schemes which may need extremely fine mesh to obtain the same accuracy. The computing costs may be lessened by inducting high-order numerical schemes relative to employing lower-order numerical schemes, given that the former are not overly complex in formation and can be well implemented (Jiang X. , 2011). In numerical simulations of geological carbon storage, higher-order finite difference schemes including the compact schemes (Sanjiva, 1992) , (Nicoud, 2000), (Desjardins, Blanquart, Balarac, & Pitsch, 2008) may be applicable. On the other hand, large numerical diffusion, which deteriorates the simulation accuracy, occurs as a result of the use of first-order up-winding scheme in the existing simulator.

Coupling of complex numerical methods and physical modelling occurs in numerical simulation of CO2 injection and storage. This process involves the multi-phase and multi-component system, requiring

efficient numerical algorithms to solve the large number of governing equations. Some of the challenges include, fluid phase front capturing and the handling of discontinuities in pressure across phase interface because of the capillary effects. An evaluation of streamline based simulation against a grid based simulation must also be performed. The different scales in the numerical scheme can be included directly when modelling phenomena of flow and transport on different scales. At present, these techniques rely heavily on simulators operated by the petroleum industry and it is important to achieve numerical accuracy in predicting the CO2 flow and transport behavior in the subsurface environment (Jiang X. , 2011).

5.3   Schlumberger`s Eclipse 2021

Eclipse is a powerful simulator used all across the globe for performing reservoir simulations for commercial as well as educational purposes. It offers a strong set of numerical solutions for quick and accurate prediction of dynamic behavior for many different types of reservoirs and their developments. It is one of the most powerful and popular software used for this purpose for the past 25 years and is well-known for its capabilities in all dynamics of reservoir simulation including black oil, compositional, thermal, finite-volume, and streamline simulation with add-on options like local grid refinement, coalbed methane, gas field operations, advanced wells, reservoir coupling, which makes it extremely beneficial (Khan N. A., 2021).

For this study, **Eclipse 300 (E300)** which is a compositional simulation software was used and its license was provided by Department of Geoscience and Petroleum at NTNU. Compositional simulation enables the user to simulate compositional models, where PVT properties of oil and gas phases are fitted to an equation of state (EOS), as a mixture of components. This is more common for modelling for reservoirs having gas, gas condensates, volatile oils and injection targets involving gas. Since, for this thesis the injection of CO_2 into a depleted gas reservoir model had to be done, E300 was the main choice. Black oil modelling on the other hand, deals with components as three phases only (oil, gas and water) and does not take into to account the distributions of components (molar %) present in the reservoir or the injection fluid. Even in the presence of many heavier or light components of hydrocarbons ranging from C1 to C10+ or more, the black oil model treats them as a single phase of gas or oil, therefore, the EOS is not applicable. Furthermore, the flow equations given in the Section 5.1.1, employ either of the three different methods of solving that are: Fully implicit, Implicit Pressure and Explicit Saturation (IMPES) and Adaptive Implicit Method (AIM). The first of the three respectively solves the pressure and saturation unknowns implicitly and finds the unknowns at the net time step using the Newton`s method for finding solutions after some iterations. This option is more stable for large time steps and is computationally time consuming. On the contrary, IMPES method solves pressure implicitly at the upcoming time step and while the saturations is explicitly updated in the next time step as well. The third option lets simulators solve the flow equations as the combination of the other two where it has the leverage of to utilize both methods depending on the complexity of the region for which the simulation is being run (Marashi, 2021). For CO_2 injection and its simulation, Eclipse uses different KEYWORDs like CO2SOL, CO2STORE, GASWAT and COAL for simulating in oil reservoirs, saline aquifers, gas reservoirs and depleted gas reservoirs respectively. The details of which option has been used is given in Section 6.1. The E300 incorporates four EOSs. The Schlumberger`s technical description manual, (Schlumberger, 2021) gives a detailed account of the EOSs

employed, and how the fluid and rock properties (saturations, relative permeability, rock compaction etc.) are calculated and handled during simulation runs. The following four are the EOSs that eclipse utilizes.

(I) PR: Peng-Robinson

(II) RK: Redlich-Kwong

(III) SRK: Soave-Redlich-Kwong

(IV) ZJ: Zudkevitch-Joffe-Redlich-Kwong.

Eclipse requires a generation of a .DATA file which was done using NOTEPAD++ which gave an easy to use workspace and made the process of creating .DATA files much smoother. They contain a set of keywords and has eight sections in total that act as input for performing simulation based on petrophysical data, fluid properties, initialization and length of the simulation runs. The main sections of the data file are summarized in the table below It is discussed in the methodology section of the report about which EOS, the methods of solving flow equations and other relevant details of the DATA file are used for this thesis. In addition to Petrel, Floviz 2021 had also been used to view some of the dynamic and static properties of the simulation model.

Table 5-1 Summary of DATA file structure in Eclipse

Section Function	Section Function
RUNSPEC	The overall basics of the simulation; title, unit system, phases present, definition of E100 or E300 run, start date, simulation grid dimensions
GRID	Grid dimensions and shape, reservoir petrophysical properties like porosity, permeability, fault etc.
EDIT (Optional)	Altering of grid structure defined in GRID section
PROPS	Fluid and rock properties; PVT data, relative permeability and saturation function tables.
REGIONS (Optional)	Defining different regions in the reservoir
SOLUTION	Data for equilibration and initialization of the model
SUMMARY (Optional)	Definition of the results that are needed to be obtained from runs
SCHEDULE	Definitions of well types, operations and time of the runs.

5.4   Schlumberger`s Petrel 2021

The user environment for the ECLIPSE family of simulators is Petrel Reservoir Engineering, Petrel is a user friendly software which aids in obtaining simulation results as graphs and visualize the static and dynamic properties of the models in a unified work flow environment. The Petrel platform gathers data from multiple disciplines, allowing experts to combine their knowledge in a single environment. And here the DATA file from Eclipse was imported and simulation was run on it to visualize the results. Petrel comes with multiple options of viewing the 2D and 3D grid blocks of the reservoir along with the graphical results according to the property to be analyzed, timescale and for making comparisons within different cases. It is shown in the methodology and results and discussion part, how this software was put to use. Figure 5-2 shows an open window of Petrel workspace with the model visualized in 3D. The panel on the left has toggle on/off options where each static and dynamic property of the model can be visualized. One additional striking feature of this software is to view animations of any chosen property for the entire simulation period (Khan N. A., 2021). In addition to this ResInsight software is also used to visualize results.
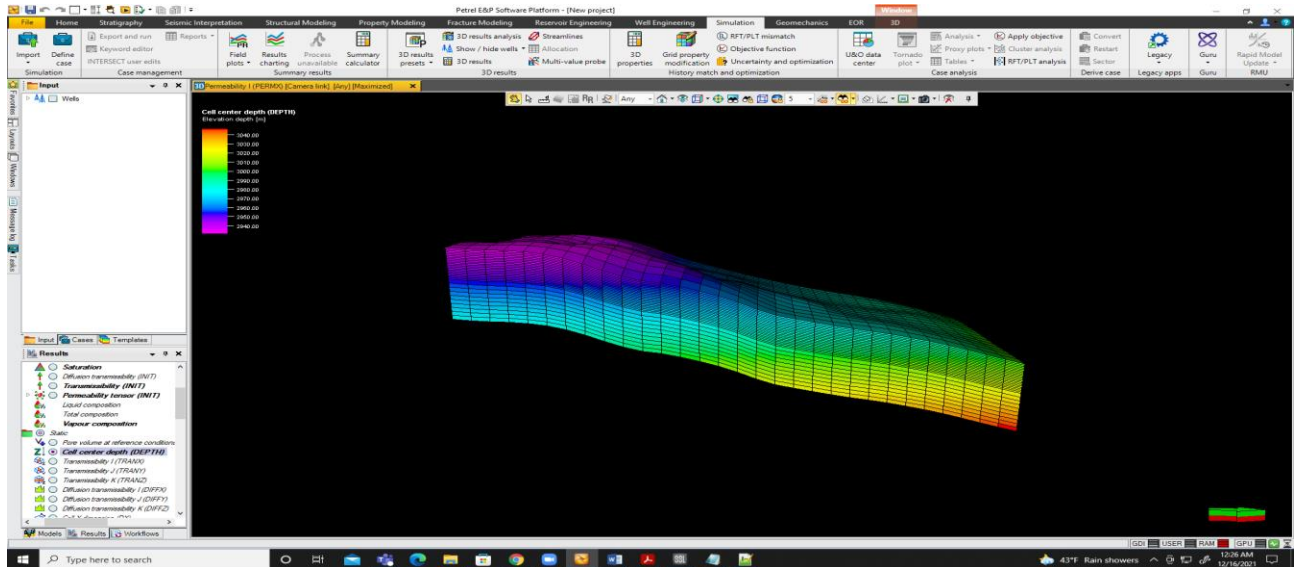
Figure 5-2 Petrel Working window

6 Methodology Used and Model Description

As mentioned previously Norne model (E-segment) was used to work on for the purpose of injection of CO_2 and modelling the short and long term effects of it by varying different input parameters like reservoir heterogeneities, initial water saturation, injection rates, salinity of reservoir, reservoir temperature, fluid contact, fluid types and aquifer presence/absence, and finally visualizing the results. For the base case, using two vertical wells, hydrocarbon gas was first produced for a period of 15 years and then using the same wells pure CO_2 was injected into the reservoir for a period of 15 years (180 months) at an injection rate of 100000 Sm3/day/well and then the wells were shut in. The simulation was run for the period of about 200 years starting from 1997. Simulations involving injection and storage scenarios, are usually run for longer periods of time to monitor the CO_2 plumes and to note if there are any problems related to storage like leakages, and/or petrophysical changes in the geological formation. This also helps in examining the redistribution of fluid saturations and compositions as well as reservoir pressure variation. The same was modelled for the base case, as well as for all the sensitivities, however modelling for any induced geo-mechanical and geochemical effects or thermal runs were beyond of the scope of this thesis. Before the reservoir initial properties (static) can be discussed, what methodology/approach was taken has to be defined initially. Norne benchmark DATA file that was based on a black oil simulation of hydrocarbon production, however for these simulations, DATA file was converted into a compositional run for CO_2 injection in a depleted gas field. All the necessary changes made and the steps taken are discussed and explained in the following sections.

6.1 Modelling approach

A compositional simulation option using Eclipse is chosen for the purpose of CO_2 injection into a depleted gas reservoir model. The aim of the study is to observe how CO_2 gets trapped in the geologic reservoir and how does it behave in the long term. According to the Schlumberger`s technical description manual and as explained in previously in section 5.4 , CO_2 storage can be activated in Eclipse by using either CO2SOL, CO2STORE, GASWAT and COAL option depending on the type of reservoir studied. For this case, a depleted gas reservoir, GASWAT and CO2SOL option is used. Sensitivity analysis based on various petrophysical parameters, fluid properties and initializations is performed using the keyword CO2SOL only and a comparison of the base case using these two different options is also provided. The total injected CO_2, total stored CO_2, and dominant trapping mechanisms and the pressure buildup against time are predicted through this modeling.

6.1.1 GASWAT option

It is capable of solving the gas and brine phases equilibrium based on the adaptive implicit approach. It uses a modified Peng Robinson EOS to model the phase equilibriums and allows the multi-component gas phases. CO2 N2, and H2S solubility in water are treated with the Peng Robinson equation of state (EOS) modified by Soreide and Whitson. However, solubility of other gases like methane are treated by the original Peng Robinson EOS by default. "GASWAT option" provides a thorough description of this feature. Molecular diffusion between gases can be modeled using the DIFFUSE option.

The GASWAT option is two-phase only and by using it the phases of water and gases are implicitly requested and oil phase cannot be modelled. Additionally, with depth the reservoir temperature may vary and this is highlighted in EOS treatment, where coefficients of temperature are stored to get combined with

the temperature of each cell. Salinity value is added globally to correct the default EOS modifications for brine concentration. It is possible to equilibrate the reservoir with a single phase and present or with an initial gas water contact. For the case of initial gas water contact, the condition that at the contact, the two phases are in equilibrium is abided. The composition is of either of the phases is specified and the software calculates the composition of the other from the equilibrium state. The determination of the single phase as gas or water is defined by a simplified criteria called as the Li criteria, given by the equation below. It states that if the temperature is less than the pseudo critical temperature and the phase mostly contains H2O component then the phase is regarded as water otherwise gas (Schlumberger, 2021).

$$T_{mix,crit} = \frac{\sum_j T_{cj} \cdot V_{cj} z_j}{\sum_j V_{cj} z_j}$$

For single phase cells in which the bubble or dew point fluids is not present, the critical temperature found using this equation is compared with the temperature of the reservoir and it is established whether it is an oil or a gas. Formulations concerning the EOS modifications, flash calculations and viscosity evaluation are given in the Technical description manual of Eclipse (Schlumberger, 2021) . Next up, the modifications made in the various sections of the DATA file, based on fluid properties, initializations, grid properties are given.

DATA FILE STRUCURE

The DATA file structure of the base case is defined here and what changes for each sensitivity are made are explained later in Section 6.5. The DATA file usually has in total eight sections and all of them have their own importance and requirements which are defined in the Schlumberger`s reference and technical descriptions manual also explained in Section 5.3. Here the most significant sections with their respective main keywords are described.

6.1.1.1   RUNSPEC SECTION
This is the first section of the DATA file. Here the title, type of units used, start date, components, grid dimensions, type of EOS etc. are written. The following, in addition to the GASWAT, are the main KEYWORDS of this section that were used for this project.

EOS: This keyword defines the type of Equation of State to be used. For this project the Peng Robinson EOS was used.

METRIC: The working units for this simulation were metric

COMPS: It defines the number of components present in the simulation run. In this case, there are 5. Along with CO2, the simulation was run with 3 hydrocarbons including methane, ethane and propane and water. Water has to be defined as a component while using the GASWAT option.

AIM: Adaptive Implicit is the solution option for Eclipse compositional run. It is the recommended option for most studies and is also the default option. Alternatively, as defined in Section 5.3, FULLIMP (fully implicit), IMPSAT and IMPES (Implicit Pressure, and Explicit Saturation) can be used as well. In general AIM avoids the time-step restrictions added by small blocks, particularly the ones containing the wells, simultaneously not suffering the much greater expense of a fully implicit solution.

DIFFUSE: It indicates that the molecular diffusion is required. In E300, the diffusivities are calculated from the grid data and the calculated can also be modified using additional keywords like DIFFMX in the gird section. In this case, only DIFFUSE is used.

6.1.1.2   GRID SECTION

GRID section comes after the RUNSPEC section. Here the static petrophysical-properties like the permeability (in x, y, z direction), porosity, grid coordinates, faults and their transmissibility and aquifer coordinates are defined. In summary, GRID section helps in defining the shape, size and extent of the reservoir model along with the properties of each grid cell. For this thesis, the GRID data was not defined separately, instead relevant INCLUDE files were used to define the coordinates of the grids as well as the reservoir properties, faults, barriers and their transmissibility. These static properties are explained in depth in the next section of this report. Other than this the significant keywords used in this section include:

MULTIPLY: This keyword is used to give a permeability value in the z direction, based on the ratio of anisotropy. The layer 4 of the reservoir from the top is the most impermeable layer, which was previously inactive since it was considered as no flow was considered across it.

MINPV: This is used to set a threshold pore volume that a cell must exceed of it will be turned inactive. The value set for this case was 500 m^3. Cells that have been made inactive using the ACTNUM keyword remain inactive even if the PV exceeds the set value.

6.1.1.3   PROPS SECTION

Once the grid properties are defined, the PVT and SCAL data are added in the PROPS section. It is the most fundamental section of the report that defines how components that are simulated behave in the presence of each other and at given pressures and temperatures. The main properties include critical temperatures, pressure, volumes, z-factor and molecular weights and binary interaction coefficients. The values were obtained from the Table A1-B of the book Phase Behavior by Curtis Whitson given in the **Appendix A**. The main keywords of this section include:

ZI: This keyword defines the molar % of each component. The model was considered as a depleted state for a dry gas reservoir, therefore the C1 component was kept with the highest percentage from the start while the heavier components and CO_2 were relatively small. Section 6.3 gives details of each component. A sensitivity analysis case based on the initial fluid composition of the reservoir is also presented and how it is changed is discussed in the sensitivity analysis section.

WSF & GSF: Gas and water saturation functions are defined using the data provided by SINTEF from an unknown reservoir. Since this is a created scenario of a depleted gas reservoir, and PVT data is not relatable to the actual reservoir, the provided DATA was used as a good estimate for modelling purpose. These keywords define the relation between relative permeability of gas and water to their respective saturations. According to the gas and water relative permeability tables, Swi was 0.37 and maximum gas saturation was 0.63 for this model. The critical gas saturation was taken to be a value of 0.01. A sensitivity for residual gas saturation and water saturation is also performed.

DENSITY: Defines the density of the reservoir fluid at surface conditions.

RTEMP: Defines the reservoir temperature at the start of the simulation. Isothermal simulations are conducted for this thesis therefore no change of temperature in reservoir is expected. Temperature of 100°C is chosen as the base case.

6.1.1.4 REGIONS SECTION

This section is used to divide the reservoir into different sections based on the requirements and the study purposes. For this thesis, two main regions are created namely region 1 and 2. The top 4 layers in the z-direction is region 1 while the remaining 18 layers are region 2.

6.1.1.5 SOLUTION SECTION

This section is relatively shorter than the rest of the sections and only the initialization parameters are entered. The most important and the only keyword here is:

EQUIL: Simulation is initialized using it and a reference depth is chosen to define the necessary parameters of this keyword. The reference depth was set at 2750m and the initial reservoir pressure was set at 200 bars. This was done to simulate a scenario of a reservoir that has a potential of producing hydrocarbons until at least fifteen years before the depleted pressure limit of 50 bars is reached. Usually, dry gas reservoirs have a recovery factor of almost 90% and at this state the pressures reach to very low values. The base case was set with the gas-water contact within the reservoir at 2750m.

6.1.1.6 SUMMARY SECTION

As we know this section lets us enter the keywords for the results that are to be obtained, the relevant ones were entered according to the requirements of this project. These include FGIR (Field Gas Injection Rate), FCWM (Molar amount of specified component dissolved in water), FCGMM (Molar amount of specified component mobile in gas), FCGMI (Molar amount of specified component trapped in gas) and FPR (Field Pressure) & FPRP (Pressure average value (Pore-Volume Weighted)). In addition to this, for sensitivity runs for reservoir heterogeneity BPR keyword was also used in order to obtain the pressure of grid blocks near the well bore region and to make comparison of pressure within each case and determine the effects of permeability and nearby faults on storage.

6.1.1.7 SCHEDULE SECTION

This is also another important section of the DATA file and helps in defining the number, types and positioning of the wells along with the rates and maximum bottomhole pressure. The injection was done using a stream of pure CO_2 by two vertical wells. The important keywords include:

WELSPECS: This defines the specification of wells. The default well type is a vertical well. Using this keyword, the well location is also defined and it was set to be 8 by 8 (I J grid) for I1 (injector 1) and 12 16 (I J grid) for I2 (injector 2). The choice of the location of each well is decided based on certain petrophysical parameters that are discussed as a separate section. I1 11 63 1 based on horizontal permeability, gas saturation, GWC and fault sides. I1 and I2 are converted from P1 and P2.

COMPDAT: Completion data for the well was also defined for this simulation. The well is perforated from grids 5 to 18 in the z direction.

WCONINJE: It defines the rate of injection/production and the status of well, along with the maximum BHP. For this project, the base case was set at 100000 Sm3/day/well injection and the maximum BHP was set to be 200 bars, considering it be an approximate value for fracture pressure of the reservoir.

TSTEP & DATES: These were used to set the simulation time steps and total time. The injection is carried out for a period of 15 years starting Jan 1, 2010. The simulation results are viewed until 1st January 2149.

6.1.2 CO2SOL option

It is used to simulate a compositional run for simulating CO_2 injection in oil reservoirs mainly for the purpose of sequestration and EOR. In the gas or oil phases the water is not allowed to dissolve. CO_2 can be present in three phases, moreover, the other components can be in the oil and gas phases. Fugacity equilibration technique calculates the CO_2 partitioning between the oil and gas phases and a cubic EOS is models the densities and fugacity of the two phases (Schlumberger, 2021).

To compute the amount the of CO_2 dissolved in water, and other aqueous phase properties, solubility data is used that is entered using either of the keywords including SOLUBILI, SOLUBILS or SOLUBILT. Additionally, molecular diffusion between gases can be modelled using the DIFFUSE option. It is also possible to take the initial dissolved CO_2 as a function of depth using the RSWD or RSW keywords. The fugacity equation is given as the following form which matches the solubility data for aqueous CO_2 when the keyword CO2SOL is included in the simulation.

$$f_{CO_2}^A = Pa_{CO_2} \emptyset_{CO_2}$$

The equilibrium of phases between the CO_2 and the hydrocarbon phases is then defined by the conditions that fugacity values are equal. Gibbs energy contribution can also be formed for the aqueous CO_2 phase. The initial concentration of CO_2 may not be fully in equilibrium with the HC phases and the flash values modifies the input values a little. Detailed explanation of the water component properties, density, viscosity and aquifer properties can be found in the (Schlumberger, 2021) manual.

Here again as explained for the previous section, Eclipse software is used to simulate the CO2SOL case, once the setting up of a DATA file is complete. There were in total eleven sensitivity cases and a base case and different files are used to run simulations for performing the analysis, For some sections, data was linked with the already presented data set from Schlumberger`s CO2SOL file. Here the most significant sections with their respective main keywords are described that are different from the GASWAT option is used. GRID, REGIONS, SCHEDULE sections are the same as the previous case.

6.1.2.1 RUNSPEC SECTION

The following are the main KEYWORDS of this section that were used for this project. AIM is used to solve the linear iteration.

EOS: This keyword defines the type of Equation of State to be used. For this project the Peng Robinson EOS was used.

CO2SOL: It is the main keyword for this simulation. According to the Schlumberger`s Technical Description manual**Invalid source specified.**, the CO_2 solution option is activated when this keyword is used. It is used when modelling for a CO_2 injection in a depleted oil reservoir. Although it is recommended for use in depleted oil reservoirs, but it can be used for a depleted gas reservoir case as well if the OWC and GWC are made equal, or in other words, the simulation is initialized with no oil zone. It allows the CO_2 component to exist in all three phases. Along with this keyword, some other optional keyword are also added which include SALINITY, and for this project it was taken as 0.51 10^-3 kg-M/kg.

COMPS: It defines the number of components present in the simulation run. Along with CO2, the simulation was run with 3 hydrocarbons including methane, ethane and propane. Water is not defined as a separate component when modelling with CO2SOL option.

6.1.2.2   PROPS SECTION
Once the grid properties are defined, the PVT and SCAL data are added in the PROPS section. It is the most fundamental section of the report that defines how components that are simulated behave in the presence of each other and at given pressures and temperatures. The main properties include critical temperatures, pressure, volumes, z-factor and molecular weights and binary interaction coefficients. The values were obtained from the Table A1-B of the book Phase Behavior by Curtis Whitson given in the **Appendix A**. The main keywords of this section include:

ZI: This keyword defines the molar % of each component. The model was considered as a depleted state for a dry gas reservoir, therefore the C1 component was kept with the highest percentage from the start while the heavier components and CO_2 were relatively small.

SOF3, SGFN & SWFN: Oil, gas and water saturation function were defined using the data provided by SINTEF from an unknown reservoir PVT data was obtained from an unknown source and was used as a good estimate for modelling purpose for a depleted gas state. These keywords define the relation between relative permeability of oil, gas and water to their respective saturations. Oil phase is needed to run the simulation and dummy oil properties are used. According to the gas and water relative permeability tables, Swi was 0.37 and maximum gas saturation was 0.63 for this model.

SOLUTION SECTION

The most important and the only keyword here is:

EQUIL: Simulation is initialized using it and a reference depth is chosen to define the necessary parameters of this keyword. The reference depth was set at 2650m and the initial reservoir pressure was set at 200 bars. Secondly, the oil water and gas water contact were set at same depth. This was done to keep the oil zone to a zero value and was only included since CO2SOL works as a three phase option. The base case was set with the gas-water contact at the reservoir depth of 2750m.

6.2 Static Properties of the Reservoir Model

In this section static properties, the ones that remain constant throughout the simulation are defined. As mentioned previously the grid data was imported from an external file as "INCLUDE" files in the main DATA file. Before the updated model properties and the E-segment is discussed, how the original structure and model stands is defined first.

6.2.1 Original Norne Reservoir Model

The original high resolution full model was produced on a 2004 geo model. The grid of the simulation was based on updated polygon and new structural and isochore maps also produced in 2004. The RMS have been utilized to generate the grid and establish the petrophysical properties. For this original model, 113344 cells are present of which 44431 are active and the reservoir is divided into 22 lithological zones for the modelling purpose. The zonal boundaries were selected as sequence boundaries and maximum flooding surfaces. For other boundaries, lithology or defined porosity/permeability from wells 6608/10-2 and 6608/10-3 were used, and for boundary correlation the surrounding wells were utilized (Rwechungura, Suwartadi, Dadashpour, Kleppe, & Foss, 2010). The zonation of this reservoir is given in the Table 6-1 below. Figure 6-1 is a 3D pictorial representation of the original model that show the distribution of permeability and porosity in the reservoir. The permeability in the horizontal direction lies in the range of to some 100s to 1000s mD while porosity is ranging from about 0.2 to 0.33.

Table 6-1 Zonation of the reservoir from the Eclipse model

Layer number	Layer name	Layer number	Layer name
1	Garn 3	12	Tofte 2.2
2	Garn 2	13	Tofte 2.1.3
3	Garn 1	14	Tofte 2.1.2
4	Not	15	Tofte 2.1.1
5	Ile 2.2	16	Tofte 1.2.2
6	Ile 2.1.3	17	Tofte 1.2.1
7	Ile 2.1.2	18	Tofte 1.1
8	Ile 2.1.1	19	Tilje 4
9	Ile 1.3	20	Tilje 3
10	Ile 1.2	21	Tilje 2
11	Ile 1.1	22	Tilje 1

a)

b)
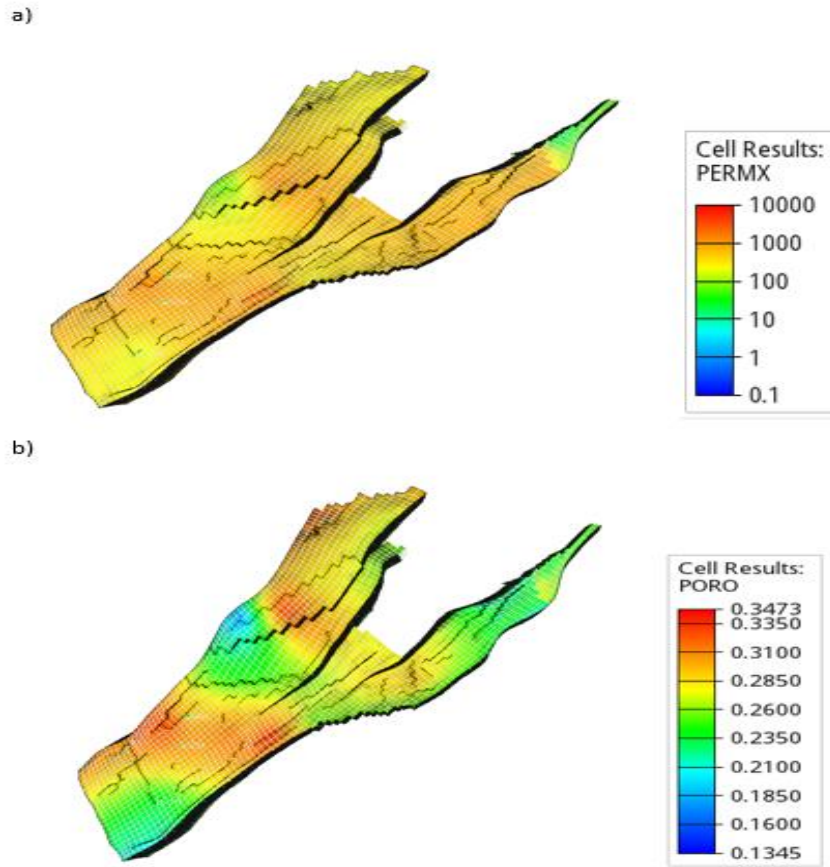
Figure 6-1 a) Permeability in x direction b) Porosity

6.2.2 E-segment

The dimension of the model has been set with 46 cells in the x-direction, 112 cells in the y-direction and 22 in the z-direction. This makes a total of 113344 cells out of which 9100 cells were kept active during the simulation runs to create the E-segment. For this model, the computational time was not very high and for one simulation it took on average 25 minutes. The size of the grids in x-direction is variable and ranges from 83.9 m to 194.2 m, for y-direction the grid size ranges from 65.7m to 155.6m and lastly in z-direction, the grids are sized in the range of 0.2m to 47.14m. The Figure 6-2 below shows the distribution of cells in the z direction. This E-segment has 22 layers with variable thickness which are consistent with the original model and have various thickness and reservoir properties. Previously, the layer 4 (Not fm.) had been kept as an inactive layer to demonstrate a highly impermeable layer across which no flow is possible. However, for these simulation runs, this layer has been activated with a low permeability value that could act as a caprock for the stored CO_2.

a)
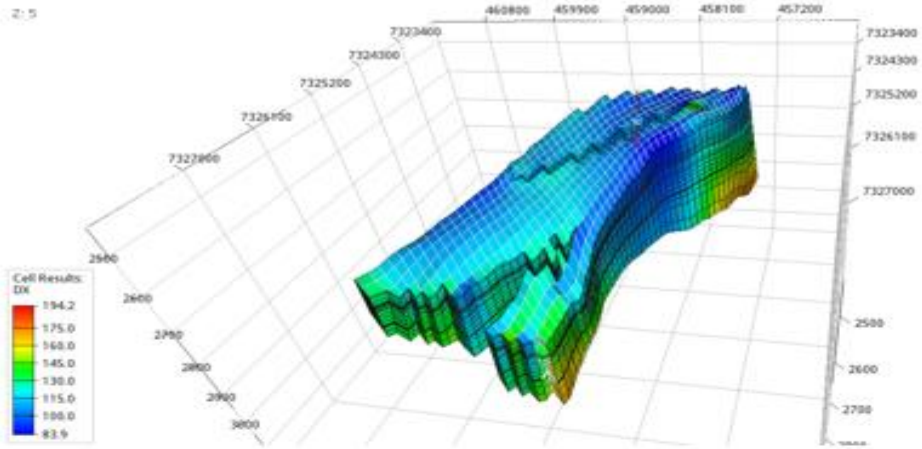
b)
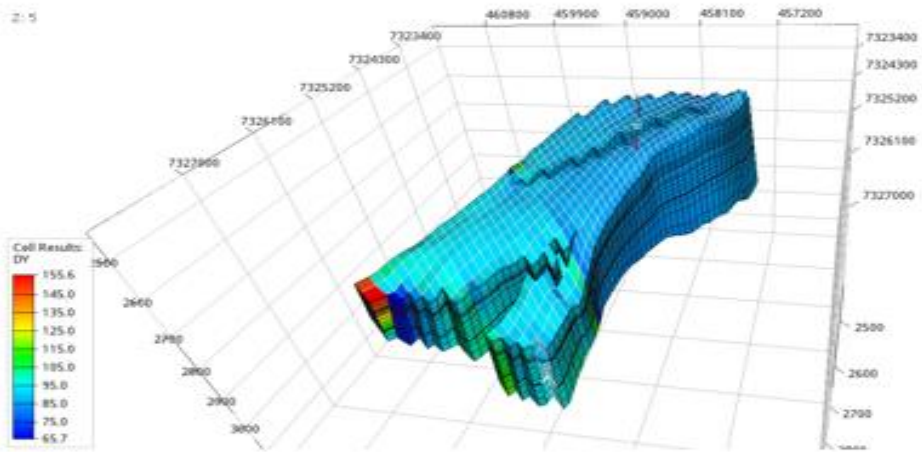
c)
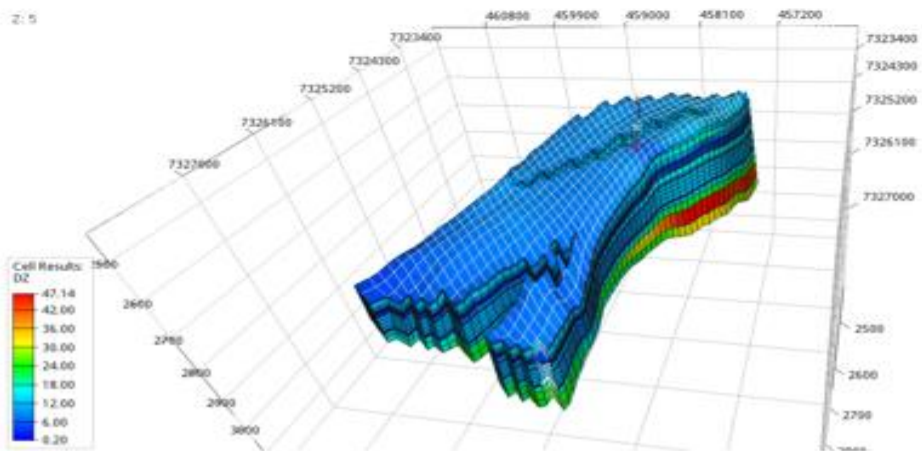
Figure 6-2 Grid cell sizes in the three dimensions. a) x-direction b) y-direction c) z-direction

52

The reservoir is arranged in a down dip manner in the North-South direction. The top depth from the surface towards this reservoir is increasing N-S. The shallower regions lie in the northern side as shown Figure 6-3. The top depth of the shallower region is 2524m, while of the deepest region it is 3051m. The reservoir thickness is almost constant and is about 220m or more on average. Thickness of a reservoir is an imperative aspect of injecting fluid into it. If the thickness is small, say < 30m, likelihoods of incurring geo-mechanical stresses on the reservoir become higher. In this case, the reservoir thickness is large enough to understand that these effects are highly unlikely to be causing any stress changes and hindering the sequestration process.
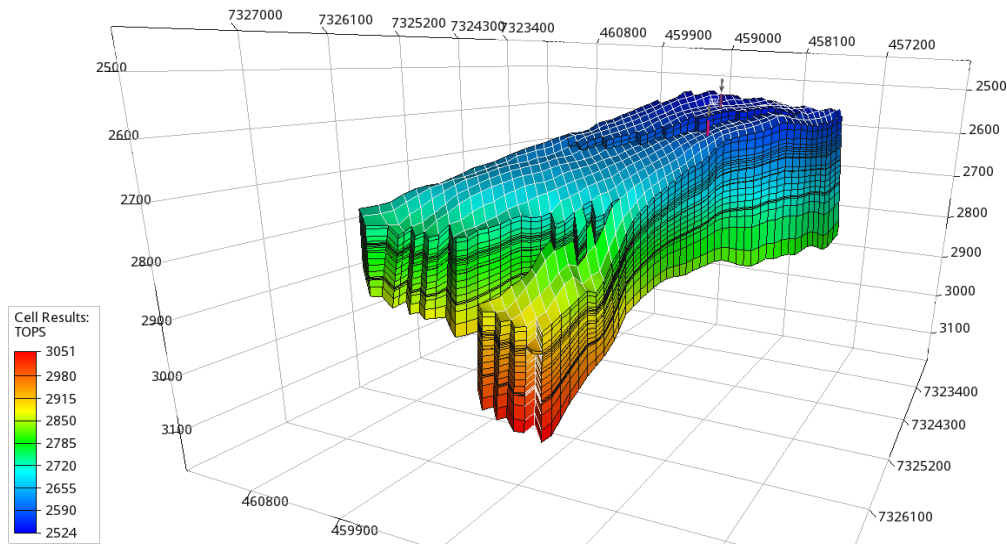
Figure 6-3 Top depth of the reservoir (viewed from the South)

As discussed in the literature review section of the report, successful storage into a reservoir is based upon how much capacity is present in the reservoir. This is determined by the pore volume of the reservoir which is reliant on porosity. The E-segment has a varied distribution of porosity ranging from values as low as 0.1554 to as high as 0.3275. On average porosity of the reservoir can be roughly estimated as 0.25, which is a relatively a good value for a reservoir rock chosen for storage. This is particular to reservoir rocks in a sandstone formation. The distribution of porosity is shown in the Figure 6-4 below. The porosity is variable between layers. But it can be seen that each layer`s porosity distribution is uniform. Total pore volume of this segment at the reference pressure is 156.53 E06 Rm^3. This segment can be considered as having a high capacity value based on the high porosity distribution. Care was taken while choosing the well location, and regions with lower porosity were avoided. Section 0 provides a detailed reasoning of choosing the well locations.
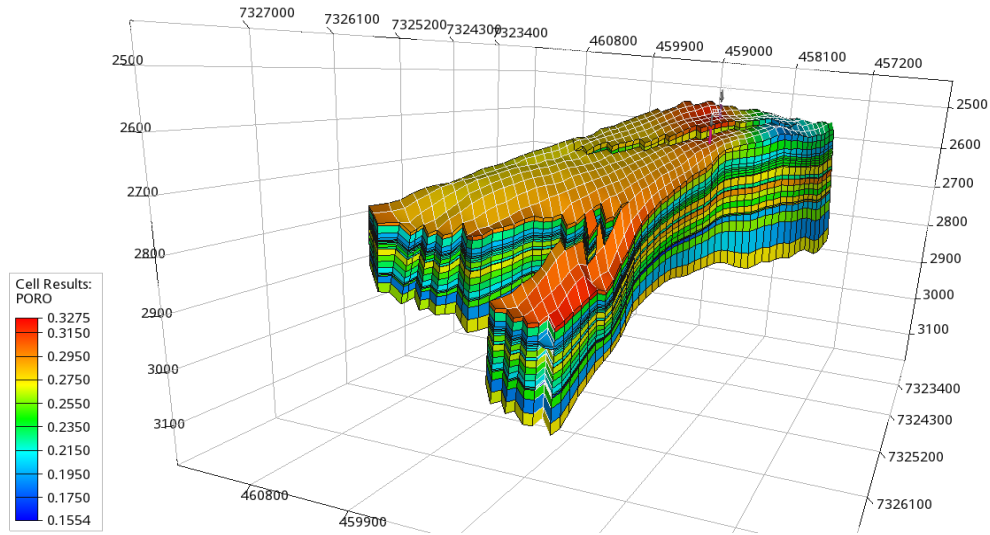
Figure 6-4 Porosity distribution of the E-segment

Permeability of the formation is a key property that assists in determining the dynamic behavior of the fluids present or injected in it. In this model it is considered as a fixed property since it is assumed that injection of CO_2, its dissolution in water and reaction with reservoir rock, does not alter the permeability of the formation. As shown in Figure 6-5 above, the permeability for this reservoir is ranging from a very small value of 1 mD to almost 10000 mD in the x-direction and 0.0001mD to 10000mD in the z-direction. The horizontal permeability (in x and y direction) is equal, while the vertical permeability has been modified based on the anisotropic ratios. Layer 4 of the formation is assigned the lowest permeability of 0.0001mD as it is considered as a caprock and injection of CO_2 is done below this layer. Caprock is an important feature of safe injection, as it confirms that the injected CO_2 can be structurally trapped in the geologic formation. In depleted oil and gas reservoirs, the most common trapping mechanism is the physical (structural trapping) mechanism and in this model, since other features like abandoned plugged wells are not defined, it is safe to assume that the CO_2 is trapped beneath the caprock. Additionally, to study the CO_2 plume movement and assess any potential leakage through this layer or from the faults within the reservoir, two regions have been created. Region 1 starts from layer 1 to layer 4 in the z direction, while Region 2 is from layer 5 until the 22nd layer which is shown in Figure 6-6 below. Total molar volumes of CO2 and hydrocarbon components present in each Region is requested as an output in the summary section of the DATA file. This helped in making a comparison of CO_2 plume movement in the short and long term.
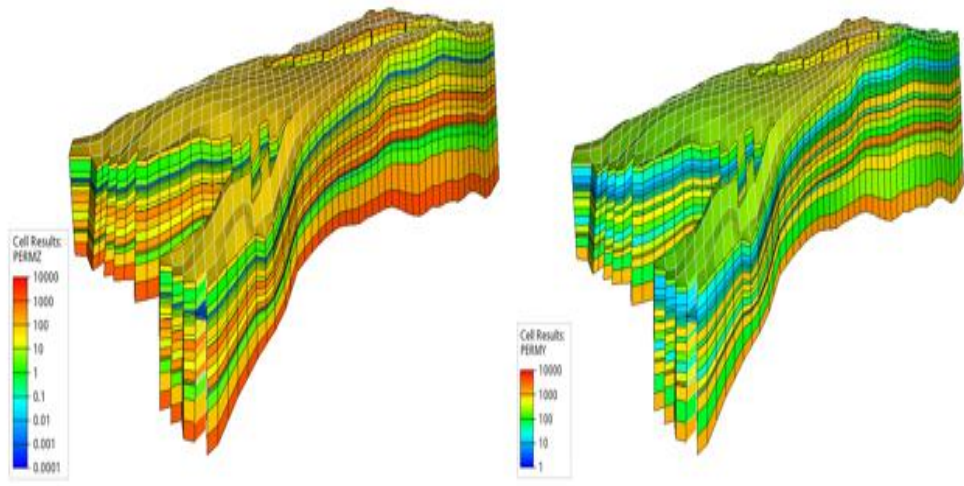
Figure 6-5 Permeability in (left) z-direction and (right) x-direction
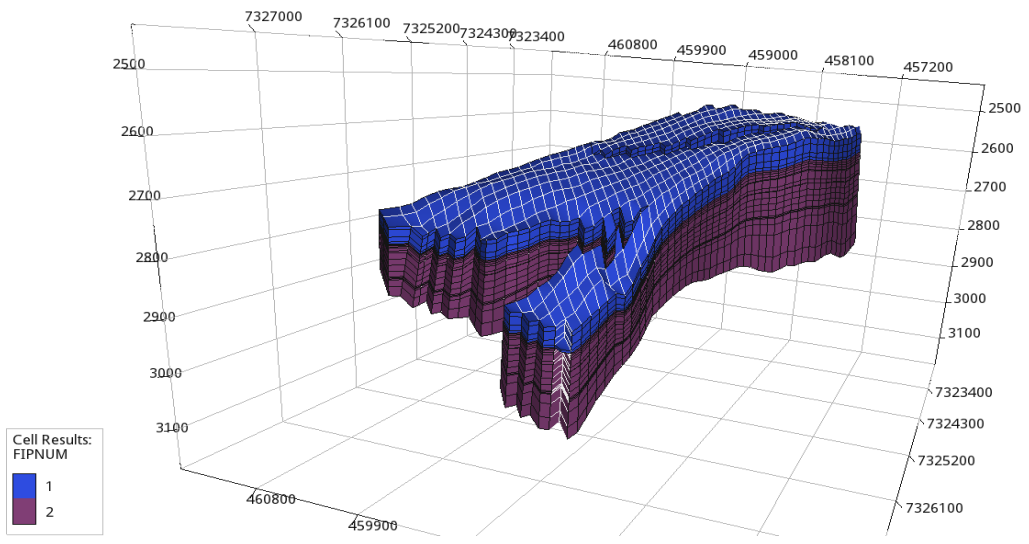
Figure 6-6 Fluid in place regions
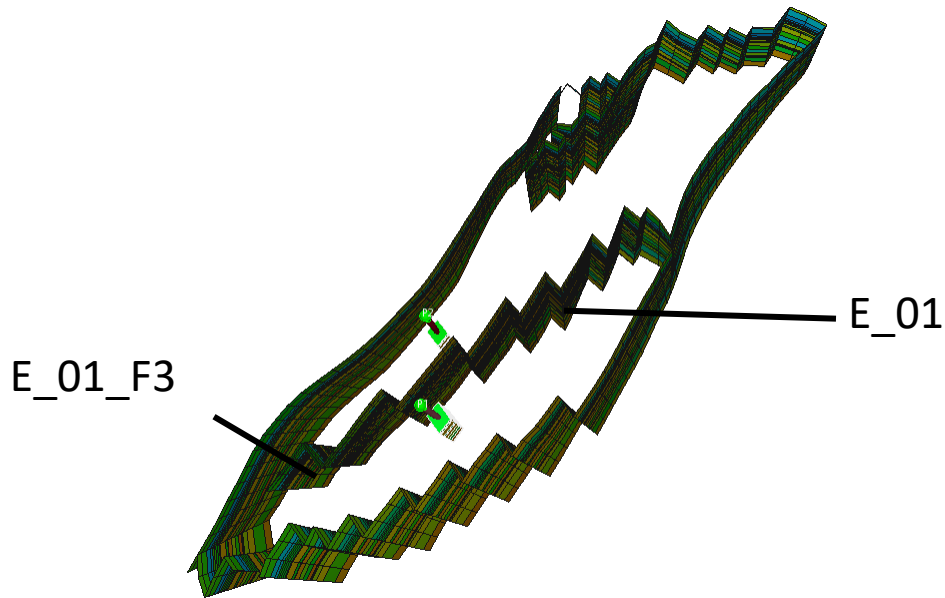
The Norne reservoir consists of many faults. The E-segment has two main faults that are extended to a relatively larger areal extent as compared to the other minor ones present. They are named as E_01 and E_01_F3 and are shown in Figure 6-7. Faults are an important feature of consideration during the process of reservoir management, depletion and injection strategies. The transmissibility of the faults can be set using the keyword MULTFLT in the GRID section, and for these two main faults it was set at 0.01. This means the faults are relatively impermeable and flow across them would only occur as a result of leakage pathway formation due to a change in the stress states caused by production or injection from the area close to it.

Overall, the static properties are key in determining the flow of CO_2 in the reservoir. They determine the distribution of pressure profiles, CO_2 plume and overall storage would occur. Therefore, these properties must be addressed in advance, and to accurately predict the reservoir engineering scenarios, the seismic and geological studies must be correctly and comprehensively done so that the reservoir simulations and the models are as close to reality as possible.

6.3   Fluid properties and simulations initialization

This section describes the relevant fluid properties that are used in the model. It also defines the initial conditions and simulation options that are used in the runs to inject and store CO_2 in a depleted gas reservoir after a period of production mainly for the base cases. Necessary changes that are made in the initializations for all sensitivity analysis cases are explained in the next section.

Reservoir simulations were carried using the two main methods elucidated in Section 6.1. GASWAT uses a two phase approach while the CO2SOL includes all the three phases. The flow characteristics, dissolution and the movement of the CO_2 in the reservoir depend on a number initial values including reservoir temperature, density, salinity, relative permeability, residual gas saturations, irreducible water saturations,

capillary pressures, densities, viscosities, fluid contacts, number of components and their compositions. All runs were carried out using isothermal conditions which is not an ideal approach for reservoir simulations as the reservoir is not in isothermal condition and with injection the near well temperatures change dramatically depending on a number of factors like those mentioned in Section 3.33.3

In this model properties of gas, water and CO_2 (i.e. critical pressure, critical temperature, acentric factors and binary coefficients are obtained from (Whitson & Brulé, 2000) Phase behavior book. The Appendix A gives the values of these properties. The injected CO2 is assumed to be in a supercritical state according to the pressure temperature at the reservoir depth. All the simulation runs are carried out with no effect of hysteresis

The relative permeability data used here was obtained from an unknown gas reservoir of similar lithology and wettability. The name of the source is kept confidential. The following graphs (Figure 6-8) give the fluid saturations of the reservoir at initial conditions. The permeability data as explained in the Section 6.1 is added in the PROPS section using the keyword WSF (Water Saturations Functions) and GSF (Gas Saturation Functions) for the GASWAT and SWOF, SGOF and SOF3 for CO2SOL case. The connate water saturation is 0.37 and the maximum gas saturation is 0.63. The critical gas saturation (S_{gr}) is 0.01. Critical saturations are the highest value of saturation for which the associated relative permeability is zero. At saturation above this value, gas is mobile. The maximum water saturation $S_{wmax} = 1.0$, which results in the water zone being fully saturated with water. Saturation data determines the dynamics of fluid being able to flow in the reservoir. These can also influence the trapping mechanisms, particularly residual gas trapping and impact how the CO_2 is distributed especially when hysteresis option is also activated.

The reservoir simulation is initialized with a GWC at a depth of 2750m for GASWAT case. For CO2SOL case, as three phases are needed to be defined, the OWC and GOC are made equal, and no oil zone is present, hence making simulator deal with gas and water only. Figure 6-9 below shows the water saturation of the reservoir at the start of the simulation period. This helps in visually understanding the location of the GWC. Fluid contacts are extremely significant in determining well completions as it is important to perforate in hydrocarbon zones to maximize production, and similarly to achieve increased injectivity, perforate the injection wells in a non-aqueous zone. In addition to this, since this study is about a gas reservoir and compositional simulation (E300) is employed, it is important to define the components as well. Table 6-2 and

Table 6-3 below show the components and their compositions in the reservoir at the initial conditions. Methane content is kept highest as this reservoir is considered a dry gas reservoir.
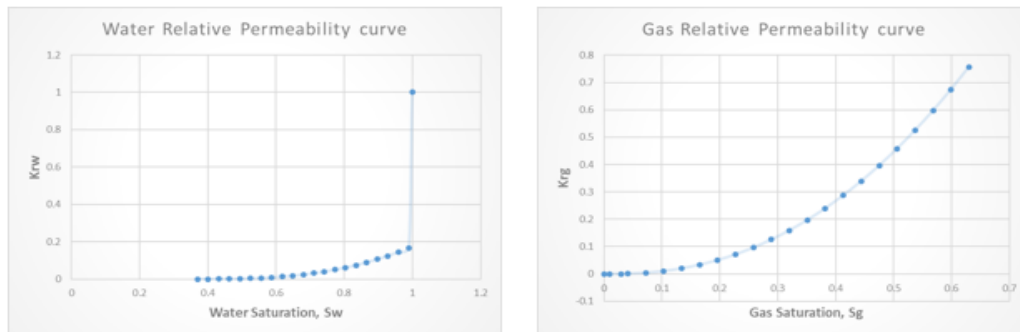
Figure 6-8 Relative permeability curves
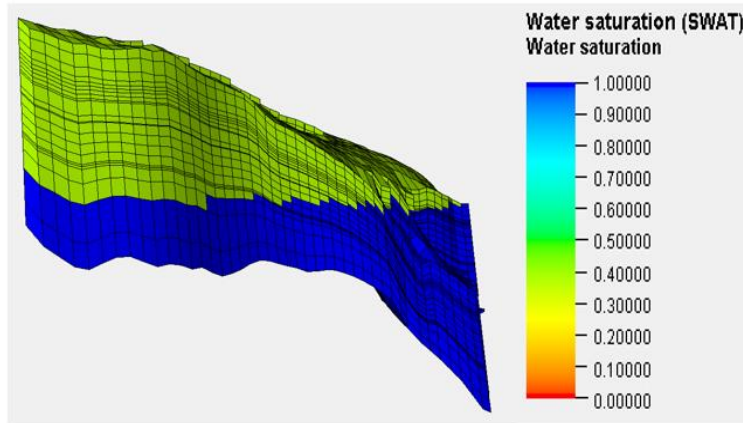
Figure 6-9 Water saturation table (viewed from the East)

Table 6-2 Molar composition of components in the GASWAT case

Component symbol	CO2	H20	C1	C2	C3
Component Name	Carbon Dioxide	Water	Methane	Ethane	Propane
Composition	0.0115	0.02	0.65	0.18	0.1385

Table 6-3 Molar compositions of components in the CO2SOL case

Component symbol	CO2	C1	C2	C3
Component Name	Carbon Dioxide	Methane	Ethane	Propane
Composition	0.0115	0.67	0.18	0.1385

As explained before, the model is simulated for a fifteen year production period followed by a fifteen year injection period using equal injection and production rate by having two wells. At the start, the reservoir has a pressure of 200 bar and is simulated to produce gas until it reaches 50 bar based on an assumed economic limit as well as a limit to prevent any serious stress changes causing alterations in reservoir petrophysical properties like porosity and permeability. Injection of CO_2 is done until the reservoir pressure reaches the value of 200 bar, which again is a good estimate of fracture pressure at this depth. The Table 6-4 below summarizes all the relevant details about initializations and some of the fluid properties as well.

Table 6-4 Initialization parameter and fluid properties

Symbol	Variable	Value	Units (metric)
N	Total grid blocks	113344	
	Active grid blocks	9100	
Cr	Rock compressibility @ 150bar	0.00005	1/bar
Temp	Reservoir temperature	100	°C
S	Salinity	0.51	10^{-3} kg-M/kg
ρ_o	Oil density at surface conditions	600	Kg/m^3
ρ_w	Brine density at surface conditions	1050	Kg/m^3
ρ_g	Gas density at surface conditions	0.062428	Kg/m^3
Kh	Horizontal Permeability	1-10000	mD
Ø	Porosity	15.54-32.275 %	
GWC	Gas-Water Contact	2750	m
P.V	Pore Volume (initial)	156.529731	$10^6 Rm^3$
S_{wc}	Connate water saturation	0.37	
S_{gr}	Critical gas saturation	0.01	
S_{gmax}	Maximum Gas Saturation	0.63	
Q_p	Gas production rate	1.8 E06	Sm^3/d
Q_i	Gas injection rate	1.8 E06	Sm^3/d
xCO_2	CO_2 mole fraction in injection stream	1.0	
T_prod	Period of production	15	years
T_inj	Period of injection	15	Years
P_{init}	Initial pressure @ 2750m	200	bar
P_{frac}	Fracture pressure	200	bar
P_{bhp_limit}	Bottom-hole pressure limit	200	bar
Start	Simulation start date	06 Nov 1997	
End	Simulation end date	01 Jan 2200	

6.4 Selection of Injection Wells` Location

The effect of the CO_2 injection well location within the geological site on the CO_2 dynamic storage capacity, and on the value of CO_2 storage efficiency, is a critical issue that has still not be fully addressed fully in literature. Some works like (Okwen, Yang, & Frailey, 2014) used numerical simulations to evaluate the gas storage efficiency for diverse sedimentation environments at 5 separate CO_2 injection well locations and this allowed them to investigate the variability in magnitude of this efficiency at these locations. In the study by (Jun, Kim, & Shin, 2019) four well patterns to express the optimal injection well pattern, placement, and operating conditions were examined. The outcomes showed the optimal location and fluid rate that enabled a nearly eight times greater volume of CO_2 to be stored compared to the base case. Therefore, choosing an optimal location for carrying out injection and storage is also a significant part of the project design. The locations and their relevant reasoning are discussed below. It is important to note before that these wells locations might not be the optimal, but based on the scope of the project, it can be considered as one of the best options to produce gas from and then inject CO_2.

The reservoir model is setup to inject CO_2 using two verticals wells. The horizontal wells were not selected as the permeability distribution of the model shows that it has greater permeability in the x and y direction and lower values in the vertical direction, making horizontal wells less effective as they are more beneficial for low permeability reservoirs. If the vertical permeability value was high in each layer, probability of radial flow in horizontal well increases hence, making vertical wells more viable in such a reservoir. The injection wells` location was selected by analyzing the permeability of the reservoir. As seen in the literature review section, permeability of a reservoir is a key factor in determining firstly the suitable location of the injection wells and secondly to inspect the plume of injected CO_2 in the long run after the injection is halted. An obvious advantage of the depleted oil and gas reservoir as explained in Section 2.4 is the availability of production wells and structures that can be easily converted into injection wells. Using the same concept, a simulation scenario is created where production wells after producing and reaching the economic and pressure limit, have been converted into injection wells. It is also important to keep a safe distance between the two wells. In addition to avoiding a steep decline in pressure and causing a movement of the gas-water contact leading to increased water content during production phase, this is also done to prevent build-up of pressures more than the fracture pressure in the near wellbore region during injection, as this could lead to stress induced fractures and may result in loss of CO_2 containment. It was also important to choose the well location that was far from the outer boundary of the reservoir and the nearby faults, again considering the geo-mechanical effects of injection that are discussed in detail in the Section 3.1. Figure 6-10 shows the location of the two wells in the reservoir model.
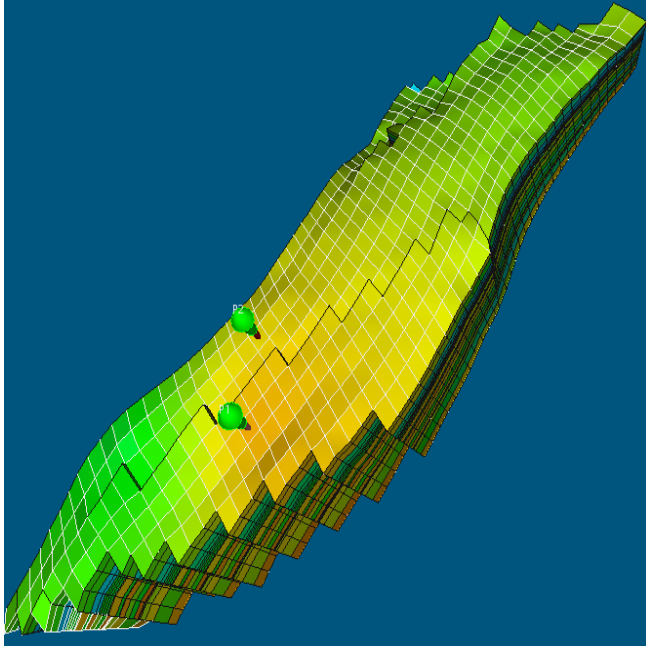
Figure 6-10 Well locations (Visualized in ResInsight)

The selected location for the first well (I1 and P1) was cell 11x63. And the second well (I2 and P2) is placed at 8x66, while the perforation intervals for both the wells were from grid 7 to 18 in the z-direction. It can clearly be seen in the Figure 6-11 below that is showing the cross section of the model`s grid cells on which the wells have been placed, that the I and J permeability in the connected and nearby layers of the well locations are relatively high. This is appropriable for injection for two main reasons: (i) CO_2 that is injected can easily migrate to the neighboring layers hence, the pressure buildup will not be high enough to cause fractures or reactivation of any faults (ii) Due to higher permeability and resulting lower pressure buildup, chances of JT effects which as explained in the literature review section, become less. JT cooling can lead to thermal stresses which ultimately lower the fracture pressure. If appropriately managed, the hydrates are not formed and the nearby well region is not compromised. In case of a simulation for a real field as this one, it is important to consider the boundary of the reservoir and distance from the fault to the wells. Keeping in line with this theoretical reasoning behind well location analysis, both wells are placed at a plausible distance from the fault and the boundary. I1 is at a distance of almost 350 meters from the boundary and 150 meters away from the fault in the x direction, while I2 is at a distance of 230 meters and 145 meters away from the boundary and fault respectively. The main faults present here are the E_01 and E_01_F3 shown in Figure 6-7. The transmissibility of these faults have been set as 0.01 which means that flow across the faults is relatively limited and communication between the near well regions of both the wells is almost non-existent or extremely low. Therefore, it is safe to assume that during depletion and injection, the pressure profiles and fluids are not travelling across the fault.

Perforation for wells were decided according to the gas-water contact which is at the depth of 2750m. The start of the perforation was from layer 7 to ensure that CO_2 is not directly released into the layer just below the caprock (layer 4). The wells are located on an up-dip direction while the gas water contact is below. Hence, the injected CO_2, may travel downwards due to gravity as well, alongside flowing laterally. This may mean that the injected CO_2 can be trapped in the reservoir due to dissolution into the formation water present underneath.
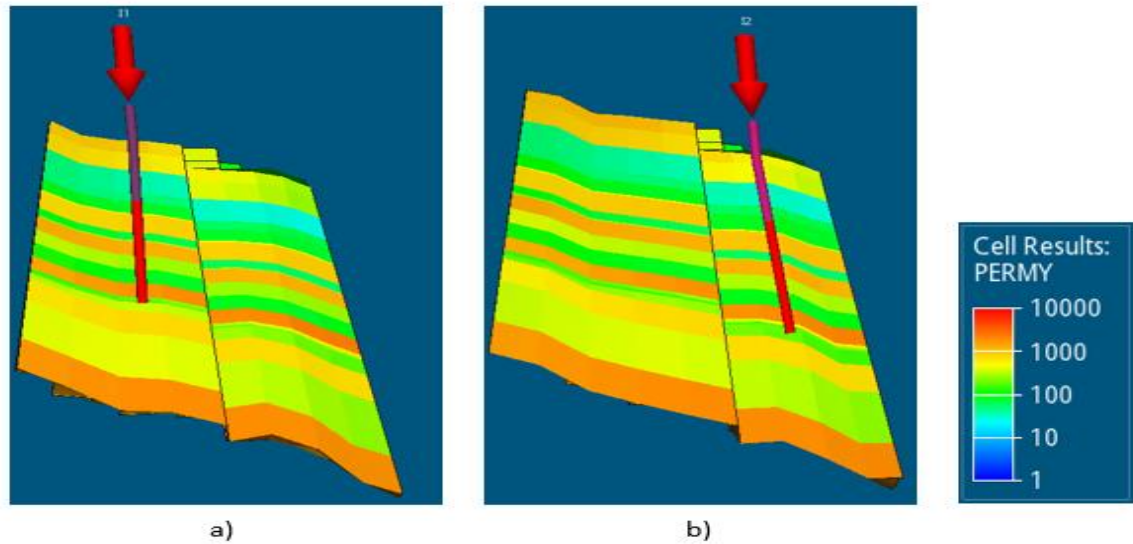
Figure 6-11 Well location based on permeability. (Visualized in ResInsight)

6.5   Sensitivity Analysis Cases

One of the main tasks of the thesis was to examine the effects of different scenarios of injection on reservoir behavior and long term CO_2 plume development. These cases are listed below and what changes were made in the DATA file are also explained within each of them. Pressure limit was set at 200 bar for all runs.

(1) High Permeability: Reservoir heterogeneity as explained previously is a vital factor that can impact the injectivity of CO_2 storage procedure. Numerous studies like the (Akai, Okabe, Hiyama, & Saito, 2021), have been conducted in past to see the effects of it on injectivity and reservoir behavior (Khan N. A., 2021). High permeability case was set up using the keyword MULTIPLY in the GRID section. Both permeability in X and Y direction were multiplied by 10.

(2) Low permeability: Similar to the Case 1, MULTIPLY keyword was used here as well and both X and Y permeability were multiplied by 0.1.

(3) Deeper gas-water contact: For the sensitivity analysis, GWC was moved to 2950m which covers almost the whole of the reservoir. This was done using the EQUIL keyword of the SOLUTION section.

(4) Initial water saturation (20%): SCAL data was altered in the PROPS section in order to make changes in the initial water saturation value. This was done by altering the WSF and GSF endpoint saturations. The base case initial water saturation was set at 37%. It was changed to 20% and $1-S_{wi} = S_g$ was set at 80%.

(5) Critical gas saturation (2.5%): Here the SGFN and SWFN tables were modified to make S_{gc}=0.025 from a previous value of 0.01. This is done to observe the effect of how the hydrocarbon production occurs and during injection which major changes are observed in the displacement of hydrocarbons by CO_2 and long term storage of CO_2.

62

(6) High injection and production rate: This was done by setting the rate to be 2.5E06 SM3/day in the WCONINJE keyword.

(7) Low injection rate: An injection rate of 1.2E06 Sm^3/day was set up by modifying the WCONINJE keyword.

8) High Reservoir Temperature: Reservoir temperature is an integral element of determining phase behavior and transport in porous media. Its variability can impact greatly, in how CO_2 acts in the reservoir. As explained in Section 2.6, properties of CO_2 and brine are explained and what impacts reservoir temperature can have on the sequestration process is also highlighted. The reservoir temperature is increased to 150 C, using the RTEMP keyword in the PROPS section.

9) High Salinity: Similar to reservoir temperature, salinity of formation brine can impact injectivity of CO_2 and storage. The trapping mechanisms can also be influenced

10) Low CH4 content gas: Fluid compositions is again an important feature determining injection and production of fluids in a porous media. Dry gas majorly contains a high volume of methane while wet gases have a greater content of C3+ compounds. The new compositions using the same five components in the GASWAT case are used that are given in the following table.

Table 6-5 Molar composition for wet gas case.

Component symbol	CO2	H20	C1	C2	C3
Component Name	Carbon Dioxide	Water	Methane	Ethane	Propane
Composition	0.0115	0.02	0.65	0.18	0.1385

(8a) With large aquifer: A numerical aquifer with properties defined in the Table 6-6 below was selected and connected to the reservoir on the cells 7 - 16 in x direction, 90-100 in Y direction and 1-22 in the z direction using the keyword AQUNUM for a numerical aquifer, AQUCON in the GRID section and AQUIDIM in the RUNSPEC section. The cells connected to the numerical aquifer are shown in the Figure 6-12 below.

Table 6-6 Numerical aquifer properties for large aquifer

Cross sectional Area (m^2)	Length (m)	Porosity	Permeability (mD)	Depth (m)
1000	2000	0.9	100	3000

(8b) With small aquifer: Using the same grid blocks, a smaller numerical aquifer case is also simulated where the cross sectional area of the aquifer has been reduced as depicted in Table 6-7, to see influences it has on the injectivity, storage, trapping or long term security of CO_2 in the depleted gas reservoir.

Table 6-7 Numerical aquifer properties for small aquifer

Cross sectional Area (m^2)	Length (m)	Porosity	Permeability (mD)	Depth (m)
100000	2000	0.9	100	3000
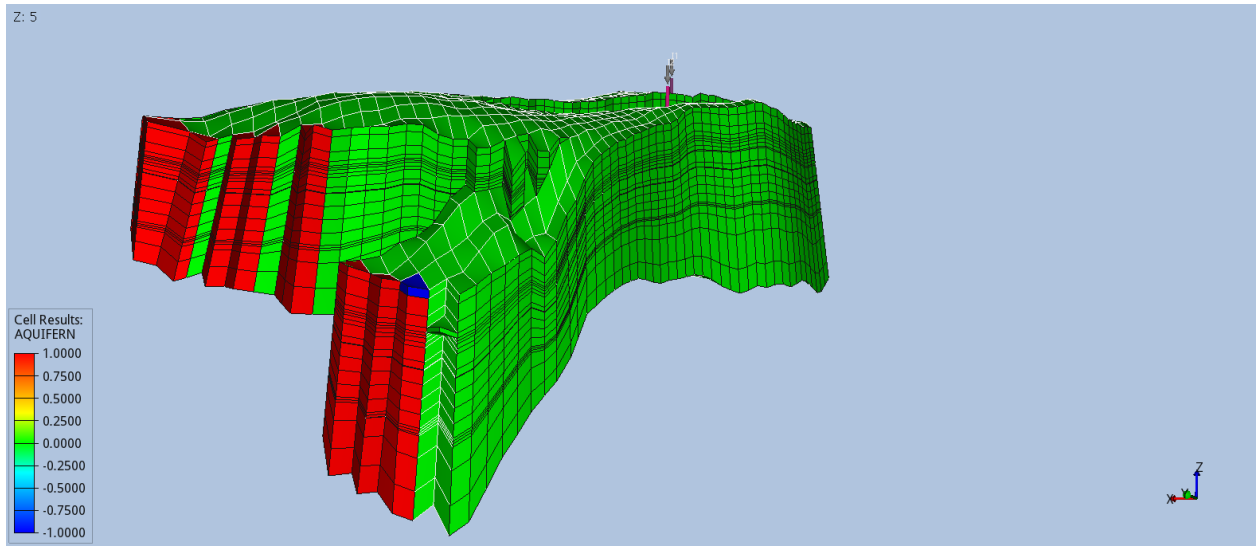
Figure 6-12 Cells connected to the numerical aquifer. (Visualized in ResInsight)

7 Results and Discussion

The impact of reservoir characteristics on CO_2 storage is studied in this thesis. Initially, in Section 7.1, a comparison of results is made between the two approaches of numerical simulation which are explained thoroughly in the previous section. For sensitivity analysis, different areas of reservoir properties are chosen that include reservoir heterogeneity discussed in Section 7.2.1, different initial water saturations and presence of GWC in Section 7.2.2, the impact of reservoir temperature, brine salinity and components of natural gas on CO_2 sequestration is presented Section 7.2.3 and finally the effect of presence of an aquifer nearby are argued in Section 7.2.5. The effect of injection rate is explained in Section 7.2.4. For all cases, the start of injection of pure CO_2 is from June 2012 once the fifteen year production period is stopped. Injection ends fifteen years later until December 2027, initial pressure conditions and the injection limit is kept similar in all runs. Pressures profiles of the field, bottom-hole pressures and grid block pressures (for reservoir heterogeneity only) are observed along with the total moles of injected of CO_2. Volumetric calculations based on analytical approach are also compared with the numerical results, explaining that the amount of CO_2 injected is within the capacity of produced hydrocarbon with differences in density attributing to different molecular mass and structure. Any effect of CO_2–water interaction with formation rock causing precipitation and dissolution during injection and ultimately causing any changes to the reservoir properties like porosity and permeability, (Raza, et al., 2018) is neglected in these cases mainly because of the limitation of the software used and since the model chosen has dominance in sandstone layers, it is considered as unreactive to the injected CO_2. History matching was not employed as the Norne field mainly has oil production, while the study is based on depleted gas reservoir.

The following flow and transport mechanisms control the distribution of CO_2 in depleted gas fields: (i) CO_2 migration because of the imposed pressure gradient formed after injection; (ii) CO_2 migration initiated by natural hydraulic gradients and capillary pressures; (ii) Density differences between the injected CO_2 and the fluids present in the reservoir initially, could result in buoyant and gravitational forces and are majorly controlled by the pressure and temperature behavior of the reservoir; (iv) Mobility differences between the initial reservoir fluids and heterogeneity and the injected CO_2 induces fingering and dispersion; (v) Dissolution of CO_2 in reservoir fluids and vaporization of H_2O and (vi) Diffusion caused by concentration gradients (Metz, Davidson, de Coninck, Loos, & Meyer, 2005). These flow and transport mechanisms are highlighted and explained according to the results obtained and their applicability. Note that the simulations are carried out isothermally therefore any induced thermal effects are beyond the scope of this work.

7.1 Comparison of GASWAT and CO2SOL

The base case for this thesis is run using the two numerical simulation approaches. Both these approaches involve compositional simulation where the effects of each component influences the flow and transport behavior during production of hydrocarbons and injection of CO_2. For both cases, the field is producing hydrocarbon until an abandonment pressure of 50bar and an attempt is made to ensure that the pressure buildup does not enhance the fracture pressure (200 bar limit) during the injection period. The main differential in both approaches would be due to the handling of PVT parameters and interaction with the reservoir. The theory behind the two approaches are elucidated in detail in Sections 6.1.1 and 6.1.2.

Initially, due to production from the two production wells, reservoir pressure is depleted from the starting initial pressure value of 200 bar to the abandonment limit set of 50 bars. For both cases as shown in Figure 7-1a (obtained using the keyword WBHP), the decline in the BHP in both wells is almost linear however, the gradient of decline is different in each case. CO2SOL case reaches the BHP limit of 50 around January 2010, while the GASWAT case reaches this limit at a slightly later time i.e. April 2011. Similar, to production, during the injection period the pressure buildup is alike for both cases at the start, but CO2SOL, as shown in Figure 7-1b, has a greater overall buildup of pressure. This is due to the flow and transport mechanisms variability caused by the differences in density calculations as well the fact that during production a lower volume of hydrocarbon gas has been produced making available space for CO_2 injection slightly less than the case of GASWAT. Furthermore, an important thing to notice is that overall injection of the similar volume of gas does not result in pressure buildup to the initial reservoir pressure, therefore leaving room for increased injection rate or a larger period of injection. Additionally, the wells display a similar behavior during both periods, which indicates a similar productivity and injectivity in the near well regions. This is self-explanatory to some extent as the chosen locations, as described in Section 0, were based on similar considerations including permeability, distance from boundaries and faults, GWC and the storage capacity for each well. The field pressure behavior displays an almost similar behavior to the bottom-hole pressures. After the end of injection period the field reaches a final value of 181.02 bar and 173.27 bar for the CO2SOL and the GASWAT case respectively and is shown in Figure 7-2. The pressures then stabilize across the whole reservoir until the end of simulation run. This behavior is attributed to the flow equations and the pressure and temperature adjustments during the simulation runs of the two approaches. The set production rate was 9E05 Sm3/day/well making a total of 1.8E06 Sm3/day. This production rate shown by Figure 7-3 is relatively high making the depletion to the abandonment pressure slightly earlier than the targeted fifteen years of production. This causes a readjustment in production rates and overall plateau rate is no longer achieved and the cumulative hydrocarbon produced after production period is 9.2645 E09 Sm^3 and 8.1884 E09 Sm^3 for GASWAT and CO2SOL respectively while the injected volume of CO_2 for both cases is 9.72E9 Sm^3 which is 1.049 times more and 1.1870 times respectively. These values are in accordance with results of some of the studies conducted earlier like (Lekic, Jukic, Arnaut, & Macenic, 2019) which concluded that the injected volume of CO_2 is slightly larger than what can be produced from a reservoir which is attributed to the high compressibility of the carbon dioxide gas in comparison to methane. According to the pressure distribution and dissipation in the reservoir, room for more injection is available in this reservoir.

a)

b)
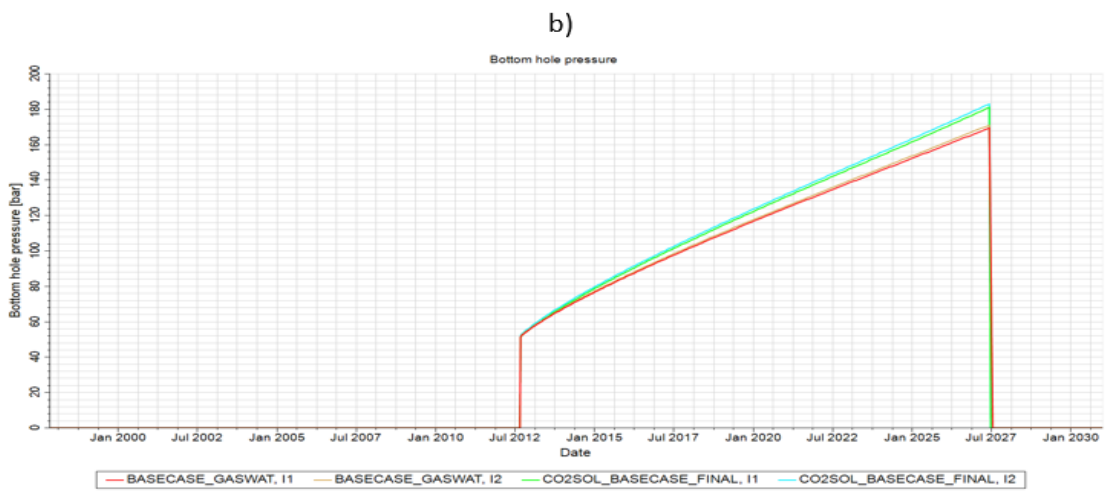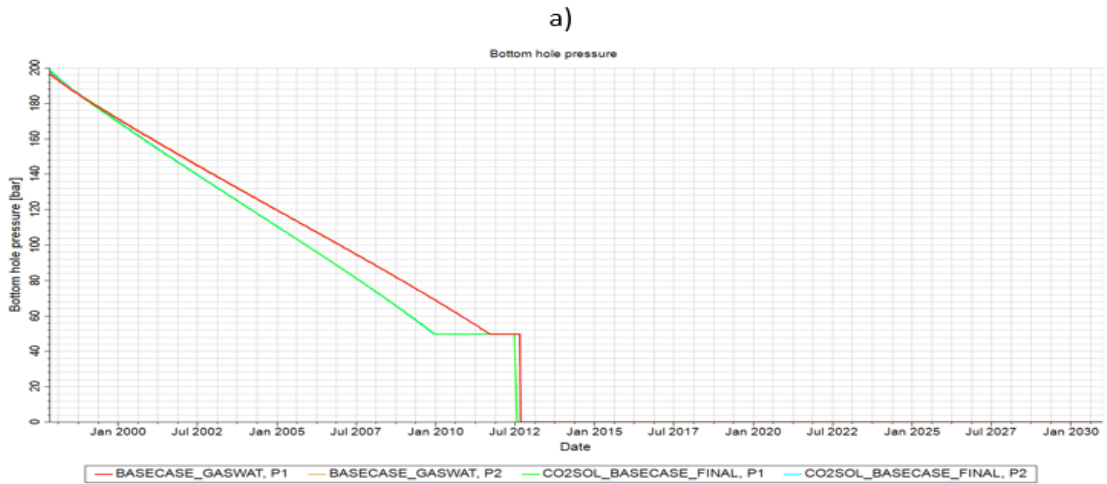
Figure 7-1 Bottom hole pressure (a) Production wells P1 and P2 b) Injection wells I1 and I2.
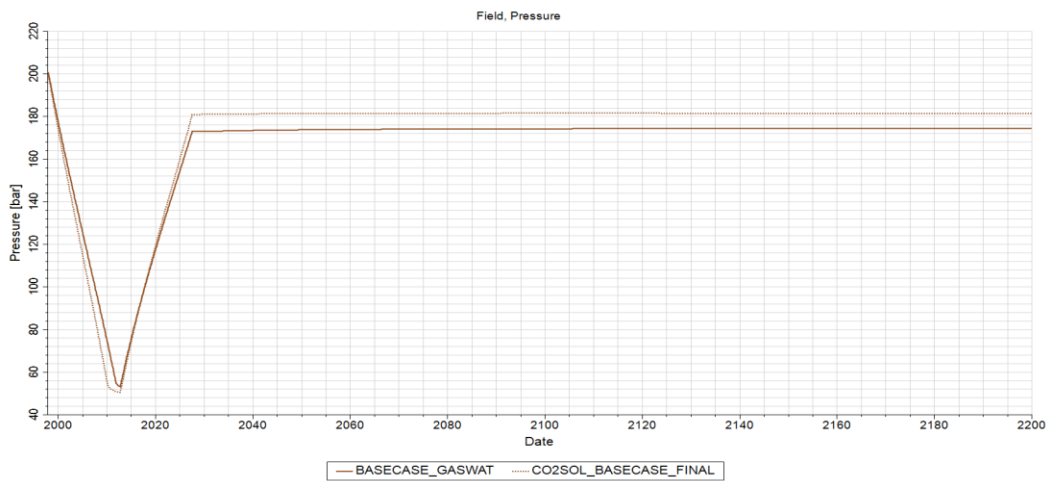
Figure 7-2 Field pressure for both cases
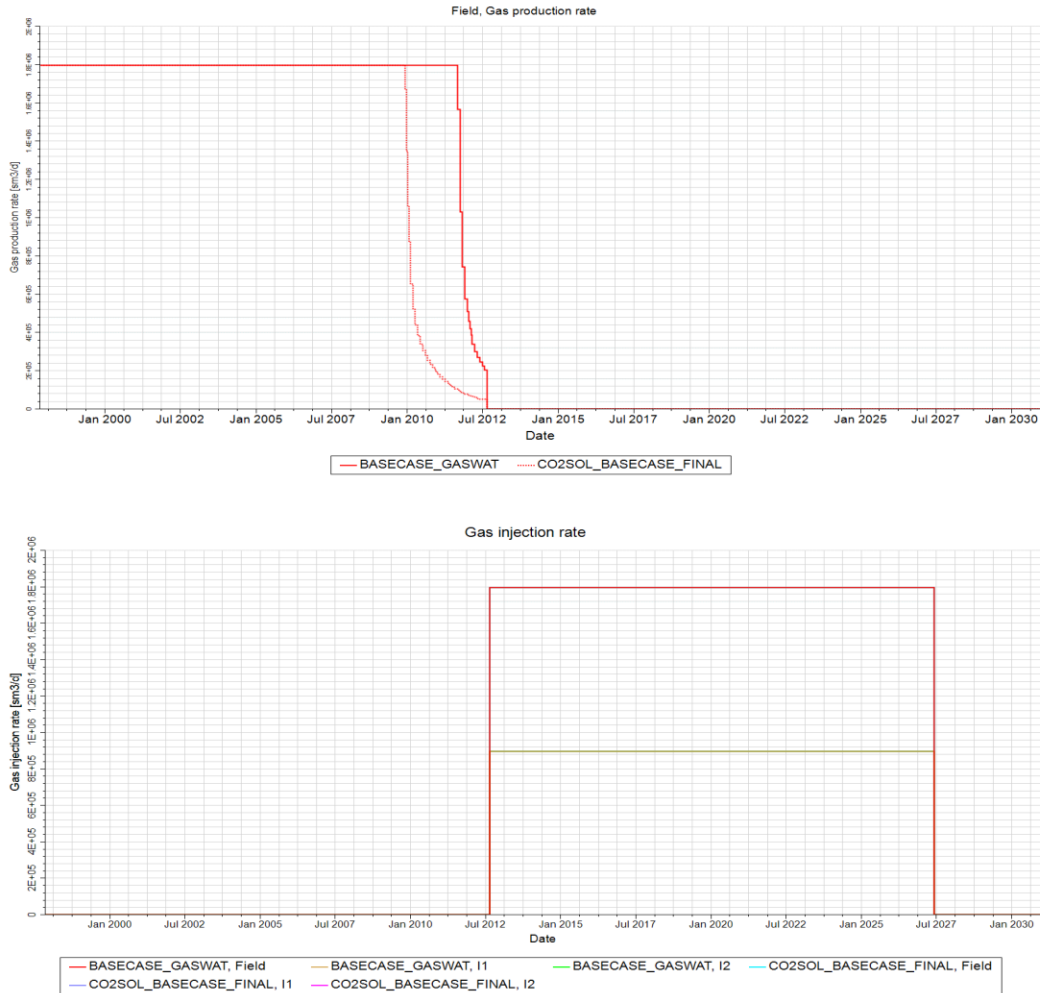
Figure 7-3 CO2 production (top) and the injection rate (bottom) for the whole field for a period of 15 years each

For projects involving CO_2 injection for the purpose of storage or enhanced oil recovery, the amount of injected CO_2 is defined using total mass rather than volumetric values as the latter depend on the P and T of the medium, therefore can vary greatly in various conditions. Volumes can be converted to mass by the conversion factors given in **Appendix B** and according to this conversion the injected CO_2 amount is 18.2022MT. From the PRT files generated at the end of both these compositional simulation runs, along with the graphs obtained using the keywords FCGMM, FCGMI and FCWM i.e. molar amount of specified component mobile, trapped in gas and dissolved in water respectively total CO_2 molar amounts are obtained. These amounts give an estimate of how the injected CO_2 is stored in the reservoir and help in predicting the dominating trapping mechanisms. The total amount of moles in kg-moles for the field and for the two sub-regions is reported.

In depleted gas reservoirs, the expected dominant trapping mechanism is free-gas/structural trapping particularly at greater depths of reservoir where the injected CO_2 is in a supercritical state and is less than water making buoyant forces stronger. Additionally, the three other trapping mechanisms (residual,

dissolution and mineral trapping) that are highlighted in Section 2.3.3 are also present. In this thesis, the mineral trapping mechanism is not taken into consideration.
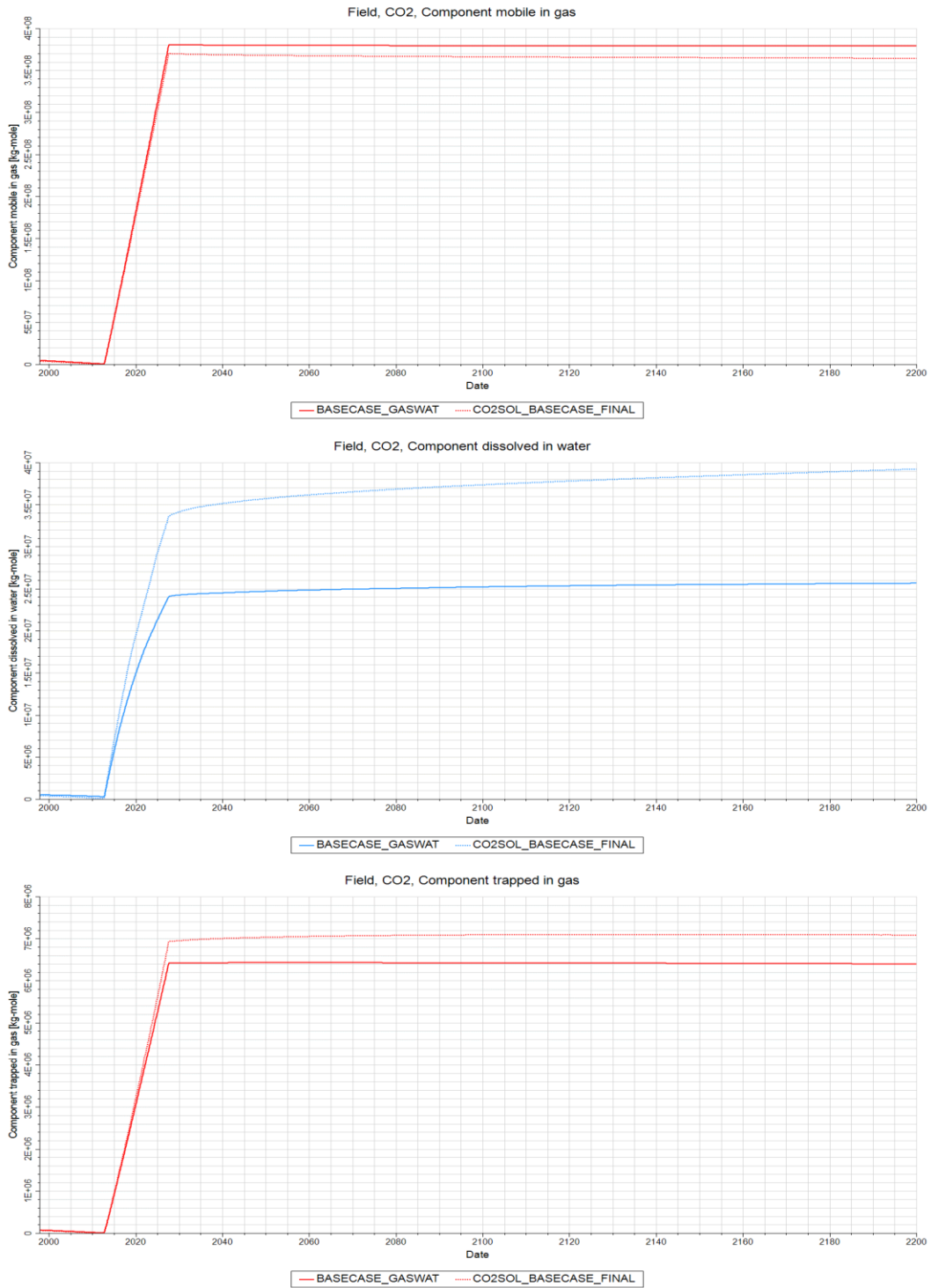
Figure 7-4 CO2 trapping mechanisms: (Top) Free/mobile gas trapping. (Middle) Dissolution trapping in water. (Bottom) Residual gas trapping.

It can be seen in the Figure 7-4 that for both cases the most prominent mode of trapping is the structural trapping which is mainly due to the fact that the injected CO_2 is in a supercritical state as the depth of the reservoir is above 3000m. At the end of the injection period, in 2027, a total of 3.81 E08 kg-mole and 3.71 E08 kg-mole is present in mobile phase for GASWAT and CO2SOL cases respectively, while dissolved trapping has 2.41E07 kg-mole and 3.35 E07g-mole in the two methods respectively. The dissolution trapping is more than the residual gas trapping because of higher irreducible water saturation. This means that the injected CO_2 is able to push away only 63% of brine in the pores while the remaining 37% is held back. This leads to a larger amount of brine being available for the CO_2 to be dissolved. The residual gas trapping was the least dominant trapping mechanism in both the methods mainly due to a low value of critical gas saturation, however, CO2SOL case had 6.95 E0 kg-mole relative to GASWAT`s 6.44E06 kg-mole of CO_2 which may be due to differences in the equations used for mobility and the redistribution of pressure in the reservoir caused by density differences. At the end of relaxation period, the dominant trapping mechanism is still the structural trapping in both cases where a very slight decrease is noticed. The amount of dissolved gas in both cases has increased relatively higher than the other two mechanisms. In Dec 2199, 2.57 E07kkg-mole and 3.93 E07 kg-mole of dissolved CO_2 is present respectively. During relaxation periods, a bit of mobile CO_2 gets dissolved in brine and some part gets trapped.

Another significant results were the number of moles of CO_2 present in each region. This is done to estimate the amount of CO_2 that moves from the main reservoir region to the top of the reservoir while the layer 4th (Not fm.) was considered as an impermeable layer by assigning it a value of 0.0001mD. The **Error! Reference source not found.** below makes a comparison of the total amount of CO_2 moles present in each region at the end of injection period and provides a rough estimate of how much CO_2 has been leaked a cross the layer or through the fault which although has a lower transmissibility value but maybe providing a leakage path way. The injection of CO_2 is done in the layer 7 to 18 in the z-direction that lie beneath the assumed caprock. Different years are chosen to make a comparison of CO_2 plume movement across time and space. Just before the start of injection slightly different moles of CO_2 are present in each region because the differences in initializations in the two approaches. GASWAT uses five components while CO2SOL has four components. The end of injection occurs in the year 2027, and it can be seen that a significant portion of CO_2 has migrated from region 2 to region 1 across the fault or the impermeable layer 4. The amount of injected CO_2 is same for both cases however, the differences in numbers can be attributed to the initial moles already present and during production some CO_2 might have produced differently in each case. Overall, once the injection stops the loss in CO_2 into the first region is very low, for instance in GASWAT case, Region 1 had 366.79 M kg-mole of CO_2 present in 2027 and this amount reduced to a value of 362.45 M kg-mole in 2200, while Region 2 increased from 45.23 M kg-mole in 2027 to 49.58 M kg-mole of CO_2 in 2200. This therefore indicates some of the CO_2 has been lost to the top of the formation above anticipated caprock.

Table 7-1Molar distribution of CO2 in region 1 and region 2 of the E-segment

	GASWAT		Total moles	CO2SOL		Total moles
	Total CO₂ Moles			Total CO₂ Moles		
	Region 1	Region2		Region 1	Region2	
	M kg-mole	M kg-mole	M kg-mole	M kg-mole	M kg-mole	M kg-mole
2012	0.39	1.36	1.75	0.34	1.00	1.34

2027	45.23	366.79	412.02	48.02	361.39	409.41
2100	46.34	365.70	412.04	52.18	359.46	411.63
2200	49.58	362.45	412.04	55.42	356.21	411.63

The output of the CO_2 mole fraction is also requested during the simulation runs that gives an idea of the movement of the injected plume in the reservoir. It helps in visualizing whether the inserted gas is diffusing across the formation laterally or the vertical movement is dominant. Figure 7-5 shows an i-j slice of the layers into which the well I2 has been placed. The layers look fully saturated with CO_2 at the end of injection period. With time the plume migrates downwards due to gravity as the reservoir is at a down-dip angle. Both GASWAT and CO2SOL cases, show a similar distribution of the plume except for the fact that some grid cells near the fluids contact have a higher proportion of CO_2 mole fraction in the CO2SOL case. It can also be observed that in both cases the GWC has been shifted slightly downwards. Plume redistributes itself in the observed layers. With time molar fraction of CO2 is also seen to increase in the upper layers. Buoyant forces are the main cause of this rise in addition to the fact that a proportion of it is transmissible across the already present faults in the system having high transmissibility values.
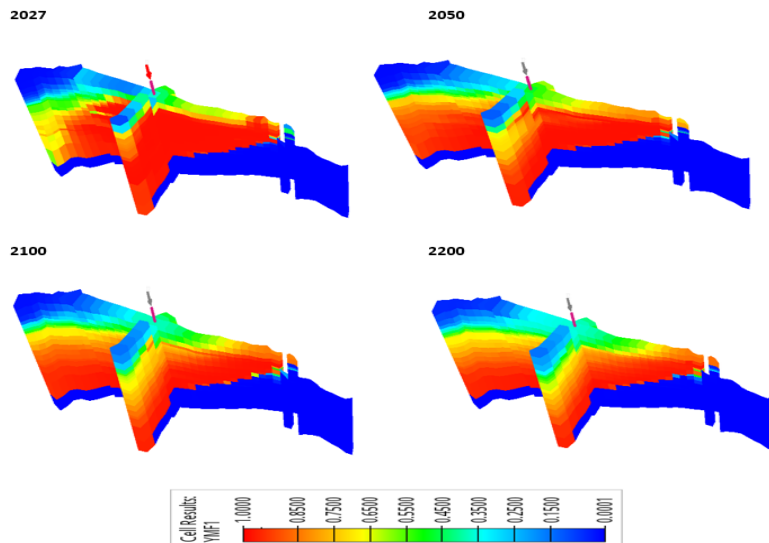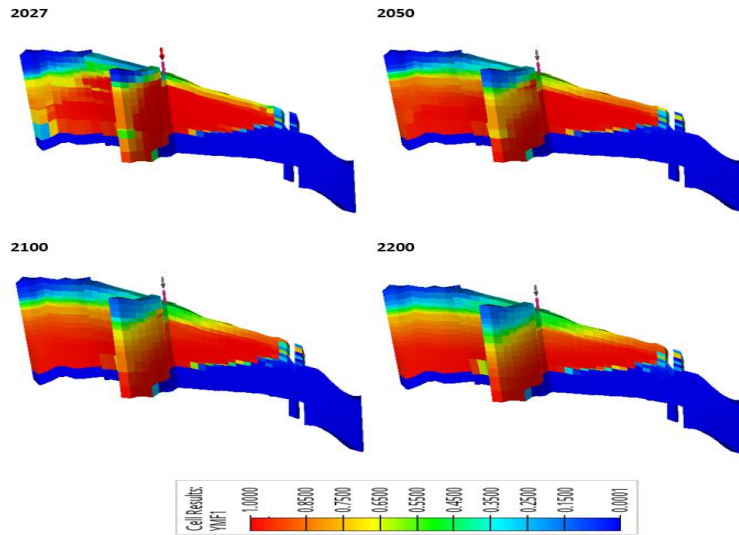
Figure 7-5 Mole fraction of CO2 (top) GASWAT (bottom) CO2SOL

As mentioned earlier, some of the CO_2 travels to the top layers of the formation above the fourth layer. This is shown in Figure 7-5 that makes a comparison between the two cases. The migration of CO_2 either vertical or horizontal has been approximately similar at the end of injection period and during the relaxation period for both cases. CO_2 plume dominantly moves downwards and away from the injection area due to the gravity effect and pressure redistribution in the reservoir.
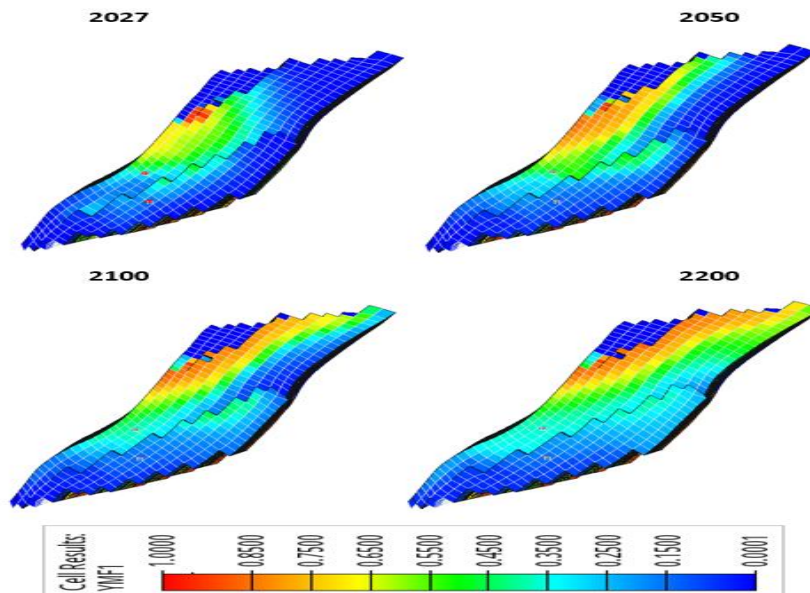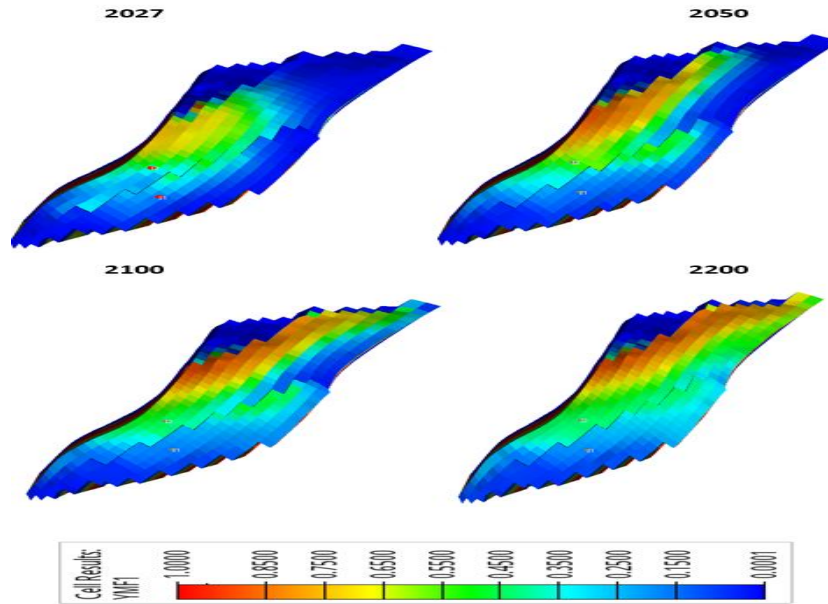
Figure 7-6 Top view of the Co2 mole fraction in the reservoir (top) GASWAT (bottom) CO2SOL

Adaptive implicit (AIM) approach was used to simulate both cases. The simulation runs were not very long in each case because a smaller number of grid cells were active, only four or five components are present and overall simulation period is only for almost 203 years. It can be noticed from Figure 7-7 below that the number of linear iterations for the CO2SOL were greater than that of the GASWAT case mainly due to the fact that CO2SOL deals in three phases while GASWAT is applicable for two phases only. Linear iterations are higher for each case as compared to the Newton iterations. No convergence errors were observed in both cases.
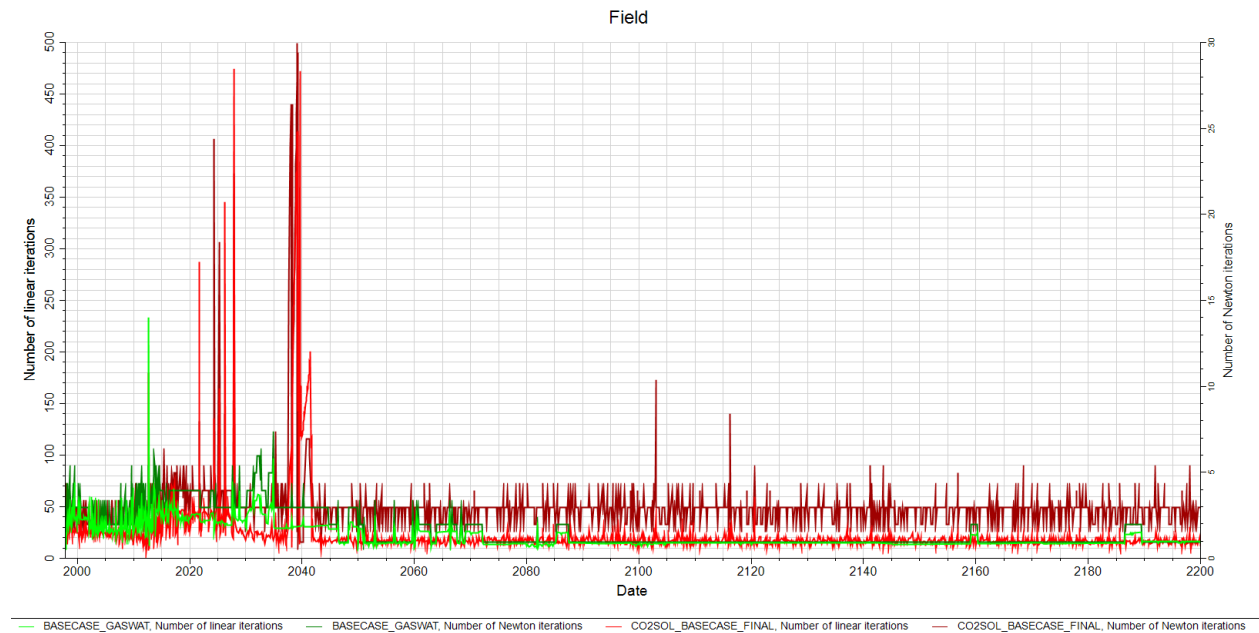
Figure 7-7 Number of iterations taken for the simulation runs

Overall, the two suggested method for CO_2 injection for the purpose of storage can be really handy in accomplishing the research and development in the area of energy transition. It is seen from the results that for both cases the dominant trapping mechanism is structural trapping where almost 90% of the CO_2 injected is stored in this way, followed by dissolution trapping and residual gas trapping. This means that the buoyant forces are dominant since the injected CO_2 is in a supercritical condition and the distribution of the plume from the near well area towards the down dip end of the reservoir in both cases explains the high mobility of reservoir which is due to the higher value of relative permeability of gas and a relatively smaller residual gas saturation which traps CO_2 residually. Pressures do not reach the set fracture pressure limit indicative of a possible elongated period of injection or a greater injection rate. It is however important to study how the pressure develops around the wells to determine the injectivity of the formation particularly within the near well are. Here, the bottomhole pressures and also the pressures in nearby grids were in accordance with the reservoir pressure. It is important to understand the driving mechanisms` including viscous, capillary and gravity forces contribution to injection process. These forces in turn are dependent on the reservoir properties, well locations, dip angle, pressure of the reservoir, mobility ratios and density and temperature. Capillary forces were not present in the runs. Therefore, the dominating forces are the viscous and gravity forces. In the region near the wells viscous forces were stronger and pushing the hydrocarbon and brine behind by miscible displacement process, and available gases are mixed overtime by molecular diffusion. However, when the CO_2 diffusion coefficient at reservoir conditions is less than the value of $10^{-6}\,m^2/sec$, the diffusion effect on the mixing of gas and CO_2 dispersion can be ignored. For these simulation runs, the set value is greater than this limit, making diffusion effects significant. This diffusion makes sure that gas inter blocks diffusive flows by describing the diffusivity input for each component. The concerning equations for diffusivity can be found in the (Schlumberger, 2021) manual. After the lateral migration of CO_2, the plume starts migrating vertically into the top of the formation. From the figures showing CO_2 vapor mole fraction over the years, it is clear that most CO_2 gets stored away from the wells and towards the dipping end of the reservoir. This shift from a viscous dominated lateral movement to a gravity dominated vertical movement is attributed mainly because of the pressure gradient of the reservoir being low and a creation of density differential as the supercritical CO_2 is less dense than the methane and brine. This is also an added advantage to the storage job since the probability of leakage across the wells is also minimalized.

7.2   Sensitivity Analysis

Reservoir simulations using numerical techniques are composed of static and dynamic models that are based on petrophysical studies like logging, seismic interpretations, geological studies, production history matching and field observations and monitoring. However, what exactly is present in the subsurface and what factors are controlling the drive mechanisms, productivity, injectivity or storage are highly uncertain. This is particularly in cases of early field development. Although, depleted oil and gas reservoirs have a slight edge over other geological formations in terms of availability of data leading to reduced uncertainty, yet it is extremely important to study various aspects of reservoir rock and fluid properties and initialization of the simulation runs that could influence the project development and can help in assessing the associated pros and cons before hefty investments are made. Some of these influencing factors including reservoir heterogeneity, GWC and initial fluid saturations, varying injection rate, reservoir fluid properties and aquifer presence are studied in detail in the following sections. These sections mainly describe pressure development during production and injection phase, CO_2 footprint highlighted by defining the total number of moles present in both regions (above and below the seal) and displaying the gaseous CO_2 mole fraction with time, and overall trapping mechanisms in short term (during injection) and over a period of more than 170 years, i.e. the relaxation period.

7.2.1   Reservoir Heterogeneity

The simulations were run for high and low permeability cases and the necessary amendments made in the DATA file are explained in Section 6.5. Before injection is begun the reservoir has been kept under production for a fifteen year period. The targeted rate of production is 1.8E09 Sm3 until the reservoir reaches the abandonment pressure limit of 50bar. Permeability is a key parameter affecting the productivity of a reservoir and pressure profile of a geological reservoir. According to the Darcy`s law, the pressure drop in a porous medium is inversely proportional to the absolute and relative permeability in a reservoir. In case of production it is expected for a higher permeable zone to be able to produce hydrocarbon from it for a greater time period and reaches the pressure limit of end of production at a later time. According to Figure 7-8 the least permeable reservoir, the case having a reduced permeability depletes much faster than the base case and the high permeability case. The production well P2 has a higher productivity compared to the production well P2, which can mainly be attributed to a higher permeability in that region and lower pressure drawdown. BHP limit for the low permeability case for both wells is reached in the first half of 2010 almost two years before the target production date. For the base case, this BHP limit is reached towards the end of 2011, almost eight months before targeted end of period, while in the highest permeability case, both wells manage to produce hydrocarbons up until six months before the production period ends with the desired rate of production. The field pressures are similarly distributed based on the pressure profile of the wells` BHP. For low permeability case the overall reservoir pressure depletion is the lowest, i.e. a value of 58.68 bar since the BHP limit is reached earliest and production rates are rearranged to cater for that limitation. Similarly the base case pressure reaches to a value of 53.6 bar and the least value, 52.2 bar is for the highest permeability case. These field pressures shown in Figure 7-10 are the initial pressures for the start of injection. The field`s rate of production and the cumulative production is shown in Figure 7-11. The

total produced volumetric amount of hydrocarbon gas is 8.94 E09 Sm3, 9.26E09 Sm^3 and 9.34E09 Sm^3 from the low, base and high case respectively. Similar to productivity, injectivity also greatly depends on the permeability of the reservoir. For injection, the buildup is highest in the low permeability case. The BHP as well as the overall field pressure is highest. This is mainly because reservoir layers having low permeability, makes it difficult for the injected CO_2 to displace the reservoir fluids. The field pressure values reach 177.5, 173, 172 bar respectively for low, base and high permeability case. Which again are much less compared to the fracture pressure limit. The injected amount of CO_2 in all three cases is 9.72E09 which is greater than the produced amount from it. Volume of the two gases and the compressibility in the subsurface is the main reason why more volumetric injection of CO_2 is possible in comparison to the amount of hydrocarbons that can be produced from it. CO_2 is more compressible than methane. Once CO_2 (in a supercritical state) is injected into a geological formation it rises to the upper layers due to buoyancy factor or the differences in the density of the formation fluids and the injected CO_2. Permeability also determines how the CO_2 plume is distributed in time and space. Mostly highly permeable reservoirs are better at aiding in lateral movement of the CO_2 plume, particularly in this case when horizontal permeability is relatively higher than the vertical one, therefore, making viscous forces more dominant. This is also why the number of moles of CO_2 at the end of injection are lowest in the high permeability case in Region 1, as the lateral movement of CO_2 is favored then the vertical one and the opposite is true for low permeability case. Table 7-2 summarizes the molar distribution in M kg-mole of CO_2 in the years 2027 (end of injection period), 2100 and 2200 in the two regions above and below the caprock. At the end of injection, Region 1 in the high permeability case, had 32.60 M g-moles of CO_2 while 48.78 M kg-moles in low permeability case.
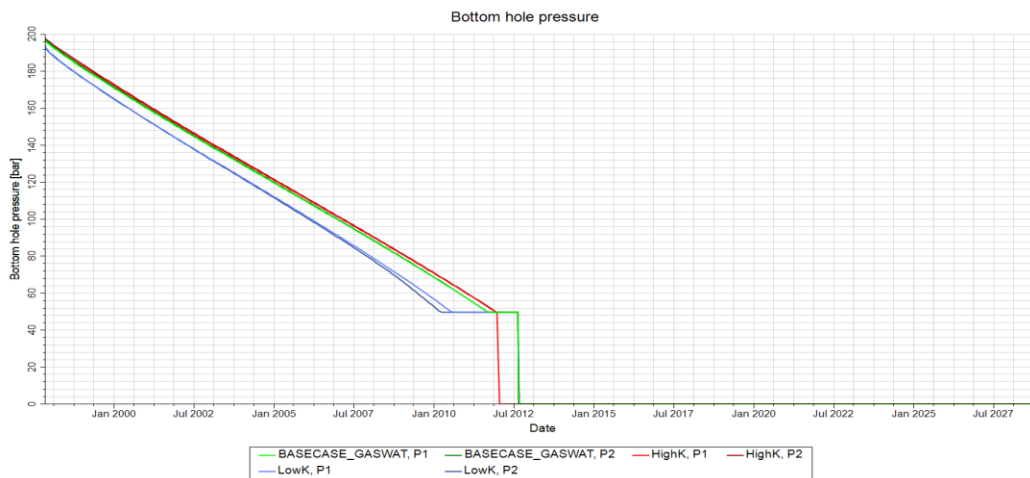
Figure 7-8 Bottomhole pressures for the production period for high & low permeability and base case.
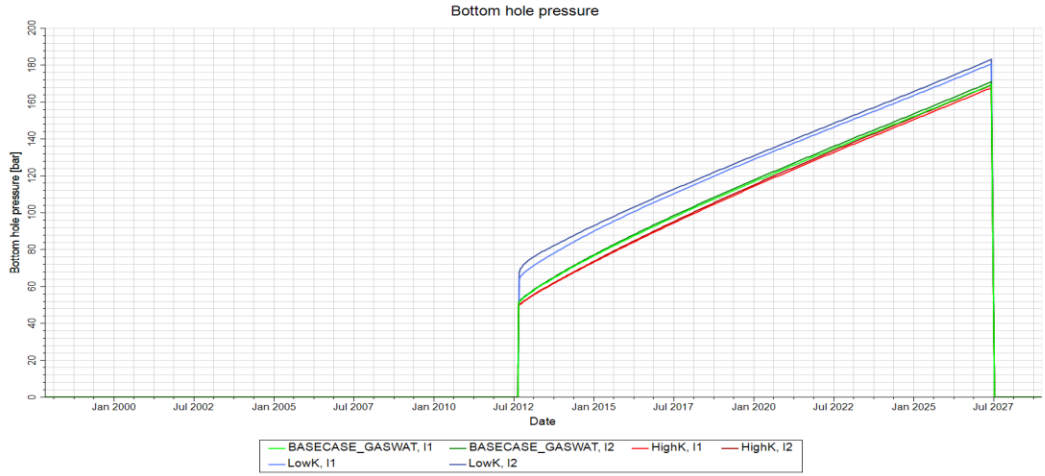
Figure 7-9 Bottomhole pressures for the injection period for high & low permeability and base case.
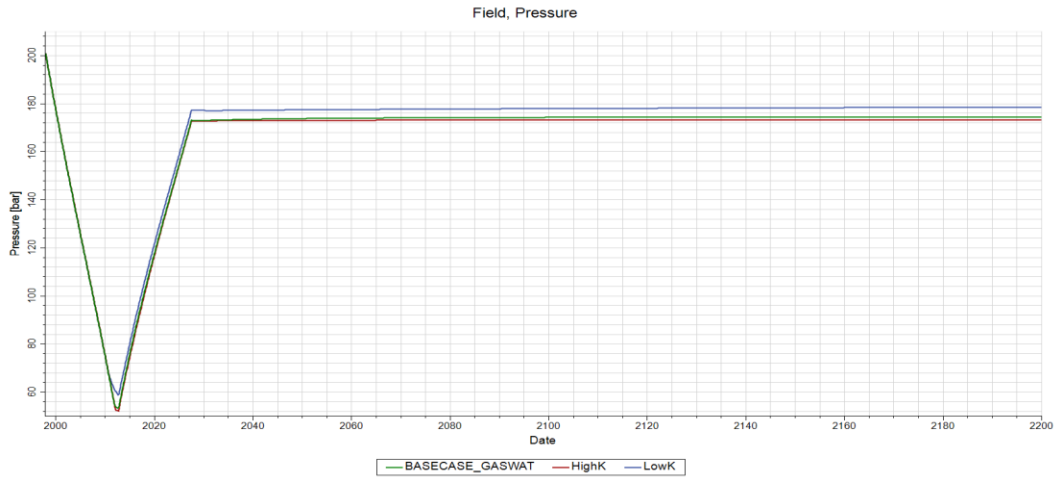
Figure 7-10 Field reservoir pressure

a)
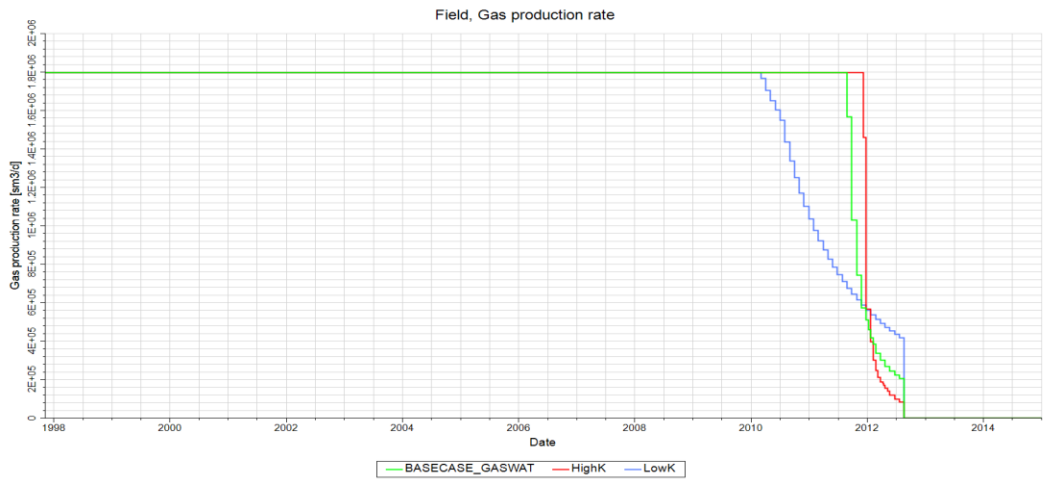
b)
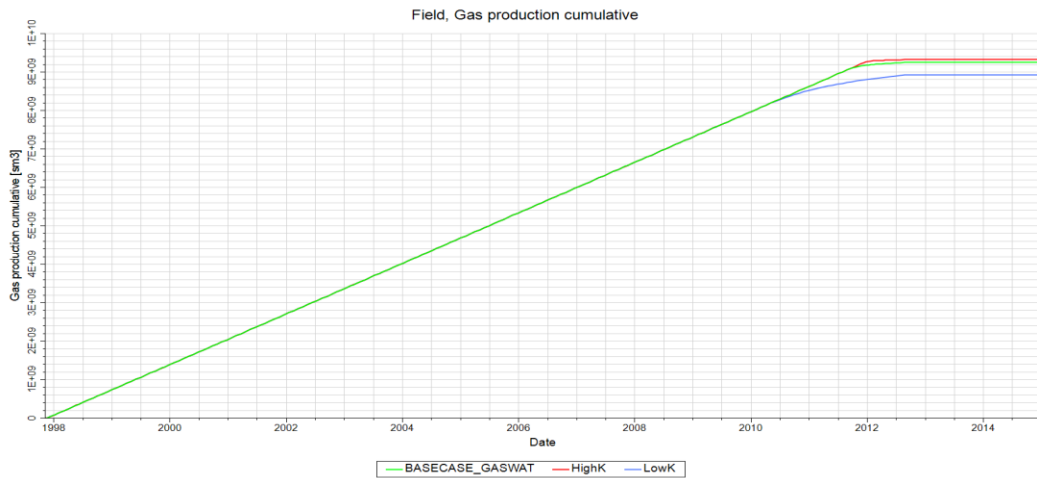
Figure 7-11 Gas Production (a) Rates (b) Cumulative

Table 7-2 Molar distribution of CO2 in the years 2027, 2100 and 2200

	LOW K		Base		High	
	Total CO_2 Moles		Total CO_2 Moles		Total CO_2 Moles	
	Region 1	Region2	Region 1	Region2	Region 1	Region2
	M kg-mole	M kg-mole	M kg-mole	M kg-mole	M kg-mole	M kg-mole
2027	48.78	361.18	45.23	366.79	32.60	377.19
2100	52.54	359.66	46.34	365.70	42.75	369.25
2200	50.93	361.27	49.58	362.45	49.89	362.11

Although, a seal layer is present in the reservoir, yet some of the CO_2 moves to upper layers of the formation. This movement could be mainly across some of the faults that have not been made fully impermeable by having their transmissibility reduced. However, based on the pressure buildup in the reservoir, even for low permeability case, the pressure is not high enough that could result in fracturing or making the faults a complete leakage pathway. CO_2 molar fraction is also greatly impacted by permeability of the reservoir. As can be seen in Figure 7-12 CO_2 mole fraction is very densely present in near the well area in the low permeability case relative to the high permeability one after the end of injection. This is due to the fact that lateral movement in the reservoir is limited and more CO_2 stays within this area. It can also be seen that the redistribution of the plume is also different in each case. High permeability allows the reservoir moles to distribute across a greater extent with respect to time. In high permeability case at the end of simulation period, the CO_2 mole fraction is almost 0.875 compared to almost 1 value of the low permeability case in perforated intervals. Some of the CO_2 can also be seen in the top layers above the seal particularly for the low permeability case, which have migrated vertically because of buoyancy forces due to gravity effect and density differences at the same time viscous forces are not very supportive. Vertical movement of the plume was seen to be similar in all cases according to the molar fraction of CO_2 vapor present in Region 1, mainly because of the fact that vertical permeability had been kept constant in all simulation runs.

79
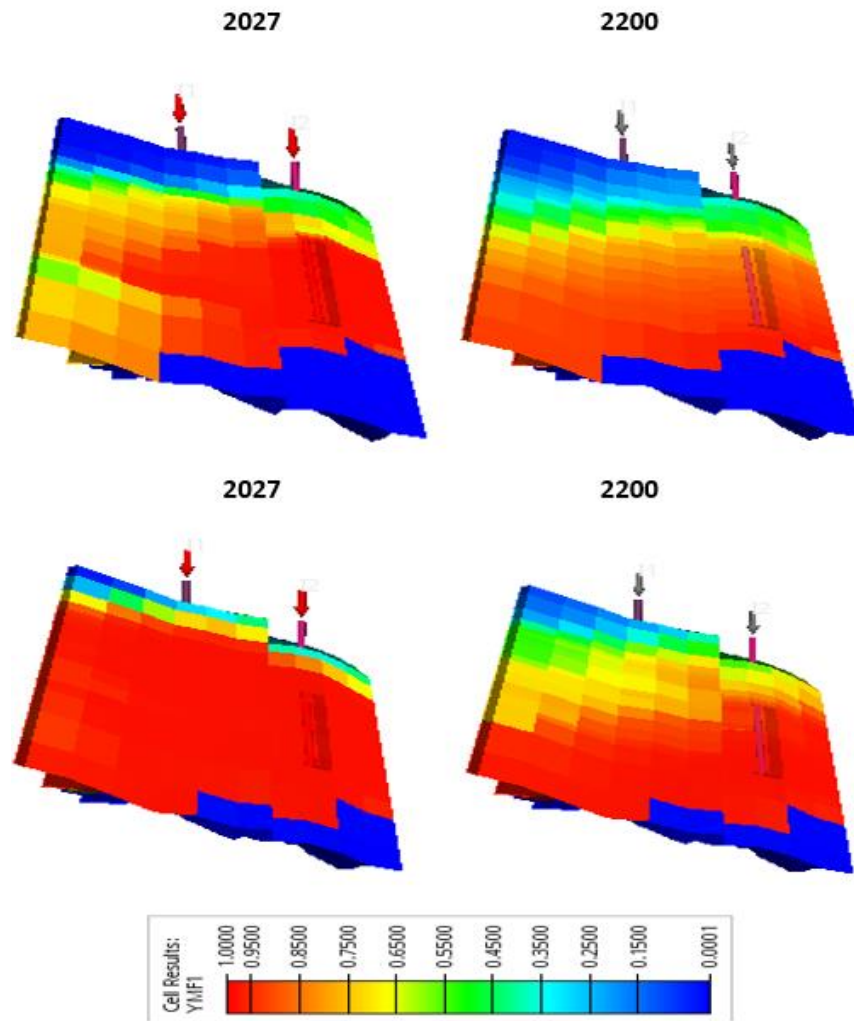
Figure 7-12 Cross-sectional view of the molar fraction of gaseous CO2 in the layer of injected well I2 (upper) High Permeability (lower) Low Permeability

In addition to pressure profiles, permeability of a reservoir can impact the trapping mechanism of the injected CO_2. Study of trapping mechanism as discussed in earlier chapters of this thesis, is an important aspect of safe and long term CO_2 sequestration. When CO_2 is injected in a gas reservoir, it displaces the brine and the hydrocarbon gas, and mixes with the resident gas along with flowing upwards due to buoyancy forces caused by density differences. During this process, in the short term, a proportion of CO_2 is capillary trapped as the residual CO_2 saturation in narrow pore throats. For longer periods, dissolution of CO_2 in brines can occur forming an immobilized dissolved phase. Similarly, some of the injected CO_2 is immobilized as free gas in the storage medium. Reservoir heterogeneity can impact this trapping procedure to a certain degree.

With increased permeability of the reservoir, injected CO_2 is expected to have an increased mobility, while on the other hand, with a reduced permeability the mobility of CO_2 is hindered. Hence, one may expect the CO_2 to stay in pore spaces of one particular grid for a longer time period. This gives an opportunity for it

dissolve more in the formation brine. According to the graph showing the relationship of CO_2 component dissolved in water, component in mobile gas, and component trapped in gas against the injection and relaxation period, given by Figure 7-13(top) the case with the lowest permeability had the greatest component dissolved in water relative to the other two cases. Structural trapping is once again the dominant trapping mechanism in all of these cases. After the injection period ends, about 2.52 E07 kg-mole of CO_2 is dissolved in brine which is slightly higher than the values of 2.41 E07 kg-mole and 2.38 E07 kg-mole of CO_2 respectively. In all three cases, the CO_2 in the mobile phase is almost equal in the year of injection as well until the period of relaxation ends. According to Figure 7-13(middle), this value is 3.80 E08 kg-mole of CO2 which makes almost 92% of overall injected CO_2. In addition to this, the least dominant trapping in all the three cases is component trapped in gas phase and shown in Figure 7-13 (bottom), the low permeability case has the most amount of CO_2 trapped in this way amongst all of them. This again is due to the mobility of fluids in the reservoir. When reservoir is relatively immobile, CO2 injected tends to be held back more by the pore throat as the residual CO_2 saturation once buoyancy forces come into play. However, relative to other defined trapping mechanisms, this is the least dominant one. The primary reason is because the critical gas saturation is only 1%. This means that most of the injected CO2 manages to displace the resident gas and the brine and only 1% of the total pore space is left to residually immobilize gas. This is also confirmed by the findings in the study conducted by (Raza, et al., 2017) where the effect of residual gas saturation on CO_2 was examined. A sensitivity study by using a higher residual gas saturation is also conducted and is discussed in Section 7.2.2. Overall the graphs reflect that during the initial period of injection and almost until the end of injection as well, the trapping mechanisms follow a similar pattern during all cases. This may be due to the fact that other fluid properties, temperature and depth of injection are same and overall CO_2 phase behavior is identical. During injection the principal mode of trapping is largely structural, while once the injection stops dissolution trapping can also become prominent as explained in the literature review. The value of salinity used here is 0.51E-03 kg-M/kg which can be one of the explanations why dissolution trapping is not very dominant as it decreases with larger salinity. Mineral trapping may also be present, however, it is not modelled in these simulation runs. The post injection behavior clearly reflects that component trapped and free in space has remained fairly constant that shows that there was very minute change in trapping mechanism once the injection stopped.
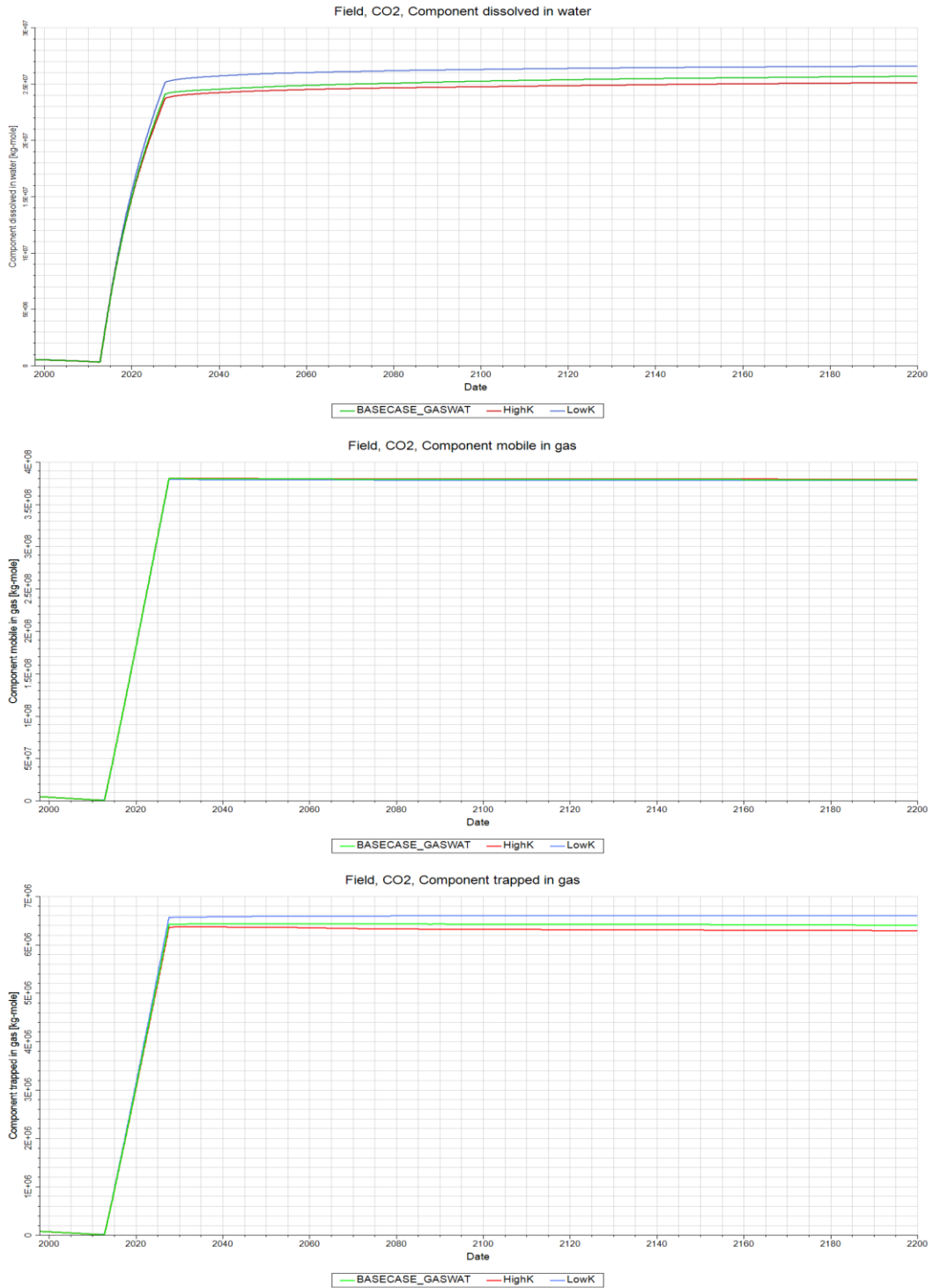
Figure 7-13 Trapping mechanisms in the low base and high permeability case (top) Dissolution trapping (middle) Structural trapping (bottom) Residual gas trapping

To further investigate injectivity of the reservoir near well grid blocks are observed and pressures are determined. The selected grid blocks have variable permeability and can be used to further confirm the

notion that due to low permeability injectivity and productivity can be affected negatively. The table below summarizes the locations of the chosen grid blocks and their corresponding permeability values.

Table 7-3 Permeability in grid blocks close to the injector/production wells

Locations	Permeability (mD)		
	Low	Base	High
10 63 15 (near I1/P1)	8.1	81.4	813.6
11 64 16 (near I1/P1)	156.6	1566.0	15660.0
7 66 11 (near I2/P2)	5.3	52.9	529.2
8 65 16 (near I2/P2)	172.0	1720.0	17200.0
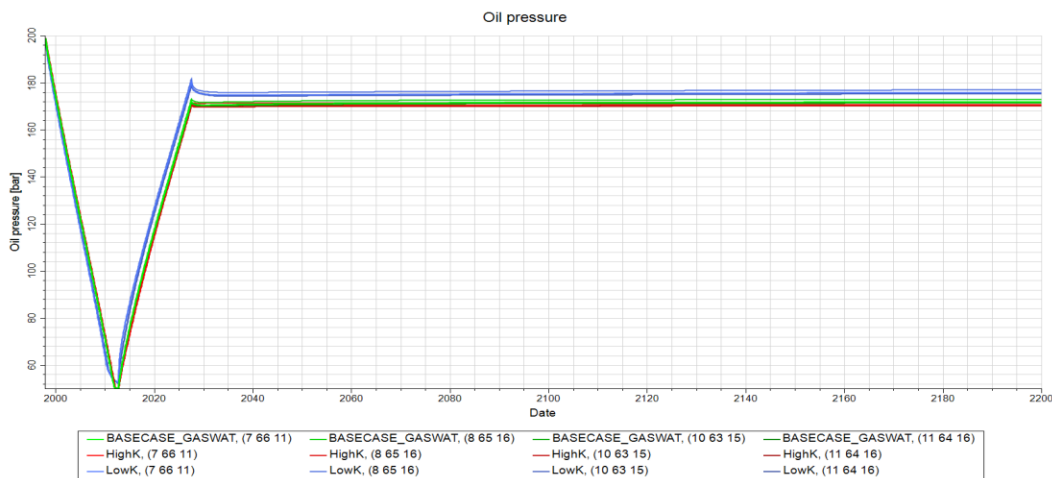
Figure 7-14 Grid bloc pressures in the near well region

The results` chart shown in Figure 7-14 above clearly demonstrates the predicted behavior of the case of injection in varying permeability reservoirs. The grid cells adjacent to the injection wells, particularly 10 63 15 and 7 16 11 cells for Low K case, have the highest pressure buildup in it of about 182 bars while the other two relatively more permeable grid cells are at about 172 bars. The post injection behavior is almost similar of all the grid cells and they reach a plateau after declining slightly. This decline can be because of the lateral movement of CO_2 further towards the boundaries of the reservoir model once injection stops. It can be noticed that the block pressure trend almost displays the similar behavior as the bottomhole pressure.

Overall, reservoir heterogeneity can have impacts on the multiphase flow of CO_2-brine-methane and can be shown with a variation in permeability. The storage capacity is mainly determined by porosity, while permeability can influence injectivity. From the results discussed earlier, it is revealed that the residual, dissolution and structural trapping depict a similar behavior in the initial stages of injection, however, towards the end of injection period some differences arise. The low permeability case had seen more dissolution trapping and residual gas trapping which leads us to the conclusion that Co2 immobilization in gas reservoirs after injection is enhanced due to reduction in permeability of the reservoir. This is also confirmed b one of the previous studies conducted by (Raza, et al., 2018).

7.2.2 Deep GWC and Different Initial Saturations

Depth of fluid contacts are very significant parameters that are needed to be examined when reservoir engineering is performed. They can considerably amend how particular fluids behave in terms of flow and transport in a geological formation that ultimately influence production as well as injection projects. With the base case, as mentioned previously, the GWC was kept at 2750m. Figure 7-15 displays how the water and gas saturation are distributed in the reservoir when GWC is initialized at 2900 m. The blue area represents a region of Sw =1 which lies in the south side dip of the reservoir. The majority of the reservoir in this case is covered with resident hydrocarbon gas which would mean greater volume is available for the injected CO_2 to diffuse through and thus creating less pressurization in the pores since the injected CO_2 volume remains constant throughout. Similar to the deeper GWC, the lower (Swi = 0.2) and higher (Swi =0.4) initial/connate water saturations and a high ($S_{gr} = 0.027$) critical gas saturation case is also tested. A low initial water saturation means lesser immobile water is present in the reservoir therefore the capacity to store CO_2 increases and thereby the final reservoir pressure is lower than the base and the high initial water saturation case. Similar to other cases, before injection is begun the reservoir has been kept under production for a fifteen year period with a targeted rate of production of 1.8E09 Sm3 until the reservoir reaches the abandonment pressure limit of 50 bar. Production of hydrocarbons is also affected by the depth of the fluid contacts. It can be seen from the field pressure profile that the case with deeper GWC depletes the least of all the cases to a value of 93 bars, due to a larger availability of hydrocarbons in the reservoir. Field pressure profile for all these cases is presented in Figure 7-16. Similar to the deeper GWC case, if the reservoir has a lower connate/initial water saturation, the pressure depletion is less at the same injection rate because of the availability of larger volume of hydrocarbon. In this case it depletes to a value of 79 bar. On the other hand, it is observed that high S_{wi} causes a steeper decline in pressure, the production has to be adjusted and doesn't produce at the plateau rate of $1.8E0\ 6Sm^3/day$. At the end of production period, it reaches the value of 52.8 bar. However, in the case of a higher critical gas saturation pressure is not affected and follows a similar trend as the base case and reaches a minimum field pressure value of 53.3 bar. This means that lower critical gas saturation has not caused a change in the pressurization of the reservoir. However, it does have an impact on trapping mechanisms which are explained later. Total amount produced is 9.72 E09 Sm3 for deeper GWC and low Swi case, 9.2647E09 Sm3 for base case and high critical gas saturation case and 8.85679 E09 Sm3 from the high initial for water saturation case. The production rate profiles are given below in Figure 7-17.
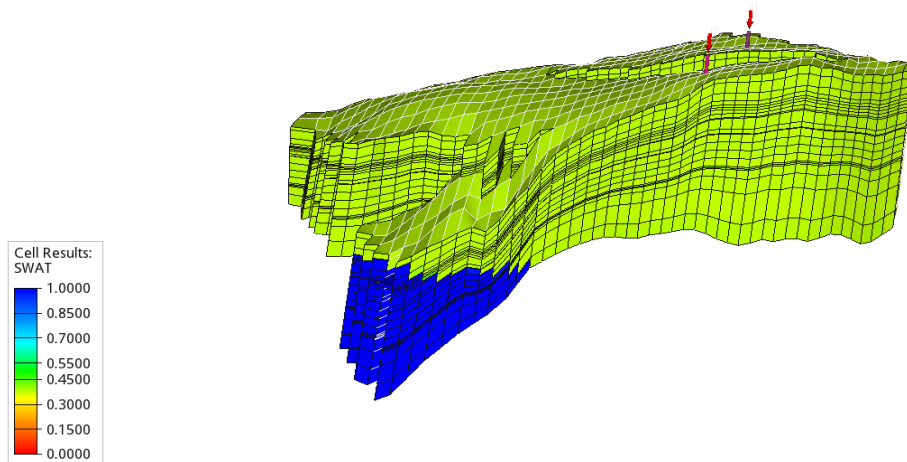
Figure 7-15 Saturation Profile

For injection an expected fluid pressure behavior in each case is observed. The initial pressure before injection in the case of deeper GWC is 93 bar. Towards the end of injection it reaches 174 bar. The total buildup in the reservoir is only 81 bar as compared to the base case`s 120 bar. This difference is significant because it gives an explanation of transport and mobility of CO_2 in the presence of other fluids. When the GWC is shallow, the injected CO_2 which is in a supercritical state must push away the reservoir brine more as compared to when the contact is deeper. This causes the additional pressure buildup. When mostly hydrocarbon is present, it is easier for the injected CO_2 to mix and diffuse into the reservoir. In the case of lower initial water saturation, the same concept applies. The pores are filled by more hydrocarbons as compared to the base case. A low initial water saturation means lesser immobile water is present in the reservoir therefore the capacity to store CO_2 increases, a lower buildup of 96.5 bar after starting at 79 bar and thereby reaching the final reservoir pressure of 175.5 bar which is quite near to the base and the high critical gas saturation case. For high initial water saturation case, the pressurization of the reservoir is similar to the base case for first three years of injection. After that it starts deviating from the base case line and shows an increasing trend, this means that with constant injection, CO_2 starts accumulating more in the near well area and migration is hindered which causes an increased buildup of pressure. This trend continues until the end of injection and the final reservoir pressure for this case reaches a value of 178 bar which is the highest value amongst these cases. Although all these cases have a varied pressure response but since the reservoir as well as the bottomhole pressures remained within the fracture pressure limit of 200 bar, total injected CO_2 amounted to 9.72E09 Sm^3 for all of them. Having a lower initial water saturation and a bigger gas cap makes a reservoir more suitable for injection.
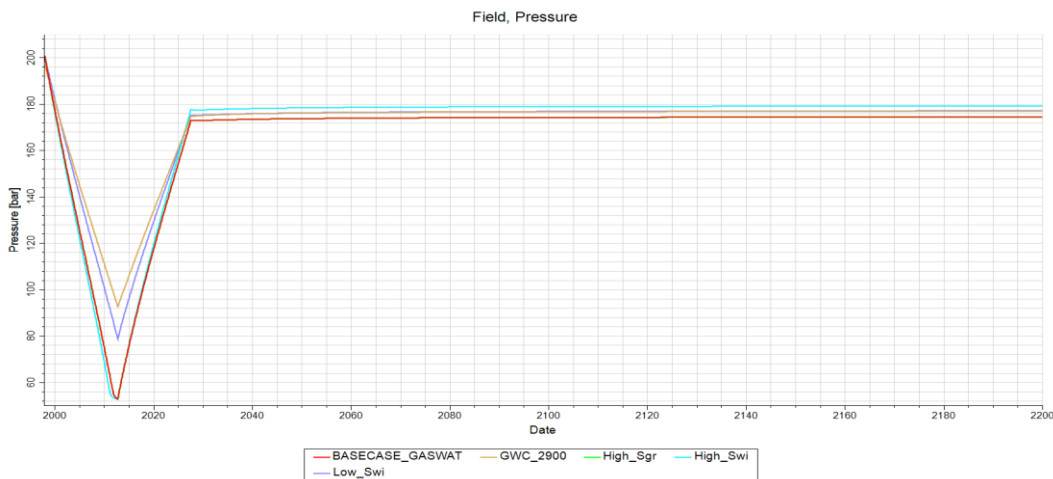
Figure 7-16 Filed reservoir pressure for different initial fluid saturation cases, deeper GWC and base case
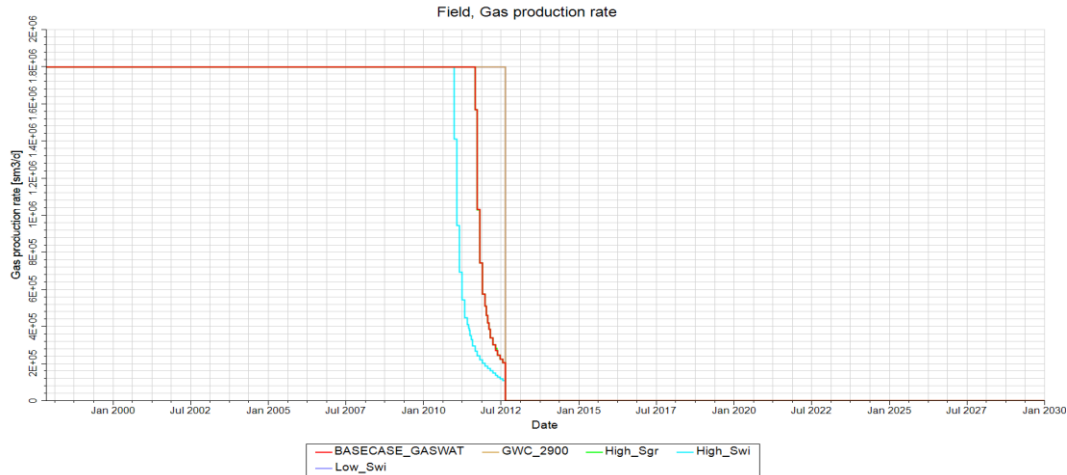
Figure 7-17 Gas production rates for deeper GWC, different initial saturations and base case.

Geological formations typically depleted oil and gas reservoirs and saline aquifers are primary sites for CO_2 sequestration. However, it is important that the injected CO_2 remains trapped in the formation and doesn't leak into the potable aquifers or rise up again. In order to study the leakage of CO_2 in this thesis, two regions are created. Region 1 lies above the caprock layer 4 and region 2 lies below it. The perforations are entirely in region 2 starting from the 7th layer until the 18th. This is done to ensure that the injected CO_2 lies in Region 2 and test if there is some leakage into the top region even in the presence of a seal. Table 7-4 below gives the total moles of CO_2 in the two regions for all the cases under consideration. Leakage rate is very less for all the cases. For low initial water saturation a higher number of CO_2 moles are present in region 2 throughout the years with a small leakage mainly because of a higher capacity is available for CO_2 to get stored in region 2. The mobility of gas is not impacted a lot therefore the number of moles of CO2 are fairly consistent with the base case.

Table 7-4 Molar distribution of CO2 in two regions for different initial fluid saturations and deeper GWC

	Base		High Sgr		Low Swi		High Swi		Deeper GWC	
	Total CO_2 Moles		Total CO_2 Moles		Total CO_2 Moles		Total CO_2 Moles		Total CO_2 Moles	
	Region 1	Region 2	Region 1	Region 2	Region 1	Region 2	Region 1	Region 2	Region 1	Region 2
	M kg-mole	M kg-mole	M kg-mole	M kg-mole	M kg-mole	M kg-mole	M kg-mole	M kg-mole	M kg-mole	M kg-mole
2027	45.23	366.79	42.28	367.51	21.48	389.60	44.06	365.67	42.28	367.51
2100	46.34	365.70	46.34	365.70	25.91	387.40	48.27	363.70	46.34	365.70
2200	49.58	362.45	49.58	362.46	29.81	383.50	51.19	360.78	49.58	362.46

High gas trapping in high critical gas saturation case near the well is expected, CO_2 plume distribution of a cross sectional view, given by Figure 7-18 below of CO2 gaseous molar fraction near injector I2 is given

with a comparison with base case after 5 years of injection and end of injection period. Due to high amount of residual gas trapping in the case of a high critical gas saturation, CO_2 is trapped more near the wells and is not seen in the above layers of the near well region. For base case, the CO_2 rises to the top as more of it is present as free gas and structurally trapped in the fifth year of injection. This flow behavior and trapping mechanism for each case is similar in throughout the injection period. . Overall, the containment is good enough to be considered a successful storage.
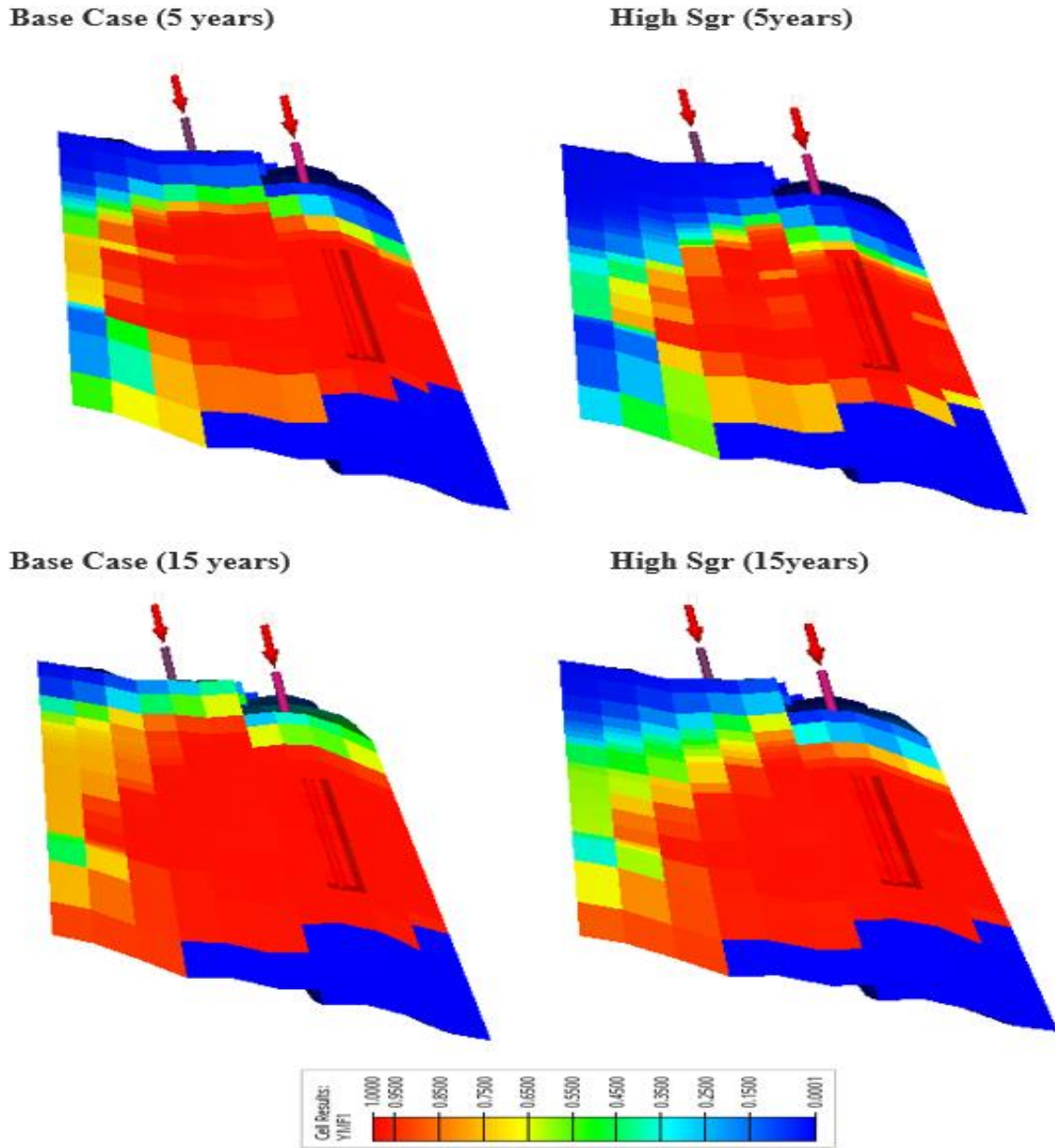
Figure 7-18 CO2 molar fraction in the near well region of base case and high critical gas saturation gas at 5 years and 15 years of injection
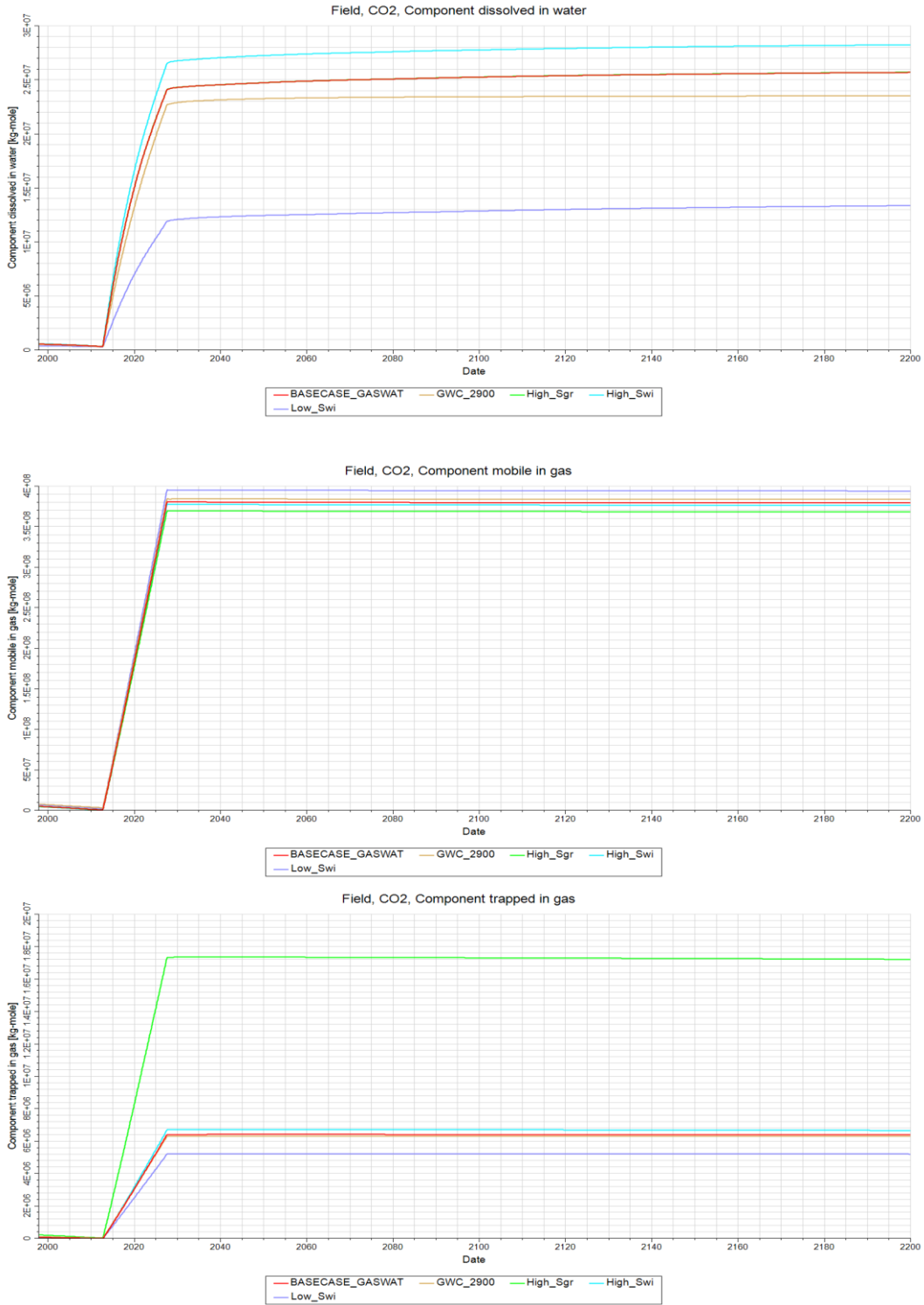
Figure 7-19 Trapping mechanism in the cases of different initial fluid saturations, deeper DWC and base case (top) Component dissolved in water (middle) Component mobile in gas (bottom) Component trapped in gas

In addition to pressure changes, high initial fluids saturation can affect the trapping mechanisms as well. Once CO_2 is injected, the most dominant trapping mechanism in a depleted gas reservoir is structural or

residual gas trapping depending on the reservoir geometry, porosity, permeability, fluid saturations and the capillary pressures.

In the Figure 7-19(top) the amount of CO_2 component dissolved in water in presented. When the initial water saturation is high meaning the pores are filled by a high amount of water, dissolution trapping must be high. This is exactly what is shown by this graph. In the year 2027 around 2.65E07 kg-mole of CO_2 is dissolved in water as compared to a value of 2.41E07 for the base case. At the end of relaxation period this value reaches to 2.83E07 kg-mole, which is due to the fact that some of the mobile phase CO_2 gets dissolved And similarly the case having lowest initial water saturation has the least amount of CO_2 dissolved in water which is 1.19E07 and 1.29E07 in 2027 and 2200 respectively. Furthermore, having a deeper GWC in the reservoir means lower amount of water available for dissolution trapping therefore this gas has around 2.27E07 kg-mole of CO_2 trapped in water which increased to 2.36E07 kg-mole in the year 2200. The amount of dissolved gas in case of a high residual gas saturation is almost same as the base case at the end of injection, which is because water component is not changed in this case. This value seems to increase with time which indicates that in the longer run, dissolution trapping is increasing.

End point saturations of the relative permeability curves, can influence the structural trapping of CO_2 as well. This is shown in Figure 7-19(middle) where the highest amount of free gas trapping is for the case of lowest initial water saturation. This is mainly because most gas has high mobility and dominant forces are viscous and as less water is present to dissolve the gas. This accounts for almost 95% of the total gas trapped for this case. In addition to this, having a deeper GWC makes the injected CO_2 more mobile, as explained previously, due to the lack of enough water to dissolve it or residually trap it due to low critical gas saturation value. Almost 93% of the injected CO2 is structurally trapped in the case of deeper GWC. In addition to this, any increase in the residual gas saturation or the volume of remaining gas alters the amount of the mobile gas phase. It should also be observed that there is an inverse relationship between the amount of free gas and remaining gas till the end of the injection period. In addition, this relationship remains the same during the observation period of 173 years. As the injected CO_2 streams upward due to buoyancy, free gas and remaining gas may limit the buoyancy process through which injected CO_2 act as a free gas. This may also be due to the capillary trapping phenomenon after stoppage of injection. Almost 89% of the injected CO_2 is trapped as mobile phase in this case which is the least of all the cases studied.

For the component trapped in gas phase, critical gas saturation value plays a vital role. From Figure 7-19(bottom) it is displayed that residual trapping increases linearly during the period of injection for all cases and reaches an almost constant value until the end of the relaxation period. It can also be perceived that the case with a higher residual gas saturation has the highest amount of gas trapped due to this capillary effect which is because presence of remaining gas would aid in achieving a high residual gas trapping. Almost 6 % of the total injected amount is trapped residually in this case. For the case of a deeper GWC, which has a high amount gas in place, traps almost 1.5 % of total injected CO_2 with this mechanism. And the least is for the low Swi case where most of the gas is viscous flow dominated making it extremely mobile and trapped mostly structurally.

Overall, the relative permeability data is very important for determining the security of the sequestration project and the fate of CO_2 in the geological formation. High critical gas saturation helps in achieving residually trapped CO2, while having a high initial water saturation makes dissolution trapping the most prominent method of immobilization. CO2 in mobile phase is dominant in case of low initial water saturation, and having a large volume of gas in place also increases the possibility of CO2 being in the mobile phase in the deeper GWC case.

7.2.3   Reservoir fluid properties

Apart from the reservoir rock properties like porosity, permeability, lithology, capillary pressures and wettability, properties of the reservoir fluids can significantly impact the hydrocarbon production or gas injection projects. In this section, the main reservoir fluid properties affecting the CO2 storage process are studied. These include salinity of resident brine, composition of reservoir gas and temperature of the reservoir at the time beginning of the injection. Although the simulations are started with an initial production period, but since they were carried out isothermally, it is safe to assume the initial temperature of the reservoir is the same from the start of injection period as well. Pressures are one of the fundamental observable elements in any reservoir engineering study. During the depletion as well as the injection state the pressure profiles significantly vary depending on the reservoir fluid properties. According to the Figure 7-20(top), bottomhole pressures for a high temperature case remain high, after starting from an initial value of 200 bar as all other cases, and ensuring the complete production of hydrocarbon gas at plateau rate of 1.8E06 Sm3/day for the complete fifteen year period. At the end of production the BHP for high temperature is almost 114 bar for both the wells. Due to high temperatures, the gas expands making larger volume available. This enlarged volume of gas reduces overall pressure loss in the reservoir and thus a reduced loss in BHP as well. The component of the reservoir gas seem to cause an effect on the pressure depletion. In the base case, methane content was 65% and for sensitivity analysis it was reduced to 50%, and the ethane and propane content has been increased. This means the new formation gas is slightly heavier than the dry gas which was dominantly methane. Although wet gases have an additional C5+ component, but for simplicity only three hydrocarbon contents are considered. The depletion is almost similar to the base case for initial five years but then the decline in pressure is less steep. As the BHP limit of 50 bars is not reached in this case, the plateau production with the 1.8E06 Sm^3/day for the complete fifteen year period is achieved hence making a total production of 9.72E09Sm^3. On the other hand, high salinity like the base case produces 9.26E09 Sm3 of total gas. Salinity does not seem to cause a big impact on the bottomhole pressure values during drawdown.

For injection as shown in Figure 7-20(bottom), bottomhole pressure in one of the wells (I2) in the higher temperature case reaches the 200 bar limit almost two months before the end of injection period, thereby not injecting completely at the assigned injection rate and cumulatively injecting a total of 9.7069E09 Sm^3 of CO_2 which is lesser than the targeted amount. For the low methane content case, bottomhole pressure reach almost 176 bars in both injection wells which is above the base and the high salinity case. Salinity again is not greatly influencing the BHP buildup in the injection wells and depict an almost similar behavior as the base case. This may be because the molality value of $0.81 \ 10^{-3}$ kg-M/kg used for this sensitivity case is not high enough to cause a big alteration in the pressure response of the reservoir. It can however impact the trapping mechanism of the storage process. Salinity values prominently influence the injectivity and the near well mobility of the injected CO_2, mainly because it causes salt precipitation and the formation of drying out zones as explained in the Section 3.2.2 .Salt precipitation can impact the injectivity of CO_2 storage process almost four times than of the storage capacity (Sokama-Neuyam, et al., 2020). However, in these simulation runs salt precipitation or CO_2-rock- brine interaction has not been modelled due to the limitation of the simulator.

Overall field pressures given by Figure 7-21 also depict a similar pattern to the bottomhole pressures in each well. The decline in high temperature case to a value of 117 bar is relatively small, mainly because of

an increased volume of fluids due to higher temperature, and similarly, the buildup (from 117 bar to 201 bar) of pressure after CO_2 injection is not very high because of greater compressibility of CO_2 in comparison with natural gas and also because of the bottom hole pressure limit causing a reduced rate in injection. Due to higher temperature, the reservoir pressure seems to increase slightly towards the end of the relaxation period to a value of 203 bar. This is caused by having a relatively greater excited state of gaseous molecules due to the reservoir being at a high temperature while redistributing the resident and injected fluids. For heavier gas case, it is seen that the field pressure declines to a value of 61.9 bar relative to base case`s value of 53 bar after production ends and reaches a slightly higher value of 178.67 bar relative to the base case`s 173.2 bar once injection is stopped. Although the pressures of lower methane content case lie above the base case, yet it can be noticed that this pressure difference decreases towards the end of injection period and this could be attributed to the varying levels of compressibility of the totally dry gas (base) case and an anticipated heavier (low methane case) gas. The study by (Raza, et al., 2017) affirms this notion in which numerical simulation is used and highest pressure buildup is observed in the dry gas case while the least buildup occurs in the retrograde gas case. The pressure response in all cases is almost linear during the injection period mainly because the injection rate remains same throughout. The pressure increases due to the increase of the pore fluid pressure by CO_2. Usually, the pressure diffusivity is almost three to five times larger than the molecular diffusivity causing reservoir pressurization quicker than the molecular diffusion (Raza, et al., 2017) . With a larger reservoir temperature, density of CO_2 is decreased making the CO_2 plume to flow at a higher rate leading to difficulties in monitoring and resulting in a high free gas saturation and over-pressurization of the medium.
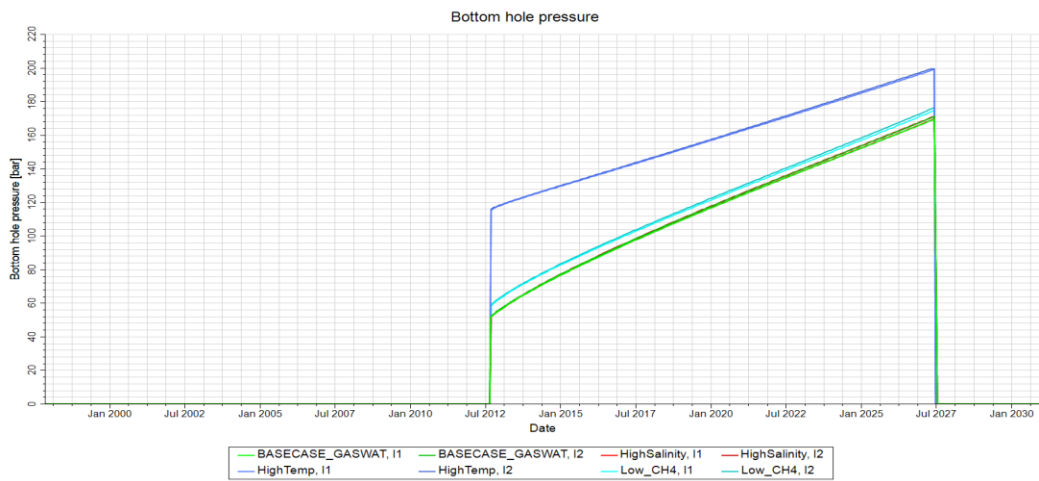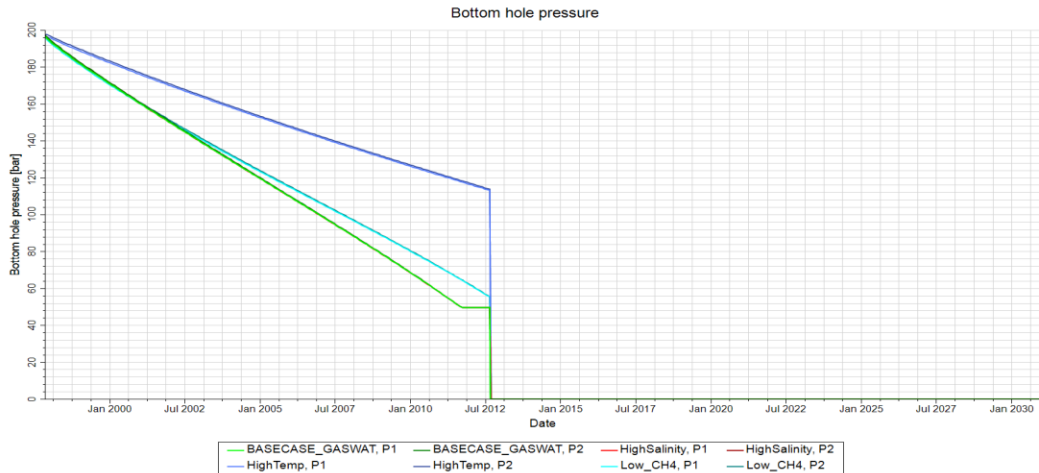
Figure 7-20 Bottomhole pressure for various reservoir fluid properties (top) Production period (bottom) Injection period
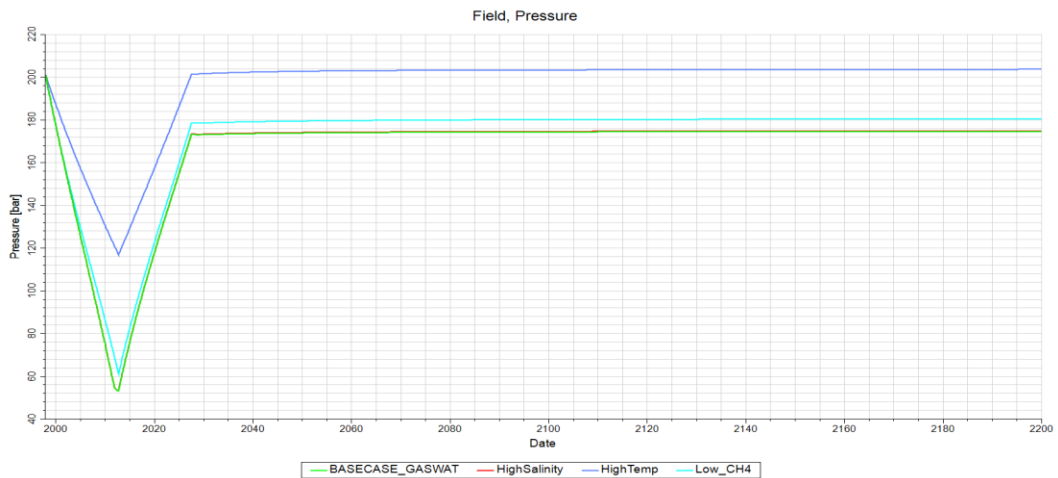
Figure 7-21 Field pressures for various reservoir fluid properties cases

Table 7-5 Molar distribution of CO2 in region 1 and region 2 for varying reservoir fluids properties

	Base		High Salinity		Low Methane		High Temperature	
	Total CO2 Moles		Total CO2 Moles		Total CO2 Moles		Total CO2 Moles	
	Region 1	Region2	Region 1	Region2	Region 1	Region2	Region 1	Region2
	M kg-mole	M kg-mole	M kg-mole	M kg-mole	M kg-mole	M kg-mole	M kg-mole	M kg-mole
2027	45.23	366.79	42.42	367.35	41.02	369.11	20.03	393.08
2100	46.34	365.70	46.45	365.56	44.52	367.86	24.13	390.71
2200	49.58	362.45	49.69	362.32	46.61	365.77	26.25	388.59
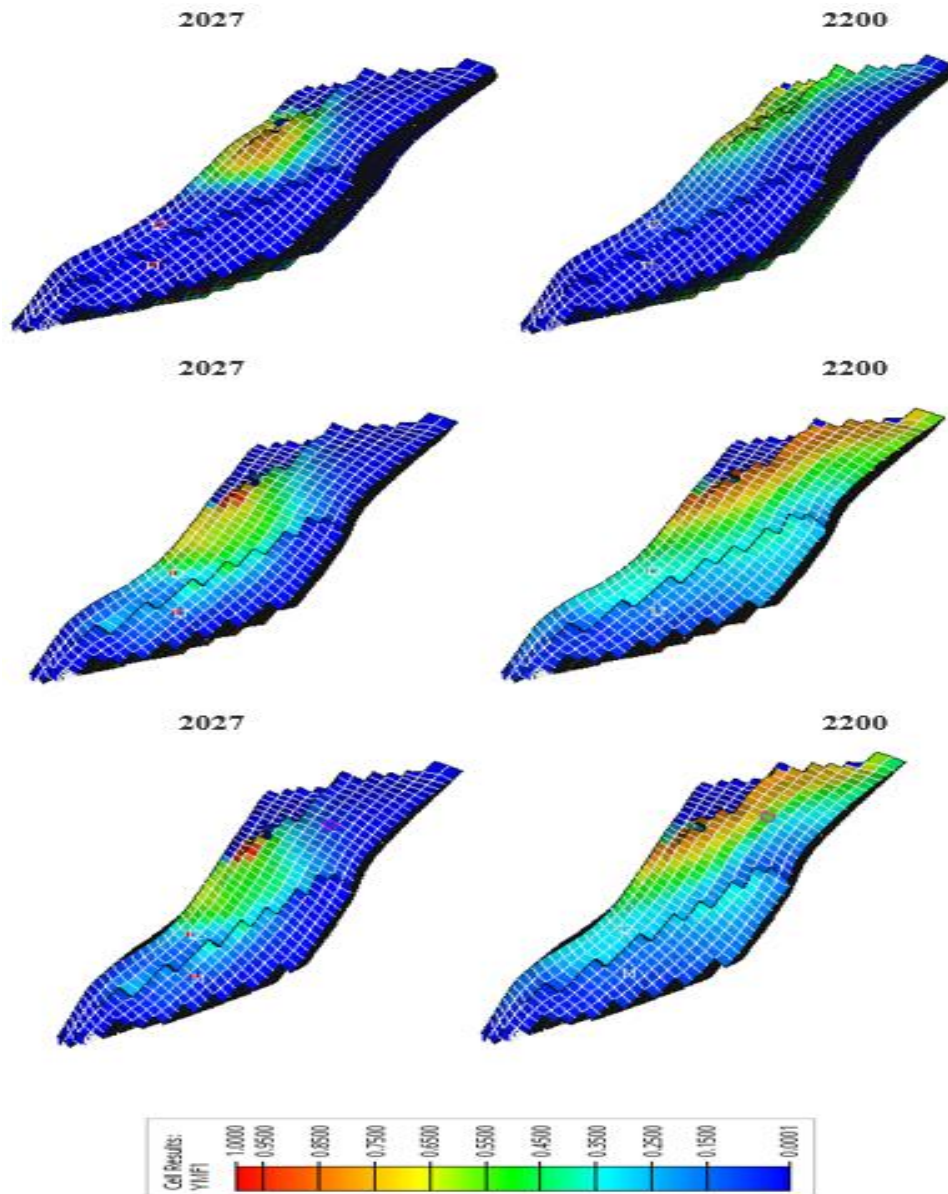
Figure 7-22 CO2 gaseous mole fraction in the years 2027 and 2200 (top layer) High Temperature case (middle layer) High Salinity (bottom layer) Low methane content case

Migration of CO_2 plume away from the injection well is an important consideration to take note of during a CO_2 sequestration project. CO_2 flow can be greatly affected by the pressure, temperature, resident gas content and reservoir brine salinity. The dynamics of the CO_2 plume is governed partly by CO_2 density (Vilarrasa & Rutqvist, 2017) . In reservoirs with high temperatures, CO_2 remains in the supercritical state and a more viscous dominated flow is observed in comparison with the gravity dominated one. This is why in the high temperature case the flow of CO_2 has been mostly laterally and not vertically due to a density differential. This is confirmed by the number of moles of CO_2, i.e. 20.03 M kg-mole, present in region 1 at the end of injection in 2027 given by the Table 7-5. Towards the end of relaxation period in 2200, the number had increased slightly to 26.25 M kg-mole which helps understand the notion that leakage has been minimal in this case as the CO_2 might have not reached the more leaky faults in the formation as it had spread laterally at a larger distance in a quick span. Figure 7-22(top) confirms the claim that reservoir moles lies mostly in the region 2 which is below the caprock (layer 4). It can also be seen from these distributions that most of the plume flows into the southern downward dip of the reservoir, mainly influenced by gravity. For high salinity case, the number of moles of CO_2 in both regions are similar. This can be either due to the fact that the reservoir simulations were carried without any effect of salt precipitation causing changes in permeability/capacity or injectivity of the reservoir, or maybe because the used value of 0.81 10^{-3} kg-M/kg is not high enough to cause significant change. The case with lower methane content has a slightly higher molar number i.e. 369.11, 367.86 and 365.77 M kg-mole in region 2 in the years 2027, 2100 and 2200 respectively, reflecting that a heavier reservoir gas due to a lower methane content can be slightly difficult to push back, consequently most of the CO_2 is staying in Region 2 below the caprock.

Trapping mechanisms also get impacted by the initial reservoir properties. In case of high initial reservoir temperature, it can be seen from Figure 7-23(top) & Figure 7-23(bottom) that increased reservoir temperature inversely affects the immobilization of CO_2 via dissolution and residual gas trapping. At the end of injection, a total of 6.74E06 kg-mole and 4.68E06 g-mole of CO2 has been stored via dissolution and residual gas trapping respectively. Almost 97.5% of CO2 is present in the reservoir as free gas in a supercritical state in case of high reservoir temperature and this value decreases to 97.1% until the end of simulation period. Due to higher temperature, viscosity of the gas is reduced and it is immensely mobile, therefore trapping via dissolution and residual gas is minimalized.

For high salinity case, there is a slight decline in dissolution trapping to a value of 2.27E07 kg-mole as compared to the base case value of 2.41E07 kg-mole at the time when injection stops. This decline is expected to occur. With an increase in salinity, greater anions and cations are present in the resident brine, thus causing a reduction in available volume for CO_2 to interact with H_2O and dissolve in it. According to the study by (Al-Khdheeaw, Vialle, Barifcan, & Sarmadivaleh, 2017), higher brine salinity leads to an increase in CO_2 mobility migration distance but reduces residually trapped CO_2. In the longer term, dissolution trapping increases slightly to 2.43E7 kg-mole as some of the mobile CO_2 is dissolved in brine. Residual gas trapping is overall much similar to the base case since it is dependent on the residual gas saturation which is equal and the injectivity of CO2 has not been compromised. In the longer time period almost same number of CO2 moles remain trapped residually.

For the case of low methane content of reservoir gas, about 2.34E07 kg-mole of CO2 is dissolved at the end of injection, and increases to 2.50E07 kg-mole in 2200. This value is slightly less than the base case value. Heavier gas seem to trap CO2 residually slightly more than the base case as at the end of injection the amount was 6.45 E06 kg-mole while in the longer to a value of 6.44E06 kg-mole compared to the base

case value of 6.44E06 and 6.41 E06 g-mole respectively. Dominant trapping mechanism here is the structural trapping with almost 92% of the total CO_2 trapped.
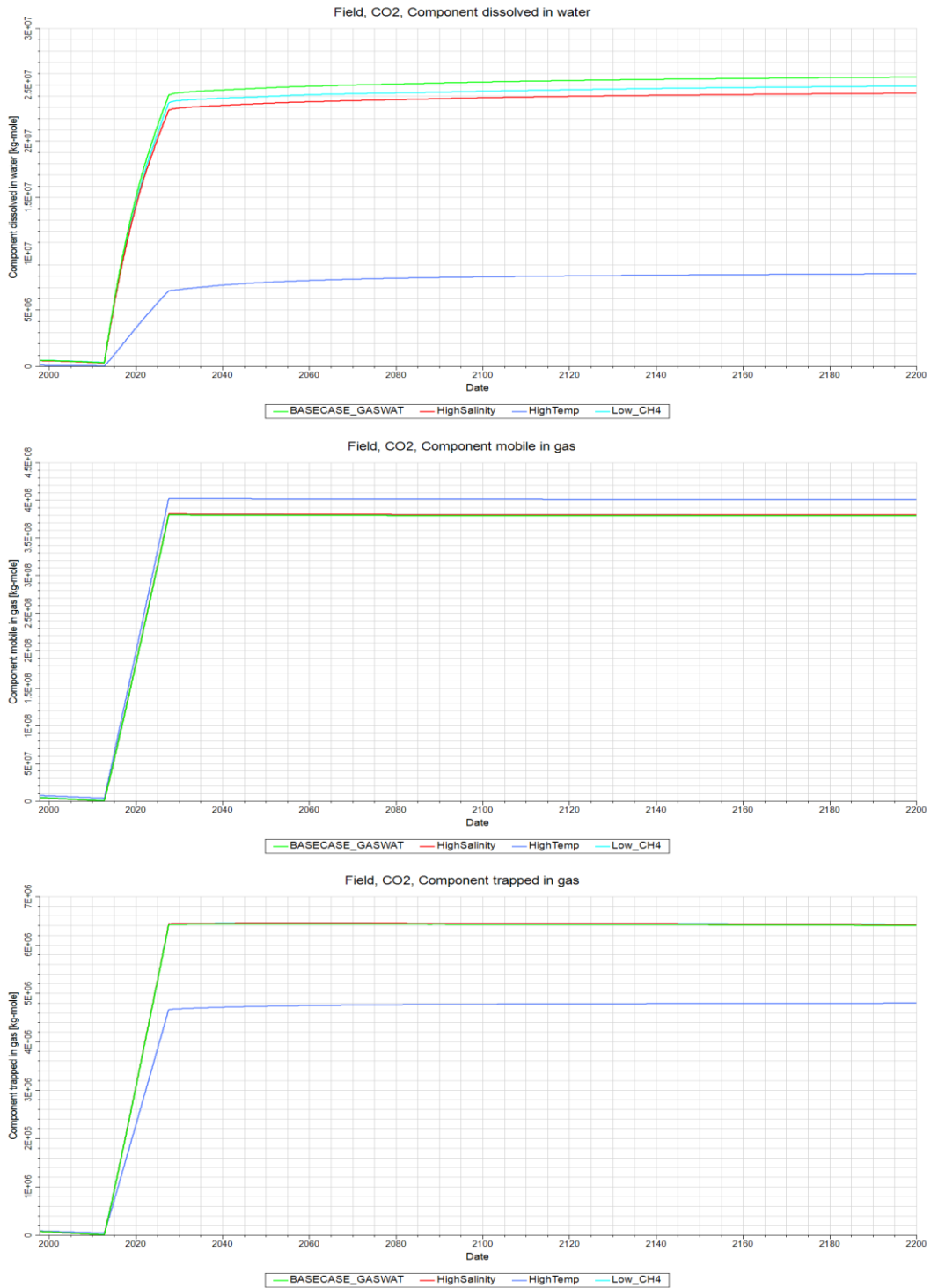
Figure 7-23 Trapping Mechanism for various reservoir fluid properties cases (top) Dissolution trapping (middle) Structural trapping (bottom) Residual Gas trapping

The results discussed above highlight some important reservoir fluid considerations that must be well-thought-out before the carbon sequestration process is initiated. As told earlier CO_2 density plays a major role in governing the dynamics of CO_2 plume since high density of CO_2 (supercritical) makes flow viscous dominated while a lower density makes it gravity dominated. Temperature and pressure are key in determining the density values of CO_2 and it may be difficult to predict accurately while the plume is in motion or during injection. Therefore density can vary greatly from high temperate reservoirs to low temperate ones, and the warmer the reservoir the lower would be its viscosity causing an increased mobility and a decrease in overpressure. Temperature can also cause an effect on surface tension and wettability angle that have significance in capillarity (Vilarrasa & Rutqvist, 2016). Although these runs were conducted isothermally, and the fact that the initial BHP for all the cases had been limited to 50 bar makes it slightly less depleted than it could have been from an actual production history and the depth of reservoir is high enough to cause the injected CO_2 to be at a higher temperature, it is safe to assume that JT cooling effects have not come into play in this reservoir. Yet, it is still important to review and understand some of the temperature effects CO_2 injection can bring in the reservoir which are discussed in depth in Section 3.3. It is seen in the simulation runs, that for a high reservoir temperature case, CO_2 as a free gas is present as almost 97% of the total injected gas and CO_2 plume movement has migrated dominantly in lateral direction because of its increased mobility due to reduced viscosity, and causing very less leakage into the region above the seal. Due to this high mobility, the residual gas trapping and dissolution trapping is reduced to very low values.

It is also observed from the results that salinity causes a reduction in dissolution trapping and an increase in the free and residual trapping. Lower methane content gas gives similar results to the base case apart from a slight decrease in dissolution trapping and an increase in residual gas trapping, which might indicate heavier gases are better capturing CO_2 residually. However, more research and different initial compositions must be tested to confirm this claim.

7.2.4 Varying Injection Rates

In determining injectivity, an efficient and long term storage, one of the key parameters is injection rate. Project planning entails a calculation on keeping injection rates high enough to make CCS economical and at the same time, the rates have to be not too high to avoid any problematic geo-mechanical or geothermal effects being caused on the reservoir. Keeping this in mind a high injection rate scenario is built. For this case, two injections wells which previously had produced for a fifteen year period are used to inject CO_2 into the reservoir at a rate of 1.2E06 Sm3/day/well. Injection rate used in this sensitivity analysis case is selected based on the available capacity of the reservoir before the pore fluid pressure reaches the fracture pressure limit. High injection rates can be considered vital for the aim of meeting the net zero goal as soon as possible, however, it is important to note that with very high injection chances of geo-mechanical fractures or reactivation of existing faults are high. For this case the production scenario is similar to the base case, therefore the initial reservoir pressure is almost 52 bar. Results of the injection rates as a function of time reflect that at this rate fracture pressure limit is reached before the injection period is completed. The injection rates shown in Figure 7-24 below show that around June 2026, almost a year before the end of fifteen year period, the pressure limit constraint (200 bar) had reached and the simulation software had to lower the injection rates until the wells were shut by the mid of 2027. Cumulatively, the amount of CO_2 injected in volumetric terms is 1.2347E10 Sm3 and in terms of mass it is 23.903 Mt. Conversion is given in **Appendix B**.

Bottomhole pressures also depict an expected behavior in high injection rate case. It is seen that both wells I1 and I2, have a higher bottomhole pressure throughout the injection period. This is because greater amount of CO_2 is being injected therefore pore fluid pressure is increasing near the injection wells ultimately causing a rise in BHP. The pressure profiles of the BHP and the field pressures are given in Figure 7-25. It can be seen from the BHP profiles that well I2 has reduced injectivity as compared to well I1 and is shut off before the injection period ends. This reduced injectivity is mainly because of a lower permeability value or the fact that it is slightly closer to an impermeable fault, causing a higher buildup in pressure. The field pressure reaches almost 204 bar as compared to base case 173 bar. It then stabilizes once CO_2 redistributes in the reservoir while interacting with brine and reservoir gas.

Figure 7-24 (top) Field Gas injection rate (bottom) Cumulative gas injection for the sensitivity of high injection rate case.
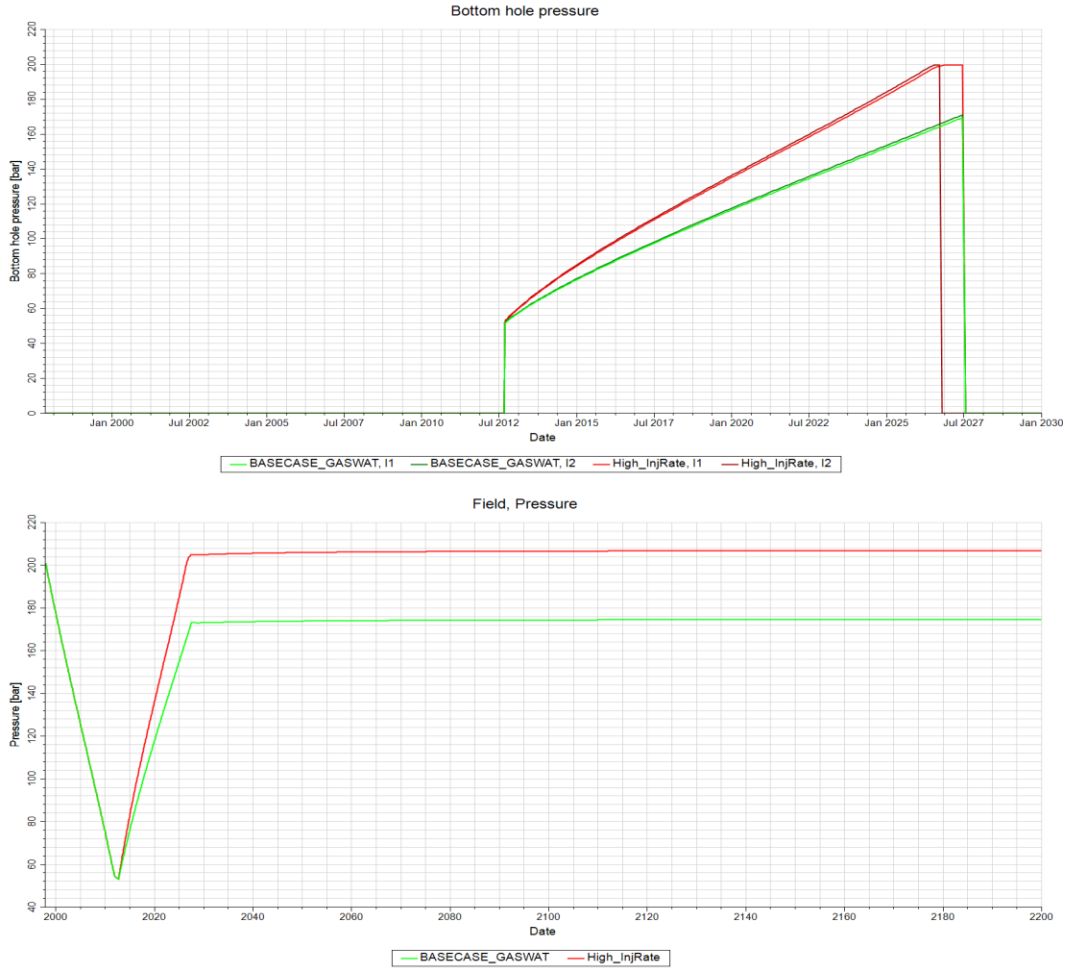
Figure 7-25 Pressures of the high injection and base case (top) Bottom hole pressure of I1 and I2 (bottom) Field Pressure

Since the injected rate is high, the total moles of CO_2 stored increase proportionally. The Table 7-6 below gives the moles in two regions of the reservoir that aid in studying the amount of CO_2 moles leaking from region 2 to 1 in the reservoir after the completion of injection period and beyond that. The amount of CO_2 present at the end of injection in region 1 is 63.32 M kg-mole while in region 2 it is 462.96 M kg-mole of CO_2. With time only about 6.4 M-kg-mole of CO2 has been lost to the region above the seal. This amount is proportionally similar to the base case value which had almost 4.4 M kg-mole of CO_2 lost. This reflects that a higher injection rate has not resulted in any leakage pathway. The CO_2 plume distribution is also in line with the base case, with greater number of CO_2 moles thereby making more grid cells having a higher CO_2 gaseous mole fraction. It is seen through the 3D grid representations that in the higher injection case, CO_2 not only migrates to the southern part of region 1, but also redistributes itself in the northern region as well. In the base case most of the CO2 mole fraction is present away from the fault E_01 and E_01_F3. This 3D representation of the plume movement is shown in Figure 7-26.

Table 7-6 Moles of CO2 in the two regions of the reservoir for sensitivity of high injection rate and base case

	Base		High Injection Rate	
	Total CO_2 Moles		Total CO_2 Moles	
	Region 1	Region 2	Region 1	Region 2
	M kg-mole	M kg-mole	M kg-mole	M kg-mole
2027	45.23	366.79	63.32	462.96
2100	46.34	365.70	66.16	460.56
2200	49.58	362.45	69.76	456.96
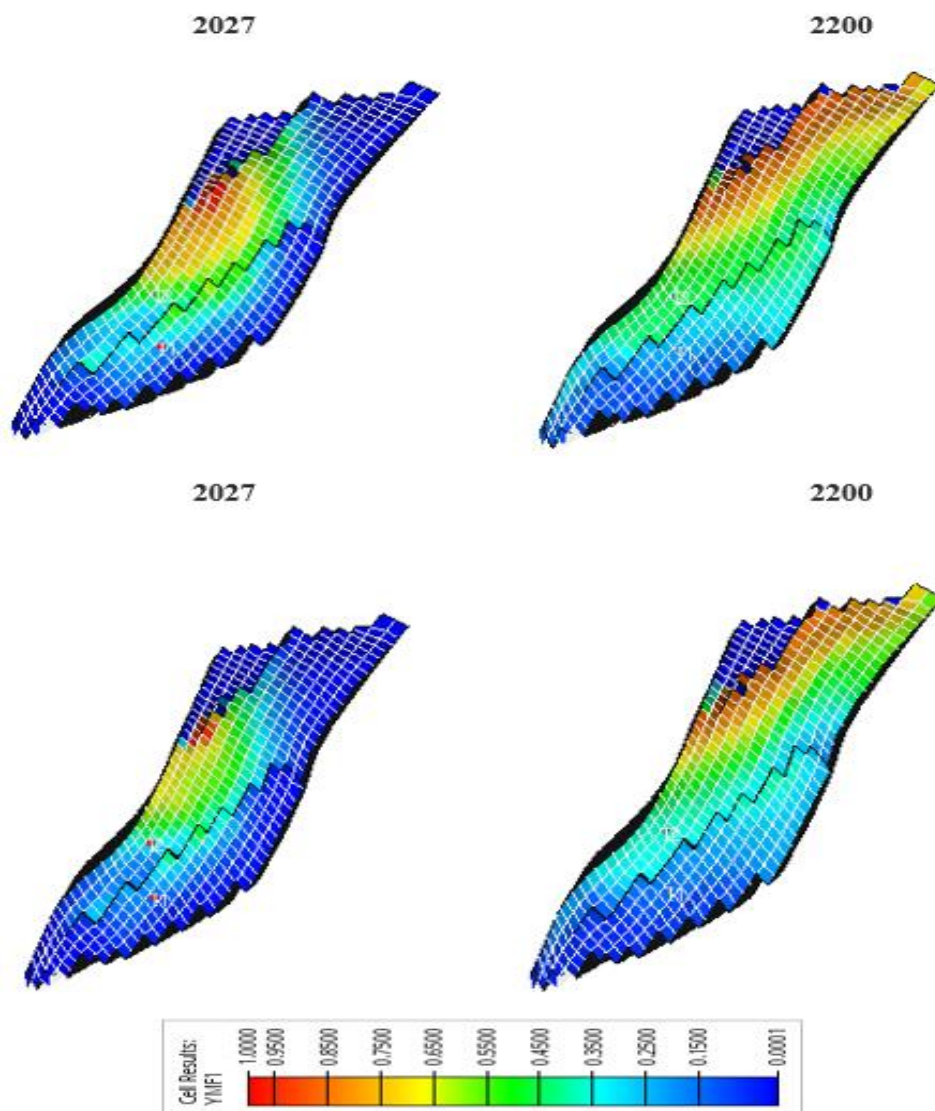
Figure 7-26 CO2 molar distribution (top) High Injection case (bottom) Base case

Figure 7-27 Trapping Mechanisms (top) Component dissolved in water (middle) Component mobile in gas phase (bottom) Component trapped in gas

To study the relevant trapping mechanisms in this case, relationship between total amounts of injected CO_2 dissolved, mobile and trapped in gas phases against time is requested. It is given by Figure 7-27 above. It

shows that the dominant mechanism in both cases is the structural free gas trapping that accounts for almost 92% of the total injected gas. This is similar to the base case in terms of ratio of CO_2 injected. This is because apart from the injection rate everything else is equal making storage pattern similar. The depth of the reservoir is almost 3000 m, making the injected fluid in a super critical condition and that being the reason why it is extremely mobile and structural trapping is more dominant than the other two. The residual gas trapping accounts for almost 6% of trapping and the least amount of gas is trapped via residual gas trapping mainly because of highly viscous injected CO_2 and low residual gas saturation. The injection of CO_2 can also cause the GWC to shift downwards slightly as well due to the pressure created by injection of CO_2. High injection rates can lead to JT effects and result in the formation of hydrates and freezing of formation water which can ultimately lead to reduced injectivity in the near well region. In this thesis, however, thermal are not modelled. Overall, this high injection rate can be assumed to be safe for injection, based on the reservoir capacity, injectivity and the length of injection period.

7.2.5 Presence of an Aquifer

In order to test, how the storage of CO_2 would behave in the presence of an aquifer numerical aquifer cases with variable sizes connected to the cells at the southern down dip end of the reservoir as shown in Figure 6-12 are modelled for this purpose. Attaching a numerical aquifer increases the pore volume of the grids to which it is attached. The first and the most significant behavior to note here is the field pressure response of the reservoir when the aquifer is present and is given in Figure 7-28. The initial reservoir pressure is above 200 bar for the case of a large aquifer (Area =100000 m^2) as compared to the base and smaller aquifer (Area = 1000 m2) case. The pressure linearly decreases during production for all the three cases. It is observed from the pressure profile that having a large aquifer near the reservoir, the pressure depletion is very less since aquifer provides the support and maintains the pressure. The drawdown for the production period is only 66 bar as the pressure reaches to a value of 138 bar once production ends. On the other hand, in the smaller aquifer case no prominent changes are seen as compared to the base case. The cumulative production from the large aquifer case is 9.72E9 Sm^3 of methane gas as the BHP never reached the limit of 50 bar for any of the wells, while for the base and smaller aquifer case it is 9.26 E09 Sm^3 due to a reduced production towards the end of the fifteen year period. During injection the total buildup in the presence of a strong aquifer is about 60 bar reaching the final reservoir pressure to 194 bar. The buildup response of smaller aquifer is similar to the base case. With a strong aquifer case, it is evident that as water replenishes easily during hydrocarbon production so it can drive away easily during injection. This is the reason why an aquifer presence can be considered helpful in achieving successful storage. The graph also shows that the pressure equilibration is better in the presence of an aquifer as compared to the base case, where it tends to increase slightly with time. There is however, an important technical aspect that has to be considered before making the judgment on selecting a reservoir with nearby aquifer for storage and that is, the volume of the aquifer. If an aquifer is relatively small and falls under the category of a weak aquifer, it can bring more damage than benefit. As explained by (Hughes, 2009) and discussed in Section 3.4, Type 2 (weak aquifer) response is considered as more challenging when CO_2 disposal is considered. This is because there will be some initial capacity squeezing the remaining HC gas but later the additional capacity will depend on the rate at which aquifer relaxes as a result of CO_2 injection, and for weak aquifers this response is very truncated for being practically applicable. For this simulation, the provided aquifer cross sectional area and length were 100000 m^2 and 2000 m for large aquifer and 1000 m^2 and 2000 m respectively with a fairly large porosity and permeability as given in Table 6-6 and Table 6-7. This large aquifer, can be safely considered as a Type 1 (strong aquifer) response, making this a good choice for storage.

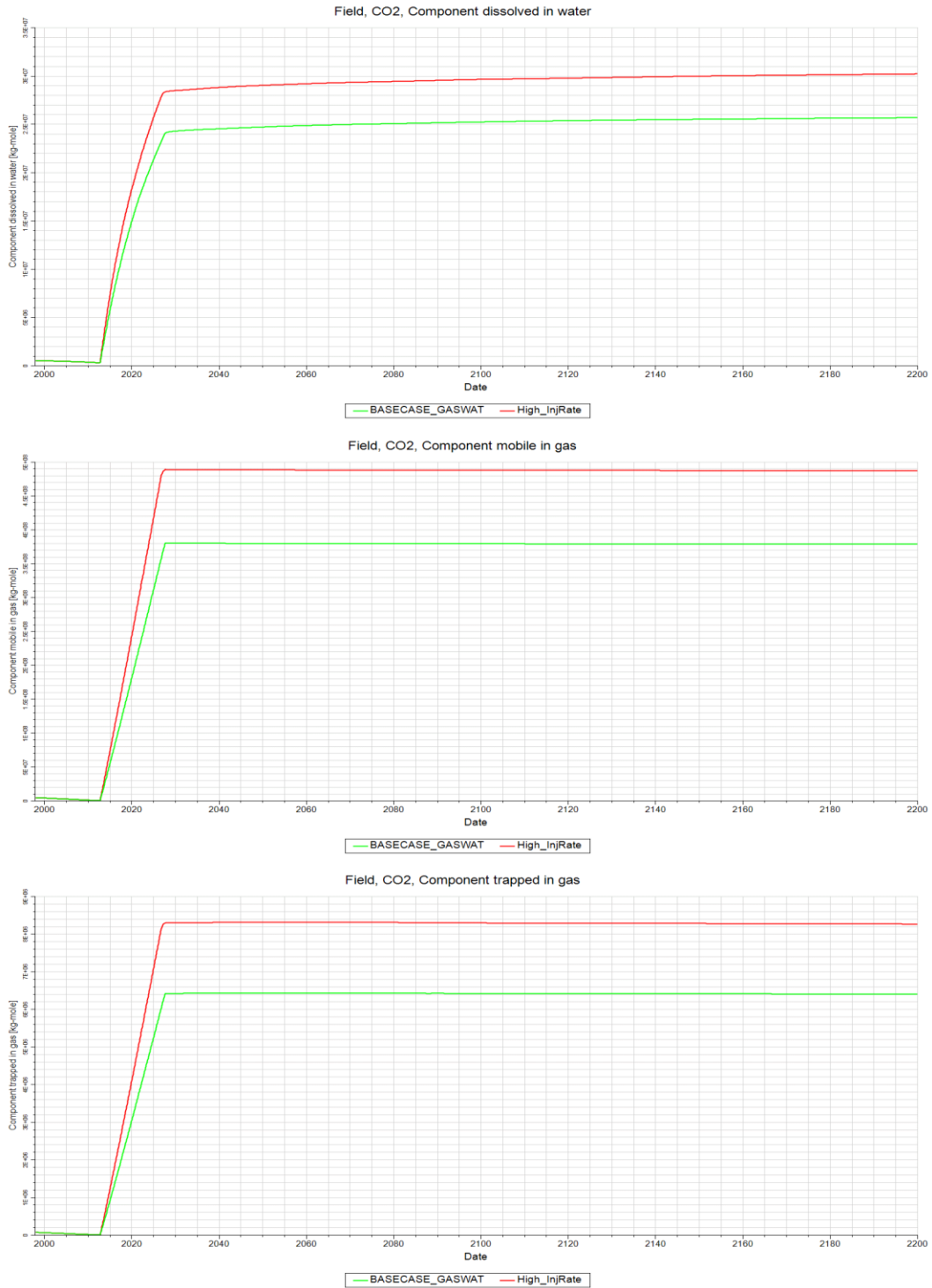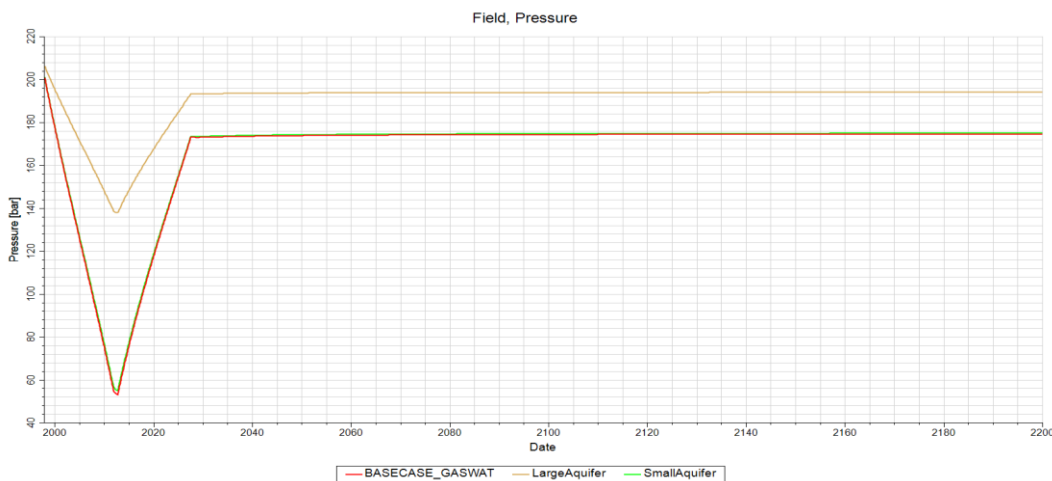*Figure 7-28 Field pressure response of large and small aquifer and base case*
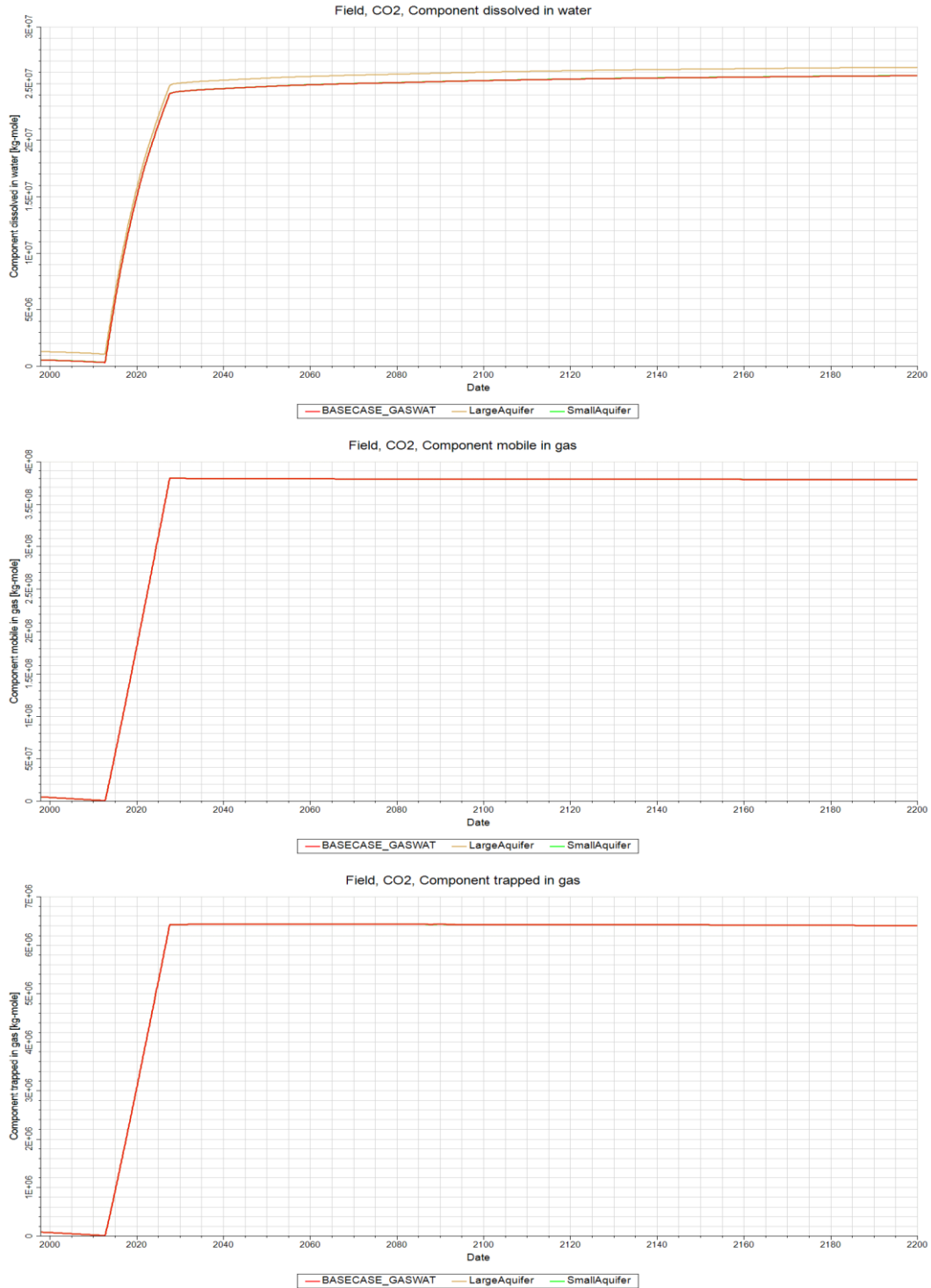
Figure 7-29 Trapping Mechanisms (top) Component dissolved in water (middle) Component mobile in gas phase (bottom) Component trapped in gas phase

When discussing about geological storage it is important to understand which trapping mechanisms are dominant in the particular storage. Figure 7-29 help in making a comparison of the main trapping

mechanisms in reservoir under the presence of two different sized aquifers. From the graphs showing the component dissolved in water the case having the larger volume of aquifer dissolves the most amount of CO_2 injected of all the cases until the end of injection with a value of 2.48E07 kg-mole in and in the relaxation period it remains at the top as well with 2.65 E07 kg-mole. This is mainly because of the injected CO_2 has more water to dissolve in. It can also be seen that the injected fluid properties do not change and the injected phase beahvior is same as all the cases, and therefore it exists in a supercritical state having a high mobility and therefore existing mainly in mobile phase for all the cases with slightly less for the large aquifer because some of the CO_2 is also dissolved. In addition to this, the component trapped in gas phase shows a similar trapping pattern for all the three phases. It increases linearly during injection to a value of 2.65E06 kg-mole of CO_2 until the end of injection and remains almost constant throughout the relaxation period as well. Residual gas trapping is the least due to the fact that in all three cases the residula gas saturation is 0.01 which means the hydrocarbons are easier to be pushed once the CO_2 is injected and when CO_2 rises due to bouyancy the capillary effects are not strong enough to cause this trapping. The number of moles of CO_2 present in each region for each case almost consistent as the base case which reflects that in the presence of aquifers the leakage of CO_2 from region 2 to region 1 is not affected.

Overall, it can be observed that size of the aquifer within the reservoir is an imporant consideration that determines the pressure response of the reservoir. Having a larger aquifer (Type 1) is a better option for injecting CO_2 in the reservoir for the purpose of sequestration, as the pressure depletion is minimal due to the replinishment of produced hydrocarbon by the aquifer warer and also because of the fact that if it can replace at a quicker rate, it can also be diplaced back easily.

8 Conclusion

In this thesis various aspects of long term storage of CO_2 into a reservoir model of a real field were studied by compositional modelling technique using the Schlumberger`s Eclipse software. Two different approaches of modelling are used which uses slightly different flow equations and transport calculations. The results obtained from both these approaches were fairly consistent with slight changes due to density and viscosity calculations therefore making mobility and phase behavior different. Two vertical wells with a production and an injection rate of 0.9E06 Sm3/day/well were used to produce hydrocarbon and inject CO_2 for a period of 15 years each and a relaxation period of almost 173 years. Sensitivity analysis based on various reservoir characteristics, fluid properties, fluid saturations, and injection rates, on injectivity and containment and trapping were examined. Results showed that the reservoir heterogeneity slightly impacted the overall field pressure as the low permeability reservoirs see an additional pressure drop Having a deeper GWC, caused an decrease in reservoir pressure buildup due to an increased volume availability for injection. Lowering initial water saturation to 20% meant, increased storage capacity for CO_2, thereby causing the pressure to remain lower than the base case. Injection at higher rates led to pressure buildup up to the 200 bar limit before the 15 year period ends, which had the highest amount of CO_2 injected. Having a high initial reservoir temperature makes the fluids to expand further and more amount of CO_2 is stored in the mobile phase a more viscous dominated flow is observed in comparison with the gravity dominated one. With a large aquifer nearby, the pressure buildup is drawdown and buildup, since aquifer acts as a medium for pressure to be dissipated while a smaller aquifer did not impact the injection process.

Some common findings of the project include: (I) Dominant trapping mechanism in all the cases was structural trapping that was indicated by the high CO_2 moles free in gas phase. In addition to this, dissolution trapping particularly in the presence of aquifer was also seen that was the second best mechanism for trapping. Residual gas trapping was lower w.r.t overall trapping as a low value of critical gas saturation is used. (II) Redistribution of pressures through movement of CO_2 occurred in all cases and pressure profiles (plateaus) showed that after injection stopped the reservoir pressure had been fairly constant until the end of simulation in 2200. (III) The loss in the amounts of CO_2 was consistent in all the cases from Region 2 to 1, indicating no increased leakage due to injection scenarios. (IV) Pressure and total moles injected increase linearly across the injection period although for the case of high temperature the overall pressure limit of 200 bar has been reached causing relatively lower amount of CO_2 injected, thus indicating warmer reservoirs as being not the best choices of injection. (V) Most of the CO_2 migrating upwards accumulated in the southern down dip area due to the effects of gravity. (VI) In all cases, viscous forces seemed to dominate and CO_2 migrated across the formation very quickly as compared to vertically, high horizontal permeability was one reason for this high mobility as well. (VII) Injection well I2 showed the most amount of pressure buildup in all cases, this can be because of a presence of a nearby grid cells having lower permeability. (V) Overall, the containment of CO_2 was fairly constant across the 173 year period and the injected CO_2 was in a supercritical state for all cases considering the depth of the reservoir is above 3000m.

This thesis provided an exceptional opportunity to model and examine the behavior of reservoir at various injection scenarios. It delivers an insight of working for other comprehensive real field scenarios that can impact injection work otherwise, which include, different fluid types such as condensate gas reservoirs and study of varying transmissibility of faults. For storage to be considered a successful effort, it has to be made sure that the injected volume of CO_2 remains intact for centuries without migrating into the potable aquifers and leaking off through the leakage pathways. This Norne model, although relatively small, can be considered a good practice model for working towards large scale projects and gives an idea of the

implications of CO_2 storage in depleted gas formation in order to lessen GHG and achieve a healthier environment for all.

Rooms for improvement and further work

Modelling the reservoir heterogeneity scenarios, with statistically produced variation in heterogeneity, for instance using Monte Carlo simulations, instead of linear heterogeneity could have given a greater understanding of its impacts on CO_2 sequestration.

Choice of well locations can be optimized based on other fault locations, horizontal permeability and porosity of the formation.

Including the effects of capillary effects and hysteresis can certainly impact the injectivity and storage of CO2 in depleted gas reservoirs. Therefore further research and work can conducted in this regard.

Using non-isothermal techniques to study the near well effects induced by injected cold CO2 in a depleted gas reservoir. Eclipse software is not compatible with non-isothermal runs with CO2SOL and GASWAT option. Other software that are mentioned in the **Appendix C** can be explored to study the thermal effects arising due to the sequestration process.

Using reservoir modelling with considerations of geo-mechanical effects and salt precipitation leading to alterations in reservoir properties like porosity, permeability and wettability ultimately leading to an altered injectivity, capacity and containment as the injection is continued can be studied.

Using coupling to simulate a wellbore model along with the reservoir model: while CO_2 is being injected at high depths various physical changes are witnessed due to changing pressure and temperature in the wellbore. Therefore these changes in the injected CO_2 properties could lead to differences in the initializations in dynamic reservoir models. Currently, this area of research is developing and further research can make predictions as close to reality as possible.

References

Agartan, E., Gaddipati, M., Yip, Y., Savage, B., & Ozgen, C. (2018). CO2 storage in depleted oil and gas fields in the Gulf of Mexico. *International Journal of Greenhouse Gas Control*, 38-48.

Ajayi, T., Gomes, J. S., & Achinta, B. (2019). A review of CO2 storage in geological formations emphasizing modeling, monitoring and capacity estimation approaches. *Petroleum Science*, 1028-1063. Retrieved from https://doi.org/10.1007/s12182-019-0340-8

Akai, T., Okabe, H., Hiyama, M., & Saito, N. (2021). Numerical Modelling on CO2Storage Capacity in DepletedGas Reservoirs. *MDPI*. Retrieved from https://doi.org/10.3390/en14133978

Al-Khdheeaw, E. A., Vialle, S., Barifcan, A., & Sarmadivaleh, M. (2017). Effect of brine salinity on CO2 plume migration and trapping capacity in deep saline aquifers. *APPEA Journal*.

André, L., Azaroual, M., & Menjoz, A. (2009). Numerical simulations of the thermal impact of supercritical CO2 injection on chemicalreactivity in a carbonate saline reservoir. *Transport in Porous media*.

Bachu, S. (2015). Review of CO2storage efficiency in deep saline aquifers. *International Journal of Greenhouse Gas Control*, 188-202.

Berge, U., Gjerset, M., KRISTOFFERSEN, B., LINDBERG, M., PALM, T., RISBERG, T., & SKRIUNG, C. S. (2011). *CARBON CAPTURE AND STORAGE.* Oslo: Zero Emission Resource Organization.

Boden, T. A., Marland, G., & Andres., R. J. (2017). Global, Regional, and National Fossil-Fuel CO2 emissions. *Carbon Dioxide Information Analysis Center*.

Burchwell, A., Gupta, N., Place, M., Kelley, M., Ravi-Ganesh, P., Sminchak, J. R., & Conner, A. (2020). *Monitoring and Modelling of CO₂ Storage: The Potential for Improving the Cost-Benefit Ratio of Reducing Risk.* Cheltenham: IEAGHG Technical Report.

CCS, I. G. (2021). *CO2 Capture.* GLOBAL CCS INSTITUTE. Retrieved December 2021, 2021, from https://www.globalccsinstitute.com/about/what-is-ccs/capture/

Chen, H., Yang, S., Zhang, X., Ren, S., Dong, K., Li, Y., . . . Ma, Q. (2015). Study of phase behaviour and physcial properties of a natural gas reservoir with high carbon dioide content. *GHG*.

Class, H., Ebigbo, A., Helmig, R., Dahle, H. K., Nordbotten, J. M., Celia, M. A., . . . Beni, A. N. (2009). A benchmark study on problems related to CO2 storage in geologic formations. *Computational Geosciences*.

Correia, G. G., & Schiozer, D. J. (2016). Reservoir characterization using electrofacies analysis in the sandstone reservoir of the Norne Field (offshore Norway). *Petroleum Geoscience, Volume 22*, 165 - 176.

Crowe, C. (2006). *Multiphase flow handbook.* CRC Press, Taylor & Francis.

Dalland, A., Worsely, D., & Ofstad, K. (1988). A lithostratigraphic scheme for the mesozoic and cenozoic and succession offshore mid-and northern norway.

Desjardins, O., Blanquart, G., Balarac, G., & Pitsch, H. (2008). High order conservative finite difference scheme for variable density low Mach number turbulent flows. *Journal of Computational Physics*, 7125-7159.

Edenhofer, O., Pichs-Madruga, R., Sokona, Y., E.Farahani, Kadner, S., Seyboth, K., . . . Minx, J. C. (2014). *"Summary for Policymakers," in Climate Change 2014: Mitigation of Climate Change. Contribution of Working Group III to the Fifth Assessment Report of the Intergovernmental Panel on Climate Change.* Cambridge, United Kingdom: Cambridge University Press.

Falenty, A., Qin, J., Salamatin, A. N., Yang, L., & Kuhs, W. F. (2016). Fluid Composition and Kinetics of the in Situ Replacement in CH_4-CO_2 Hydrate System. *ournal of Physical Chemistry C* .

Farzaneh-Gord, M., Rahbari, H. R., & Zangeneh, J. (2020). Effects of natural gas compositions on its Joule–Thomson coefficients and Joule–Thomson inversion curves. *Elsevier - Cryogenics*.

Fawad, M., & Mondol, N. H. (2021). Monitoring geological storage of CO_2: a new approach. *Scientific Reports*.

Freund, P., & Kaarstad, O. (2007). *Keeping the lights on.* Oslo: Universitetsforlaget.

Gasda, S., Bachu, S., & Celia, M. (2004). Spatial characterization of the location of po-tentially leaky wells penetrating a deep saline aquifer in a mature sedimentary basin. *Environ. Geol. 46 (6–7),*, 707–720.

GLOBAL CCS, I. (2021). *About CCUS.* CCS GLOBAL INSTITUTE. Retrieved from https://www.globalccsinstitute.com/resources/ccs-image-library/

Grobe, M., Pashin, J., & Dodge, R. (2009). Carbon dioxide sequestration in geological media—state of the science. *AAPG Stud. Geol., 59*, 59.

H.Ott, Roels, S., & Kloe, K. d. (2015). Salt precipitation due to supercritical gas injection: I. Capillary-driven flow in unimodal sandstone. *International Journal of Greenhouse Gas Control*, 247-255.

Hawkes, C., McLellan, P., & Bachu, S. (2005). Geomechanical Factors Affecting Geological Storage of CO_2 in Depleted Oil and Gas Reservoirs. *Journal of Canadian Petroleum Technologyy*, 44-54.

Hughes, D. S. (2009). Carbon storage in depleted gas fields: Key challenges . *Energy Procedia*, 3007-3014.

IEA. (2020). CCUS in Clean Energy Transitions,. *IEA, Paris*. Retrieved December 12, 2021, from https://www.iea.org/reports/ccus-in-clean-energy-transitions

IEA. (2021). About CCUS. *IEA, Paris*. Retrieved December 12, 2021, from
(https://www.iea.org/reports/about-ccus

IPCC. (2007). *Change, C. IPCC fourth assessment report. The physical sciences basis, .* IPCC.

IPCC. (2007). *IPCC Special Report. Carbon Dioxide Capture and Storage. A Special Report of Working
Group III of the Intergovernmental Panel on Climate Change.* IPCC.

Jamaloei, B. Y. (2015). The Joule-Thomson Effect in Petroleum Fields: II. CO2 Sequestration, Wellbore
Temperature Profiles, and Thermal Stresses and Wellbore Stability. *Energy Sources, Part A:
Recovery, Utilization, and Environmental Effects, Volume 37*, 236-244.

James, E. G. (2006). *Physical Properties and Process Conditions.* Houston: Gulf Publishing Company.

Jenkins, C. R., Cook, P. J., Ennis-King, J., Undershultz, J., Boreham, C., Dance, T., . . . Hortle, A. (2011). Safe
storage and effective monitoring of CO2 in depleted gas fields. *PNAS*.

Ji, X., & Zhu, C. (2015). *Novel Materials for Carbon Dioxide Mitigation Technology.* Oxford: Elsevier B.V. .
Retrieved from https://doi.org/10.1016/B978-0-444-63259-3.00010-0

Jiang, X. (2011). A review of physical modelling and numerical simulation of long-term geological storage
of CO2. *Applied Energy*.

Jiang, X., & Lai, C.-H. (2009). *Numerical techniques for direct and large-eddy simulations.* Taylor &
Francis.

Jiang, X., & Luo, K. (2001). Direct numerical simulation of the near field dynamics of a rectangular
reactive plume. *International Journal of Heat and Fluid Flow*, 633-642.

Jun, C., Kim, M., & Shin, H. (2019). Optimization of well placement and operating conditions for various
well patterns in CO2 sequestration. *Int. J. Greenh. Gas Control*.

Jun, Y.-S., Giammar, D. E., & Werth, C. J. (2013). Impacts of Geochemical Reactions on Geologic Carbon
Sequestration. *Environ. Sci. Technol.*, 1,3-8.

Khan, A. (2014). *Integrated Petrophysical and Seismic interpretation of Norne Feild, Norway.* Tromso:
The Arctic University of Norway.

Khan, N. A. (2021). *CO2 storage in depleted gas reservoirs.* Trondheim: NTNU.

Lekic, A., Jukic, L., Arnaut, M., & Macenic, M. (2019). Simulation of CO2 injection in a depleted gas
reservoir: A case study for Upper Miocene sandstone, Northern Croatia. *The Mining-Geology-
Petroleum Engineering Bulletin*.

LINDSEY, R. (2021). Climate Change: Atmospheric Carbon Dioxide. *ClimateGov*.

Loizzo, M., Lecampion, B., Berard, T., & Jammes, L. (2010). Reusing O&G-Depleted Reservoirs for CO2 Storage: Pros and Cons. *SPE Projects Facilities & Construction*.

Lorenz, S., & Muller, W. (2003). Modelling of halite formation in natural gas storage aquifers,. *TOUGH Symposium, Lawrence Berkeley National Laboratory*.

Maleki, M., Davolio, A., & Schiozer, D. J. (2017). Using simulation and production data to resolve ambiguity in interpreting 4D seismic inverted impedance in the Norne Field. *Petroleum Geoscience, 24*, 335-347.

Marashi, V. (2021). *Northern Lights Project: Aurora Investigation with Sensitivity Studies and Using Different Simulation Methods.* Trondheim: NTNU.

Metz, B. D. (2005). *Carbon dioxide capture and storage,.* Geneva: IPCC.

Metz, B., Davidson, O., de Coninck, H., Loos, M., & Meyer, L. (2005). *IPCC Special Report: Carbon Dioxide.* Cambrige, UK: Cambridge University Press,.

Muller, N., Qi, R., Mackie, E., Pruess, K., & M. J. (2009). CO2 injection impairment due to halite precipitation . *Energy Procedia 1*, 3507-3514.

Nicoud, F. (2000). Conservative high-order finite-difference schemes for low-Mach number flows. *Journal of Computaional Physics*, 71-97.

Niessner, J., & Helmig, R. (2006). *Multi-scale modelling of two-phase–two-component processes in heterogeneous porous media.*

Nikolaos, K., Zacharenia, K., Gemma, P., A., R. C., Charalampos, V., & Nikolaos, T. (2018). Assessment of the impact of CO2 storage in sandstone formations by experimental studies and geochemical modeling: the case of the Mesohellenic Trough, NW Greece .

Norouzi, A. M., Babaei, M., Han, W. S., Kim, K.-Y., & Niasar, V. (2021). CO2-plume geothermal processes: A parametric study of salt precipitation. *Chemical Engineering Journal 425*.

NPD. (2021). *NORNE.* Retrieved from https://www.norskpetroleum.no/en/facts/field/norne/

NPD. (2022). Norne Field. *Norweigian Petroleum*. Retrieved from https://www.norskpetroleum.no/en/facts/field/norne/

Okwen, R., Yang, F., & Frailey, S. (2014). Effect of geologic depositional environment on CO2 storage efficiency. *Energy Procedia*, 5247-5257.

Oldenburg, C. M. (2006). JOULE-THOMSON COOLING DUE TO CO2 INJECTION INTO NATURAL GAS RESERVOIRS. *TOUGH Symposium.* Berkeley: Lawrence Berkeley National Laboratory.

Orlic, B. (2016). Geomechanical effects of CO2 storage in depleted gas reservoirs in the Netherlands: Inferences from feasibility studies and comparison with aquifer storage. *Journal of Rock*

Mechanics and Geotechnical Engineering, 846-859. Retrieved December 14, 2021, from
https://www.sciencedirect.com/science/article/pii/S167477551630141X

Orlic, B. (2016). Geomechanical effects of CO2 storage in depleted gas reservoirs in the Netherlands:
Inferences from feasibility studies and comparison with aquifer storage. *Journal of Rock
Mechanics and Geotechnical Engineering*, 846-859.

Pan, M., Ismail, N. A., Luzi-Helbing, M., Koh, C. A., & Schicks, J. M. (2020). New insights on a μm-scale
into the transformation process of CH4 hydrates to CO2-rich mixed hydrates. *Energies MDPI*.

Pandey, J. S., Strand, Ø., Solms, N. v., Ersland, G., & Almenningen, S. (2021). Direct Visualization of
CH4/CO2 Hydrate Phase Transitions in Sandstone Pores. *Crystal Growth & Design*, 2793-2806.

Parry, M. L., Parry, O. F., F.Canziani, O., Palutikof, J. P., Linden, P. J., & Hanson, C. E. (2007). *IPCC;
Contribution of Working Group II to the Fourth Assessment Report of the Intergovernmental
Panel on Climate Change.* Cambridge, UK: Cambridge University Press.

Pentland, C., Iglauer, S., Gharbi, O., Okada, K., & Suekane, T. (2012). *The Influence of Pore Space
Geometry on the Entrapment of Carbon Dioxide by Capillary Forces.* Asia Pacific : SPE.

Raza, A., Gholami, R., Rezaee, R., Bhatti, A. A., Bing, C. H., & Rasouli, V. (2018). Suitability of depleted gas
reservoirs for geological CO2 storage: A simulation study. *Green House Gases Science and
Technology*, 876-897.

Raza, A., Gholami, R., Rezaee, R., Bing, C. H., Nagarajan, R., & Ali Hamid, M. (2017). CO2 storage in
depleted gas reservoirs: A study on the effect of residual gas saturation. *Heriot-Watt University,
Research Gateway*, 95-107.

Raza, A., Gholami, R., Rezaee, R., Bing, C. H., Nagarajan, R., & Hamid, M. A. (2017). Assessment of CO2
residual trapping in depleted reservoirs used for geosequestration. *Journal of Natural Gas
Science and Engineering*, 137-155.

Razaa, A., Rezaee, R., Gholami, R., Bing, C. H., Nagarajand, R., & Hamid, M. A. (2016). A screening
criterion for selection of suitable CO2 storage sites. *Journal of Gas Science and Engineering*, 317-
327.

Ringrose, P. S., Mathieson, A. S., Wright, I., Hansen, O., Bissell, R., Saoula, N., . . . Selama, F. (2013). The
In Salah CO2 storage project: lessons learned and knowledge transfer. *Energy Procedia GHGT-
11*, 6226-6236.

Rosenbauer, R., & Thomas, B. (2010). Carbon dioxide (CO2) sequestration in deep saline aquifers and
formations. *Developments and Innovation in Carbon Dioxide (CO2) Capture and Storage
Technology*.

Rwechungura, R., Suwartadi, E., Dadashpour, M., Kleppe, J., & Foss, B. (2010). The Norne Field Case—A
Unique Comparative Case Study . *SPE Intelligent Energy Conference and Exhibition*.

Sanjiva, K. L. (1992). Compact finite difference schemes with spectral-like resolution. *Journal of Computational Physics*, 16-42.

Schlumberger. (2021). *Eclipse Technical description.*

ShojaiKaveh, N., Rudolph, E., Rossen, W., Van Hemert, P., & Wolf, K. (2013). Interfacial tension and contact angle determination in water-sandstone systems with injection of flue gas and CO2. *Fundamental Science toDeployment: 17th European Symposiumon Improved Oil Recovery,*.

Sokama-Neuyam, Y., Boakye, P., Aggrey, W. N., Obeng, N. O., Adu-Boahene, F., Woo, S. H., & Ursin, J. R. (2020). Theoretical Modeling of the Impact of Salt Precipitation on CO2 Storage Potential in Fractured Saline Reservoirs. *ACS omega*, 14776-14785.

STATOIL. (2006). *Annual reservoir development plan.* Statoil.

Svalestuen, J., Park, A., DePaola, D., & Powell, J. (2017). Accelerating Breakthrough Innnovation in Carbon Capture, Utilization, and Storage. *Mission Innovation* (pp. 2-250). Houstan, Texas: US department of Energy.

Swiecicki, T., Gibbs, P., Farrow, G., & Coward, M. (1998). A tectonostratigraphic framework for the Mid-Norway region. *Marine and Petroleum Geology*, 245-258.

Talman, S., Shokri, A. R., Chalaturnyk, R., & Nickel, E. (2020). Salt Precipitation at an Active CO2 Injection Site. In J. J. Alice Wu, *Gas Injection into Geological Formations and Related Topics.* Alberta.

Teukolsky, .., Vetterling, W., & Flannery, B. (2007). *Numerical recipes with source code CD-ROM.* Cambridge University Press.

Tsypkin, G. G. (2016). Formation of Hydrate in Injection of Liquid Carbon Dioxide into a Reservoir Saturated with Methane and Water. *Ishlinsky Institute for Problems in Mechanics, Russian Academy of Sciences*.

Vandeweijer, V., & Hofstee, C. (2018). 13 Years Of Safe CO2 Injection at K12-B. *Fifth CO2 Geological Storage Workshop.* Utrecht: EAGE.

Vilarrasa, V., & Rutqvist, J. (2016). Thermal effects on geologic carbon storage. *3 Institute of Environmental Assessment and Water Research (IDAEA)*.

Vilarrasa, V., & Rutqvist, J. (2017). Thermal effects on geologic carbon storage. *Earth-Science Reviews*, 245-256.

Whitson, C. H., & Brulé, R. M. (2000). Phase behavior. In C. H. Whitson, & B. M. R., *Phase behavior* (p. 170). Trondheim: Society of Petroleum Engineers Inc.

Yang, J., Lian, H., & Li, L. (2020). Fracturing in coals with different fluids: an experimental comparison between water, liquid CO2, and supercritical CO2. *Scientific Reports*, 10.

Appendix A

TABLE A-1B—COMPONENT PROPERTIES IN SI METRIC UNITS											
Compound		Molecular Weight M (kg/kmol)	Specific Gravity* γ	Liquid Density ρ_{sc} (kg/m³)	Critical Constants p_c (kPa)	T_c (K)	v_c (m³/kmol)	Z_c	Acentric Factor ω	Normal Boiling Point T_b (K)	Ideal Liquid Yield L (m³/1000 m³)	Gross Heating Value H (MJ/std m³)
Nitrogen	N_2	28.02	0.4700	469.5	3 399	126.3	0.0901	0.2916	0.0450	77.39		
Carbon dioxide	CO_2	44.01	0.5000	499.5	7 382	304.2	0.0940	0.2742	0.2310	194.67		
Hydrogen sulfide	H_2S	34.08	0.5000	499.5	9 005	373.6	0.0976	0.2831	0.1000	212.83		25.04
Methane	C_1	16.04	0.3300	329.7	4 604	190.6	0.0993	0.2884	0.0115	111.67		37.71
Ethane	C_2	30.07	0.4500	449.6	4 880	305.4	0.1479	0.2843	0.0908	184.56		66.43
Propane	C_3	44.09	0.5077	507.2	4 249	369.8	0.2029	0.2804	0.1454	231.11	3.67	95.27
iso-butane	$i\text{-}C_4$	58.12	0.5613	560.7	3 648	408.2	0.2627	0.2824	0.1756	261.44	4.37	125.0
Butane	$n\text{-}C_4$	58.12	0.5844	583.8	3 797	425.2	0.2547	0.2736	0.1928	272.67	4.20	125.5
iso-pentane	$i\text{-}C_5$	72.15	0.6274	626.8	3 381	460.4	0.3058	0.2701	0.2273	301.00	4.86	149.1
Pentane	$n\text{-}C_5$	72.15	0.6301	629.5	3 369	469.7	0.3040	0.2623	0.2510	309.22	4.83	149.4
Hexane	$n\text{-}C_6$	86.17	0.6604	659.7	3 012	507.4	0.3701	0.2643	0.2957	341.89	5.51	177.2
Heptane	$n\text{-}C_7$	100.20	0.6828	682.1	2 736	540.3	0.4322	0.2633	0.3506	371.56	6.20	205.0
Octane	$n\text{-}C_8$	114.20	0.7086	707.9	2 486	568.8	0.4920	0.2587	0.3978	398.83	6.80	232.9
Nonane	$n\text{-}C_9$	128.30	0.7271	726.4	2 289	594.6	0.5477	0.2536	0.4437	423.94	7.45	260.7
Decane	$n\text{-}C_{10}$	142.30	0.7324	731.7	2 096	617.7	0.6031	0.2462	0.4902	447.33	8.20	288.5
Air		28.97	0.4700	469.5	3 771	132.8	0.0852	0.2910	0.0400	78.83		
Water	H_2O	18.02	1.0000	999.0	22 105	647.2	0.0572	0.2350	0.3440	373.11		
Oxygen	O_2	32.00	0.5000	499.5	5 047	154.4	0.0733	0.2880	0.0250	90.11		

*Water = 1.

Table A1 Component Properties (SI units) (Whitson & Brulé, 2000)

Appendix B

Conversion factors

Volume to mass

1 year = 365 days

534 Sm^3= 1 tonne

106 tonnes= 1 million tonnes

Cumulative Injection volume for a period of 15 years:

1.8E6 Sm3/day x 30 days/1 month x 12 months/year x 15 years = 9.72 E09 Sm^3

In tonnes: 9.72 E09 Sm^3 x 1 tonne / 534 Sm^3 x 1 Mt/10^6 = 18.202 Mt

Mass-mole to mass:

mol = mole = g-mole

1 mole = 1 g-mole CO2 = 44.01 g CO_2

1 kg-mole CO_2= 1000 g-mole CO_2= 1000 moles of CO_2

1 kg-mole CO_2 x ($\frac{1000 \text{ mole CO2}}{1 \text{ kg}-\text{mole CO2}}$) x ($\frac{144.01 \text{ g CO2}}{1 \text{ mole CO2}}$) x ($\frac{1 \text{ kg}}{1000 \text{ g}}$) x ($\frac{1 \text{ tonne}}{1000 \text{ kg}}$) x $\frac{1Mt}{10^6 \text{ tonnes}}$ = Mt

Appendix C

This table provides the list of simulating software and their numerical features for discretization applied It has been adapted fromm the work of (Jiang X. , 2011).

Table 0-1 List of software and their numerical features (Jiang X. , 2011)

Simulators	Main applications	Numerical features (methods for discretization/integration)
CHILLER (companion to SOLVEQ)	Multi-component multi-phase equilibrium geochemical calculation software based on minimum free-energy	Newton–Raphson method for solving a system of mass balance and mass action equations
COORES	Multi-component three-phase and 3D fluid flow in heterogeneous porous media	Finite volume method for spatial discretization; implicit temporal discretization
DUMUX	Multi-scale multi-physics toolbox for the simulation of flow and transport processes in porous media	Vertex-centered finite volume method for spatial discretization; implicit temporal discretization
ECLIPSE	Three-phase and 3D fluid flow in porous media with cubic EOS, pressure dependent permeability values, etc.	Integrated finite difference method (IFDM) with irregular spatial discretization; implicit temporal discretization
ELSA	Semi-analytical tool to estimate fluid distributions and leakage rates involving vertically integrated sharp-interface equations and local 3D well models	Spatial discretization is essentially grid free; several schemes for temporal discretization including implicit pressure explicit saturation, etc.

FEFLOW	Solving the groundwater flow equation with mass and heat transfer, including multi-component chemical kinetics	Finite element method for spatial discretization; implicit/explicit/Crank–Nicolson temporal discretization
FEHM	Fully coupled heat, mass and stress balance equations for 3D, non-isothermal, multi-phase fluid flow in porous media	Control volume finite element method for spatial discretization; implicit temporal discretization
GEM [23]	EOS compositional reservoir simulator	IFDM for spatial discretization; implicit temporal discretization
IPARS-CO2	Parallel multi-block, multi-physics approach for multi-phase flow in porous media	Mixed finite element method for space discretization; implicit pressure, explicit concentration sequential algorithm for temporal discretization
MIN3P	Multi-component reactive transport modelling in variably saturated porous media	Finite volume method for spatial discretization; implicit temporal discretization
MODFLOW	Solving the groundwater flow equation to simulate the flow through aquifers	Finite difference method for spatial discretization; implicit or Crank–Nicolson for temporal discretization
MT3DMS	Modular 3D transport model simulating convection, dispersion, and chemical reactions of dissolved constituents	Finite difference/particle-tracking based Eulerian–Lagrangian /finite-volume method for spatial discretization; implicit/explicit temporal discretization

MUFTE	Isothermal and non-isothermal multi-phase flow problems including compositional effects	Vertex-centred finite volume method for spatial discretization; implicit temporal discretization
PFLOTRAN	Parallel 3D reservoir simulator for subsurface multi-phase, multi-component reactive flow and transport based on continuum scale mass and energy conservation	Finite element method for spatial discretization; implicit/semi-implicit time integration
PHAST	Simulating groundwater flow, solute transport, and multi-component geochemical reactions	Finite difference method for spatial discretization; implicit or Crank–Nicholson for temporal discretization
PHREEQC	Low-temperature aqueous geochemical simulator	Based on an ion-association aqueous model; chemical equilibrium, kinetic, transport, and inverse-modelling calculations
RETRASO	Reactive transport of dissolved and gaseous species in non-isothermal saturated or unsaturated problems	Direct substitution approach for solving the reactive transport equations
ROCKFLOW	Multi-phase flow and solute transport processes in porous and fractured media	Finite element method for spatial discretization; implicit temporal discretization
SUTRA	Fluid movement and transport of either energy or dissolved substances in a subsurface environment	Hybrid finite element and integrated finite difference method for spatial discretization; implicit temporal discretization
TOUGHREACT	Chemically reactive multi-component, multi-phase, non-isothermal flows in porous and fractured media	IFDM for spatial discretization; implicit temporal discretization

Appendix D

DATA FILE –BASE CASE

--===
--BASE CASE DATA FILE FOR CO2 STORAGE IN DEPLETED GAS RESERVOIR USING GASWAT
KEYWORD
-- 2 PRODUCER WELLS FOR 15 YEARS, 2 INJECTORS INJECTING FOR 15 YEARS
--CREATED BY NABEEL AHMED KHAN
--===
--RUNSPEC SECTION--

-- This reservoir simulation deck is made available under the Open Database
-- License: http://opendatacommons.org/licenses/odbl/1.0/. Any rights in
-- individual contents of the database are licensed under the Database Contents
-- License: http://opendatacommons.org/licenses/dbcl/1.0/

-- Copyright (C) 2015 Statoil

-- Norne full field model for SPE ATW 2013
--
-- Simplified Generic model based on the above Norne model. PB 09/2020
--

RUNSPEC
TITLE
CO2 Gas Injection in Norne reservoir, a depleted gas reservoir study

DIMENS
46 112 22   /

GRIDOPTS
 'YES' 0 /
METRIC
GASWAT
AIM
-- components --co2 h20 c1 c2 c3
COMPS
5 /
EOS
PR /

ENDSCALE
NODIR   REVERS /

DIFFUSE

START

```
 06  'NOV' 1997 /

EQLDIMS
 1  100  20 /

--EQLOPTS
-- 'THPRES' /   no fine equilibration if swatinit is being used

REGDIMS
--ntfip  nmfipr  nrfreg  ntfreg
   22     3     1*     20   /

WELLDIMS
130  36  15  84 /

TABDIMS
--ntsfun ntpvt nssfun nppvt ntfip nrpvt ntendp
  1    1    33    60   16   60 /

--FAULTDIM
--10000
NSTACK
 40 /

UNIFIN
UNIFOUT


--------------------------------------------------------
--
--        Input of grid geometry
--
--------------------------------------------------------
GRID

-- Ask for an EGRID file; no .GRID output.
GRIDFILE
 0  1 /

-- optional for postprocessing of GRID
MAPAXES
 0. 100. 0. 0. 100. 0. /

GRIDUNIT
METRES  /
```

```
-- requests output of INIT file
INIT
MESSAGES
 8*10000  20000 10000 1000 1* /


NOECHO


-------------------------------------------------------
--
--        Grid and faults
--
-------------------------------------------------------


-- Simulation grid, with slooping faults:
-- file in UTM coordinate system, for importing to DecisionSpace
INCLUDE
 './INCLUDE/GRID/IRAP_1005.GRDECL' /

INCLUDE
 'ACTNUM_0704_inclayer4.prop' /

-- Faults
INCLUDE
'./INCLUDE/FAULT/FAULT_JUN_05.INC' /

-- Alteration of transmissibility by use of the 'MULTFLT' keyword
INCLUDE
'./INCLUDE/FAULT/FAULTMULT_AUG-2006.INC' /

-------------------------------------------------------
--
--        Input of grid parametres
--
-------------------------------------------------------
--
INCLUDE
 'PORO_0704_inclayer4.prop' /

INCLUDE
 'NTG_0704_inclayer4.prop' /

INCLUDE
 'PERM_0704_inclayer4.prop' /
```

```
COPY
  PERMX PERMY /
  PERMX PERMZ /
/
-- Remove segment G  (PB)
EQUALS
 'PORO' 0.0 30 41 70 102 1 22 /

/

-- based on same kv/kh factor
MULTIPLY
  'PERMZ' 0.2    1 46 1 112  1  1 /   Garn 3
  'PERMZ' 0.04   1 46 1 112  2  2 /   Garn 2
  'PERMZ' 0.25   1 46 1 112  3  3 /   Garn 1
  'PERMZ' 0.0001    1 46 1 112  4  4 /   Not      (made active)
  'PERMZ' 0.13   1 46 1 112  5  5 /   Ile 2.2
  'PERMZ' 0.13   1 46 1 112  6  6 /   Ile 2.1.3
  'PERMZ' 0.13   1 46 1 112  7  7 /   Ile 2.1.2
  'PERMZ' 0.13   1 46 1 112  8  8 /   Ile 2.1.1
  'PERMZ' 0.09   1 46 1 112  9  9 /   Ile 1.3
  'PERMZ' 0.07   1 46 1 112 10 10 /   Ile 1.2
  'PERMZ' 0.19   1 46 1 112 11 11 /   Ile 1.1
  'PERMZ' 0.13   1 46 1 112 12 12 /   Tofte 2.2
  'PERMZ' 0.64   1 46 1 112 13 13 /      Tofte 2.1.3
  'PERMZ' 0.64   1 46 1 112 14 14 /      Tofte 2.1.2
  'PERMZ' 0.64   1 46 1 112 15 15 /      Tofte 2.1.1
  'PERMZ' 0.64   1 46 1 112 16 16 /      Tofte 1.2.2
  'PERMZ' 0.64   1 46 1 112 17 17 /      Tofte 1.2.1
  'PERMZ' 0.016  1 46 1 112 18 18 /      Tofte 1.1
  'PERMZ' 0.004  1 46 1 112 19 19 /      Tilje 4
  'PERMZ' 0.004  1 46 1 112 20 20 /      Tilje 3
  'PERMZ' 1.0    1 46 1 112 21 21 /      Tilje 2
  'PERMZ' 1.0    1 46 1 112 22 22 /      Tilje 1
/
--------------------------------------------------------
--
--     Barriers
--
--------------------------------------------------------

-- MULTZ multiplies the transmissibility between blocks
-- (I, J, K) and (I, J, K+1), thus the barriers are at the
```

-- bottom of the given layer.

-- Region barriers
INCLUDE
 './INCLUDE/PETRO/MULTZ_HM_1.INC' /

-- Local barriers
INCLUDE
'./INCLUDE/PETRO/MULTZ_JUN_05_MOD.INC' /

INCLUDE
 'ACTNUM_E_SEG_Layer4_Act.inc' /
NOECHO
MINPV
  500 /

EDIT

PROPS

NOECHO

--COMPONENT NAMES (carbon dioxide and first three hydrocarbons)
CNAMES
'CO2' 'H2O' 'C1' 'C2' 'C3' /

-- Equation of State Peng-Robinson
EOS
PR /

-- salinity value taken from reference manual value
SALINITY
0.51 /

DENSITY
1* 1050 1* /
--diffusion gas coeffecient, for simplicity, taken to be same for other components. Co2 val obtained from internet
DIFFCGAS
0.00027987 0.00013824 0.0001 0.0001 0.0001 /
--reservoir temperature taken to be 40C as it is assumed to be in North Sea, which is colder.

RTEMP
100 /
--Crtical temperatures of each component, values taken from Whitson`s book , Appendix B, prb8
TCRIT
304.223 647.2 190.556 305.446 369.834 /

-- critical pressures taken from whitson`s book, Appendix B, prb 8
PCRIT
73.81530056 221.05 46.04320728 48.80111128 42.49240588/

--critical volumes taken from table A1-B Whitson`s book.
VCRIT
0.094 0.0572 0.0993 0.1479 0.2029/

-- compressibility factors taken from Whitson prb 7 and co2 value from co2sol data file
ZCRIT
0.274 0.235 0.2884 .2843 .2804 /

-- Molecular weight of gases from Whitson`s book table A1-B
MW
44.01 18.02 16.04 30.07 44.09 /

--accentric factor from Whitson`s book table A1-B
ACF
0.231 0.3440 0.0115 0.0908 0.1454 /

--Binary coeffecient using whitson book appendix table A3 for co2 and hydrocarbon interactions
BIC
-- explanation of BIC
--   co2   h2o   c1   c2 c3 (hydrocarbon interactions from unknown internet source and denaqa-gaswat file
--co2 -
--h2o 0.1896
--c1 0.105 0.4850
--c2 0.130 0.4920 0.002
--c3 0.125 0.4970 0.007 0.001

0.1896
0.105 0.4850
0.130 0.4920 0.002
0.125 0.4970 0.007 0.001 /

--molar composition for all the components. Dry gas reservoirs usually have a higher c1 content (made up values)
ZI
0.0115 0.02   0.65   0.18   0.1385/
--Default LBC coeffecient are used here!
LBCCOEF
0.1023 /
--Properties obtained from noname.inc file of 3component
--water saturation functions
WSF
-- Sw   krw   Pcwg
 0.3700   0.0000
 0.4010   3.8320E-05
 0.4320   2.6623E-04
 0.4630   8.2737E-04
 0.4940   0.0018
 0.5250   0.0035
 0.5560   0.0057
 0.5870   0.0088
 0.6180   0.0129
 0.6490   0.0179
 0.6800   0.0240
 0.7110   0.0313
 0.7420   0.0399
 0.7730   0.0500
 0.8040   0.0615
 0.8350   0.0745
 0.8660   0.0893
 0.8970   0.1058
 0.9280   0.1241
 0.9590   0.1444
 0.9900   0.1666
 1.0000   1.0000
/
GSF
-- Sg   krg   Pcog
 0.000   0.0000   0.0000
 0.01   0.0   0.00
 0.03   0.000001 0.000
 0.0410 8.9509E-04 0.0000
 0.0720 0.0043   0.0000
 0.1030 0.0106   0.0000
 0.1340 0.0203   0.0000
 0.1650 0.0335   0.0000

```
0.1960   0.0504     0.0000
0.2270   0.0713     0.0000
0.2580   0.0963     0.0000
0.2890   0.1256     0.0000
0.3200   0.1592     0.0000
0.3510   0.1972     0.0000
0.3820   0.2399     0.0000
0.4130   0.2872     0.0000
0.4440   0.3394     0.0000
0.4750   0.3963     0.0000
0.5060   0.4583     0.0000
0.5370   0.5253     0.0000
0.5680   0.5974     0.0000
0.5990   0.6746     0.0000
0.6300   0.7572     0.0000
/
ROCK
150 0.00005 /
--------------------------------------------------------------------------
REGIONS

EQUALS
'FIPNUM' 1 1 46 1 112 1 4 /
'FIPNUM' 2 1 46 1 112 5 22 /
/
--------------------------------------------------------------------------
SOLUTION

RPTRST
BASIC=2 KRO KRW KRG /
--------------------------------------------------------------------------
-- equilibrium data: do not include this file in case of RESTART
EQUIL
2750    200 2750 0 5* 2 1 /
/
RPTSOL
--AQPH  AQSP
PRESSURE SGAS SWAT DENG DENW VGAS VWAT XMF YMF ZMF AMF /
--------------------------------------------------------------------------
SUMMARY

NEWTON
MLINEARS
FPR
```

FVIR
--Field Water production rate
FWPR
-- water injection rate history
FWIRH
-- Field Gas injection rate
FGIR
-- Field Gas Production Rate
FGPR
--Field Gas Production Total
FGPT
--Gas Density at surface conditions
FGDN
--Gas injection rate history
FGIRH
--Reservoir Volume injection total
FVIT
--Field water injection cumulative total
FWIT
--Water Injection Total History
FWITH
-- Gas injection total
FGIT
--Gas Injection Total History
FGITH
--Pressure average value (Pore-Volume Weighted)
FPRP
--Pore volume at reservoir conditions
FRPV
--Pressure average value (Hydrocarbon Pore-Volume Weighted)
FPRH
----Gas SATuration average value
FGSAT
--Gas Reservoir Volume in Place
FGIPR
--Molar amount of specified component mobile in gas
FCGMM
/
--Molar amount of specified component trapped in gas
FCGMI
/
----Molar amount of specified dissolved in water
FCWM
/

--Gas In Place (liquid phase).
FGIPL
--Gas In Place (Gas phase).
FGIPG
--Regional molar amount of specified component mobile in gas
RCGMM
1/
2/
/
--Regional molar amount of specified component trapped in gas
RCGMI
1/
2/
/
--Regional molar amount of specified component dissolved in water
RCWM
1/
2/
/
-- Well bottomhole pressure
WBHP
/
-- Well gas injection rate.
WGIR
/
--Pressure in blocks around the well
BPR
7 66 11 / -- for well I2/P2 nearby grid Permx about 52.922mD
8 65 16 / -- for well I2/P2 nearby grid Perm x about 1720mD
10 63 15 / --for well I1/P1 nearby grid permx 81.362 mD and next to fault
11 64 16 / -- for well I1/P1 nearby grid permx 1566 mD
/

SCHEDULE

NOECHO
RPTRST
PRESSURE SWAT SGAS DENG DENW XMF YMF ZMF VGAS VWAT AMF/
TUNING
2* 0.9/
/
30 1 50/
MESSOPTS
ACCPTIME 1 /

```
WELSPECS
P1 FIELD 11 63 1* GAS /
P2 FIELD 8 66 1* GAS /
/
--Define completions

COMPDAT
P1 11 63 7 18/
P2 8 66 7 18/
/
--Define water and gas injection streams (gas stream is pure CO2)

WCONPROD
P1 OPEN BHP 2*  900000.0 2* 50.0 /
P2 OPEN BHP 2*  900000.0 2* 50.0 /
/
--Timestep monthly
TSTEP
180*30/




--shutting the production wells after 10 years or 180 months of production.
WELOPEN
'P1' 'SHUT' 5*/
'P2' 'SHUT' 5*/
/
WELSPECS
I1 FIELD 11 63 1* GAS /
I2 FIELD 8 66 1* GAS /
/
COMPDAT
I1 11 63 7 18/
I2 8 66 7 18/
/
WELLSTRE
CO2INJ 1.0 /
/

--Set water and gas injection rates

WINJGAS
I1 STREAM CO2INJ /
```

I2 STREAM CO2INJ /
--I3 STREAM CO2INJ /
--I4 STREAM CO2INJ /
/

--2000a WELLINJE is for back-compatibility, prefered keyword is WCONINJE

WCONINJE
I1 GAS OPEN RATE 900000 1* 200 /
I2 GAS OPEN RATE 900000 1* 200 /
--I3 GAS SHUT RATE 600000 1* 200 /
--I4 GAS SHUT RATE 600000 1* 200 /
/

SAVE

TSTEP
180*30/
WELOPEN
'I1' 'SHUT' 5* /
'I2' 'SHUT' 5* /
--'I3' 'SHUT' 5* /
--'I4' 'SHUT' 5* /
 /
DATES
1 JAN 2030/
/

DATES
1 JAN 2050/
/
DATES
1 JAN 2060/
/
DATES
1 JAN 2070/
/
DATES
1 JAN 2080/
/
DATES
1 JAN 2090/
/
DATES

1 JAN 2100/
/
DATES
1 JAN 2200/
/

END

Appendix D

Link for INCLUDE files

https://drive.google.com/drive/folders/1w7mTHJQI2_8vZwPanLt6gmy9UzIgq0Ga?usp=sharing

Link for DATA Files for all cases

https://drive.google.com/drive/folders/1P_R3_j7n9ww-zWX_fvQBpG2HuBCihoBL?usp=sharing

Thankyou!